

# Time Temperature Transformation (TTT) Diagrams

**R. Manna**

Assistant Professor

Centre of Advanced Study

Department of Metallurgical Engineering

Institute of Technology, Banaras Hindu University

Varanasi-221 005, India

[rmanna.met@itbhu.ac.in](mailto:rmanna.met@itbhu.ac.in)

Tata Steel-TRAERF Faculty Fellowship Visiting Scholar

Department of Materials Science and Metallurgy

University of Cambridge, Pembroke Street, Cambridge, CB2 3QZ

[rm659@cam.ac.uk](mailto:rm659@cam.ac.uk)

# TTT diagrams

TTT diagram stands for “time-temperature-transformation” diagram. It is also called isothermal transformation diagram

Definition: TTT diagrams give the kinetics of isothermal transformations.

# Determination of TTT diagram for eutectoid steel

Davenport and Bain were the first to develop the TTT diagram of eutectoid steel. They determined pearlite and bainite portions whereas Cohen later modified and included  $M_S$  and  $M_F$  temperatures for martensite. There are number of methods used to determine TTT diagrams. These are salt bath (**Figs. 1-2**) techniques combined with metallography and hardness measurement, dilatometry (**Fig. 3**), electrical resistivity method, magnetic permeability, *in situ* diffraction techniques (X-ray, neutron), acoustic emission, thermal measurement techniques, density measurement techniques and thermodynamic predictions. Salt bath technique combined with metallography and hardness measurements is the most popular and accurate method to determine TTT diagram.



Fig. 1 : Salt bath I -austenitisation heat treatment.



Fig. 2 : Bath II low-temperature salt-bath for isothermal treatment.



Fig . 3(a): Sample and fixtures for dilatometric measurements

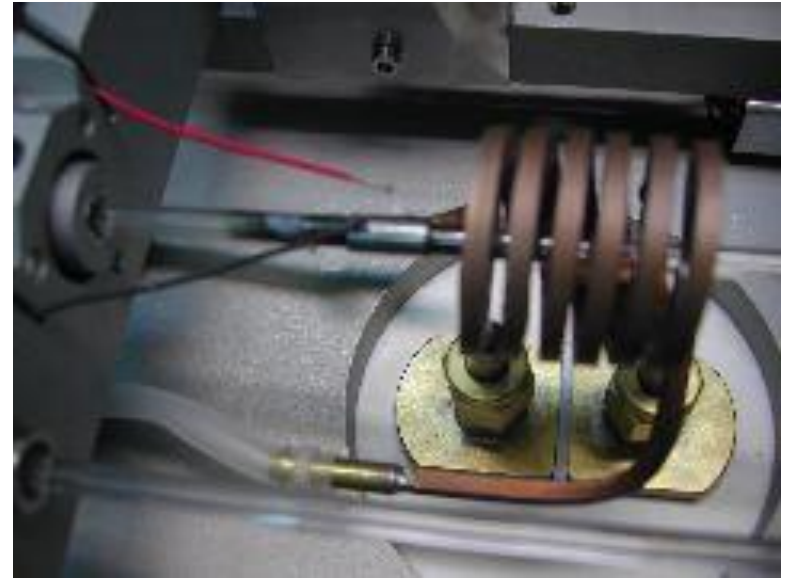


Fig. 3(b) : Dilatometer equipment

In **molten salt bath technique** two salt baths and one water bath are used. Salt bath I (**Fig. 1**) is maintained at austenitising temperature ( $780^{\circ}\text{C}$  for eutectoid steel). Salt bath II (**Fig. 2**) is maintained at specified temperature at which transformation is to be determined (below  $A_{e1}$ ), typically  $700-250^{\circ}\text{C}$  for eutectoid steel. Bath III which is a cold water bath is maintained at room temperature.

In bath I number of samples are austenitised at  $A_{C1}+20-40\text{ C}$  for eutectoid and hypereutectoid steel,  $A_{C3}+20-40\text{ C}$  for hypoeutectoid steels for about an hour. Then samples are removed from bath I and put in bath II and each one is kept for different specified period of time say  $t_1, t_2, t_3, t_4, t_n$  etc. After specified times, the samples are removed and quenched in water. The microstructure of each sample is studied using metallographic techniques. The type, as well as quantity of phases, is determined on each sample.

The time taken to 1% transformation to, say pearlite or bainite is considered as transformation start time and for 99% transformation represents transformation finish. On quenching in water austenite transforms to martensite.

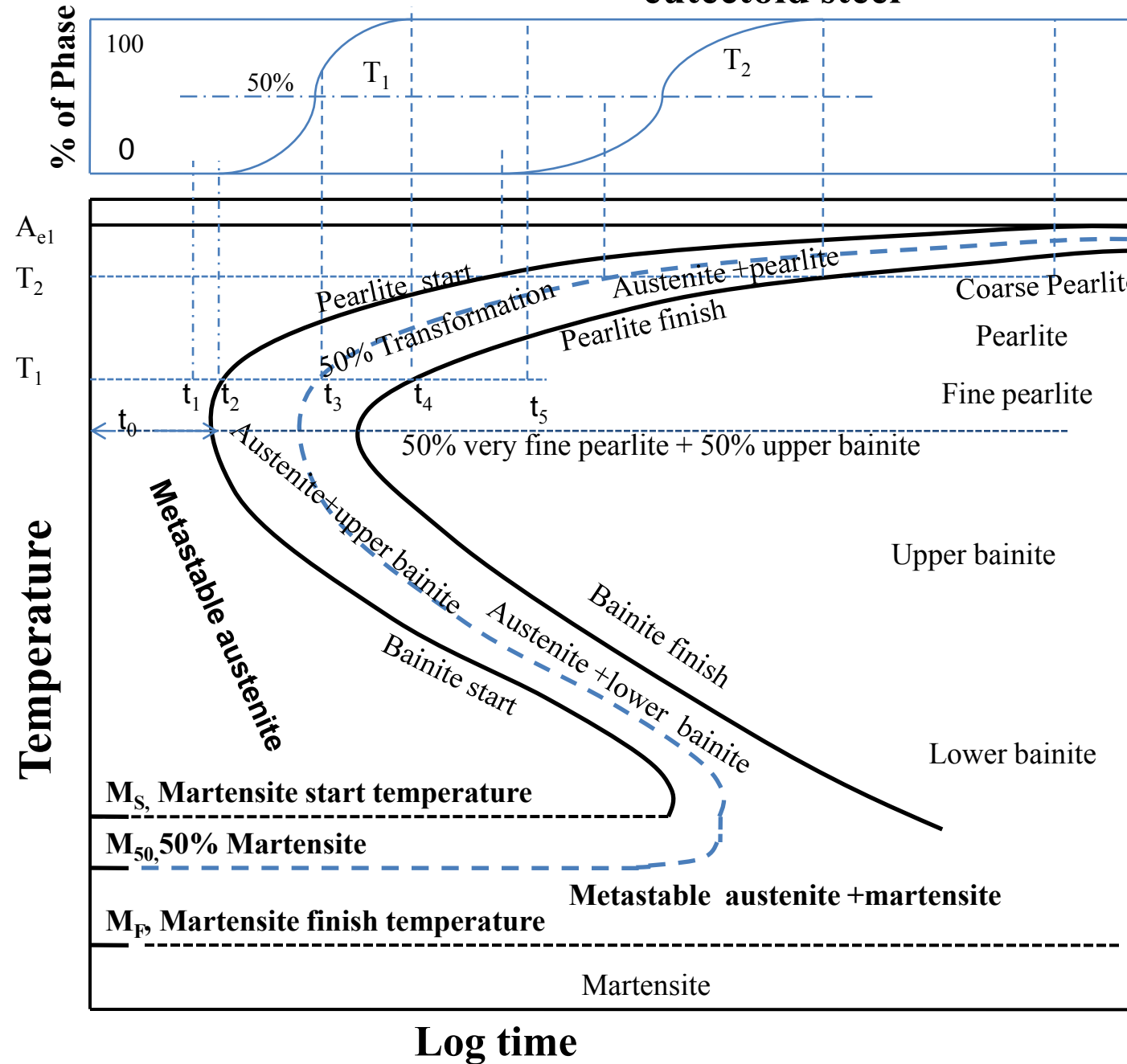
But below 230 C it appears that transformation is time independent, only function of temperature. Therefore after keeping in bath II for a few seconds it is heated to above 230 C a few degrees so that initially transformed martensite gets tempered and gives some dark appearance in an optical microscope when etched with nital to distinguish from freshly formed martensite (white appearance in optical microscope). Followed by heating above 230 C samples are water quenched. So initially transformed martensite becomes dark in microstructure and remaining austenite transform to fresh martensite (white).

Quantity of both dark and bright etching martensites are determined. Here again the temperature of bath II at which 1% dark martensite is formed upon heating a few degrees above that temperature (230 C for plain carbon eutectoid steel) is considered as the martensite start temperature (designated  $M_S$ ). The temperature of bath II at which 99 % martensite is formed is called martensite finish temperature ( $M_F$ ).

Transformation of austenite is plotted against temperature vs time on a logarithm scale to obtain the TTT diagram. The shape of diagram looks like either S or like C.

**Fig. 4** shows the schematic TTT diagram for eutectoid plain carbon steel

**Fig.4: Time temperature transformation (schematic) diagram for plain carbon eutectoid steel**



At T<sub>1</sub>, incubation period for pearlite=t<sub>2</sub>, Pearlite finish time =t<sub>4</sub>

Minimum incubation period t<sub>0</sub> at the nose of the TTT diagram,

**Hardness**

M<sub>S</sub>=Martensite start temperature  
M<sub>50</sub>=temperature for 50% martensite formation  
M<sub>F</sub>= martensite finish temperature

At close to  $A_{e1}$  temperature, coarse pearlite forms at close to  $A_{e1}$  temperature due to low driving force or nucleation rate.

At higher undercoolings or lower temperature finer pearlite forms.

At the nose of TTT diagram very fine pearlite forms

Close to the eutectoid temperature, the undercooling is low so that the driving force for the transformation is small. However, as the undercooling increases transformation accelerates until the maximum rate is obtained at the “nose” of the curve. Below this temperature the driving force for transformation continues to increase but the reaction is now impeded by slow diffusion. This is why TTT curve takes on a “C” shape with most rapid overall transformation at some intermediate temperature.

Pearlitic transformation is reconstructive. At a given temperature (say  $T_1$ ) the transformation starts after an incubation period ( $t_2$  at  $T_1$ ). Locus of  $t_2$  for different for different temperature is called transformation start line. After 50% transformation locus of that time ( $t_3$  at  $T_1$ ) for different temperatures is called 50% transformation line. While transformation completes that time ( $t_4$  at  $T_1$ ) is called transformation finish, locus of that is called transformation finish line. Therefore TTT diagram consists of different isopercentage lines of which 1%, 50% and 99% transformation lines are shown in the diagram. At high temperature while undercooling is low form coarse pearlite. At the nose temperature fine pearlite and upper bainite form simultaneously though the mechanisms of their formation are entirely different. The nose is the result of superimposition of two transformation noses that can be shown schematically as below one for pearlitic reaction other for bainitic reaction (**Fig. 6**).

Upper bainite forms at high temperature close to the nose of TTT diagram while the lower bainite forms at lower temperature but above  $M_S$  temperature.

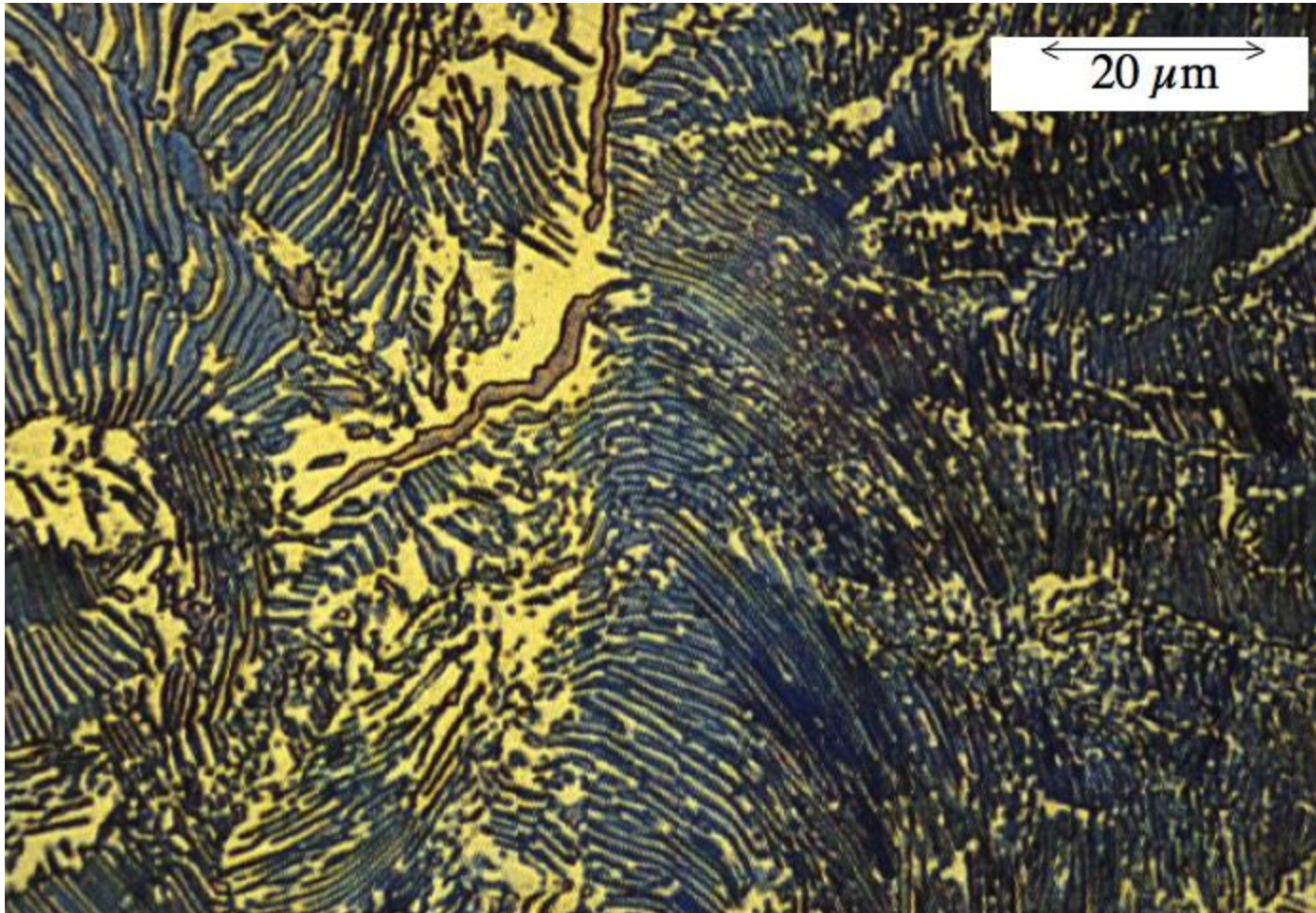


Fig. 5(a) : The appearance of a (coarse) pearlitic microstructure under optical microscope.



Fig. 5(b): A cabbage filled with water analogy of the three-dimensional structure of a single colony of pearlite, an interpenetrating bi-crystal of ferrite and cementite.

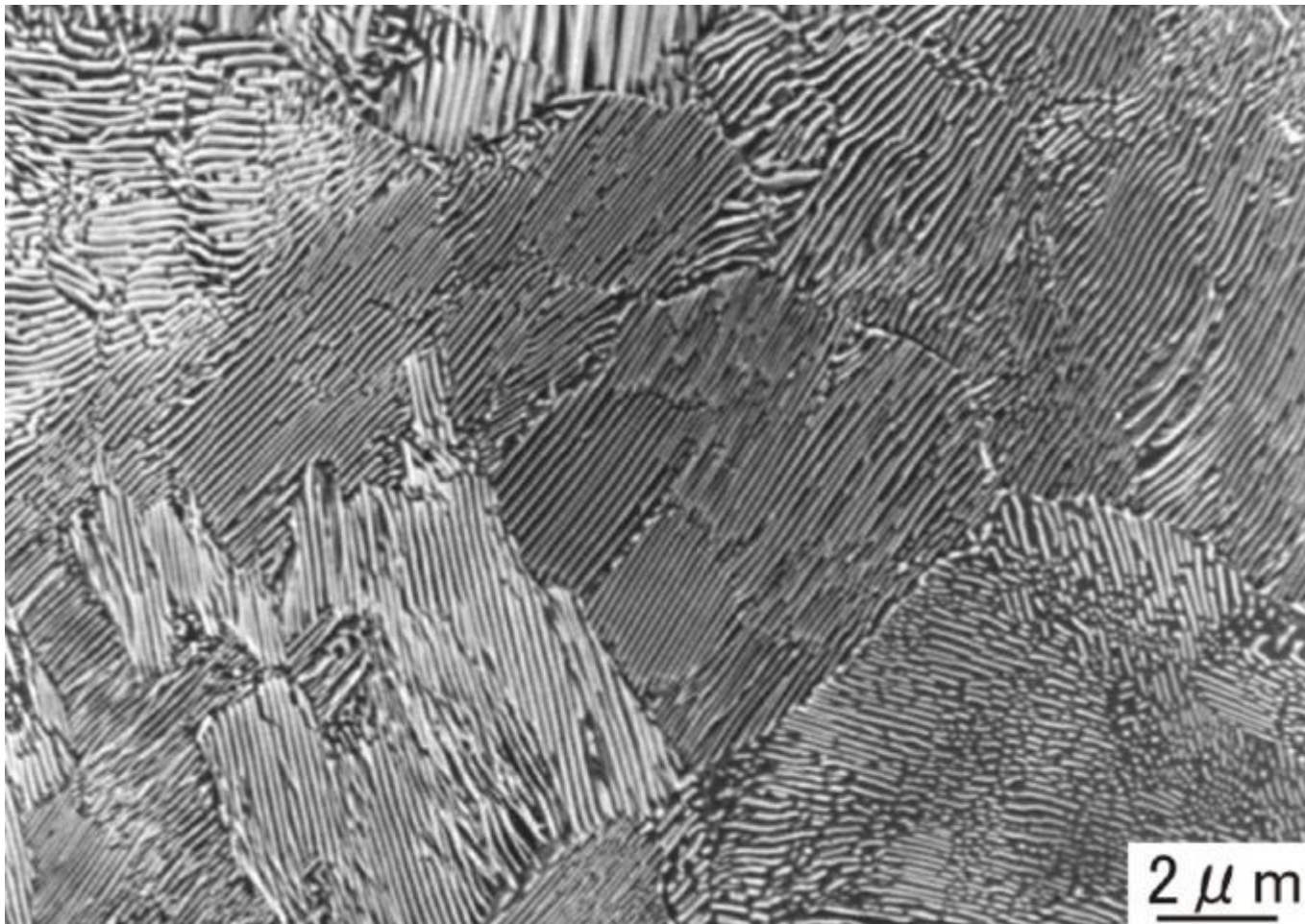


Fig. 5(c): Optical micrograph showing colonies of pearlite . Courtesy of *S. S. Babu*.

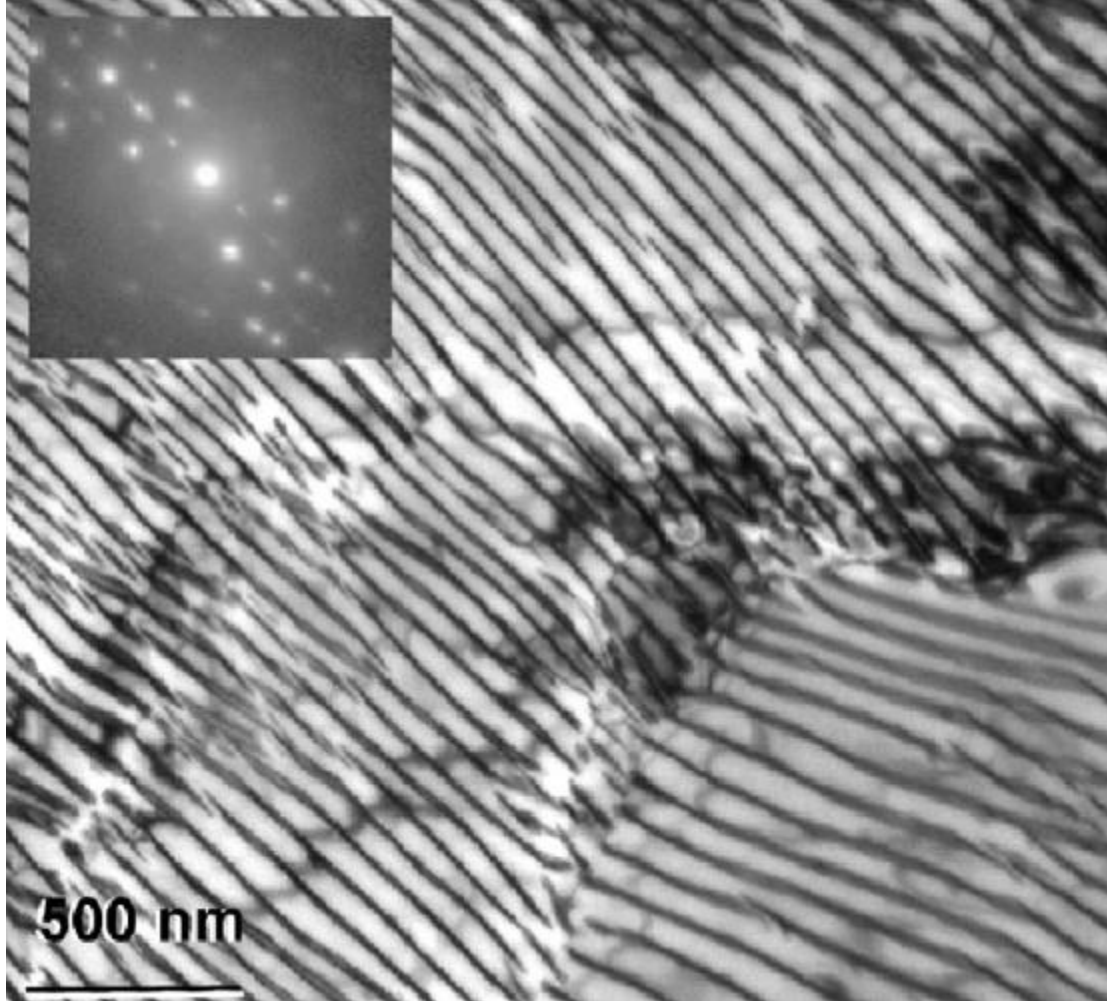


Fig. 5(d): Transmission electron micrograph of extremely fine pearlite.

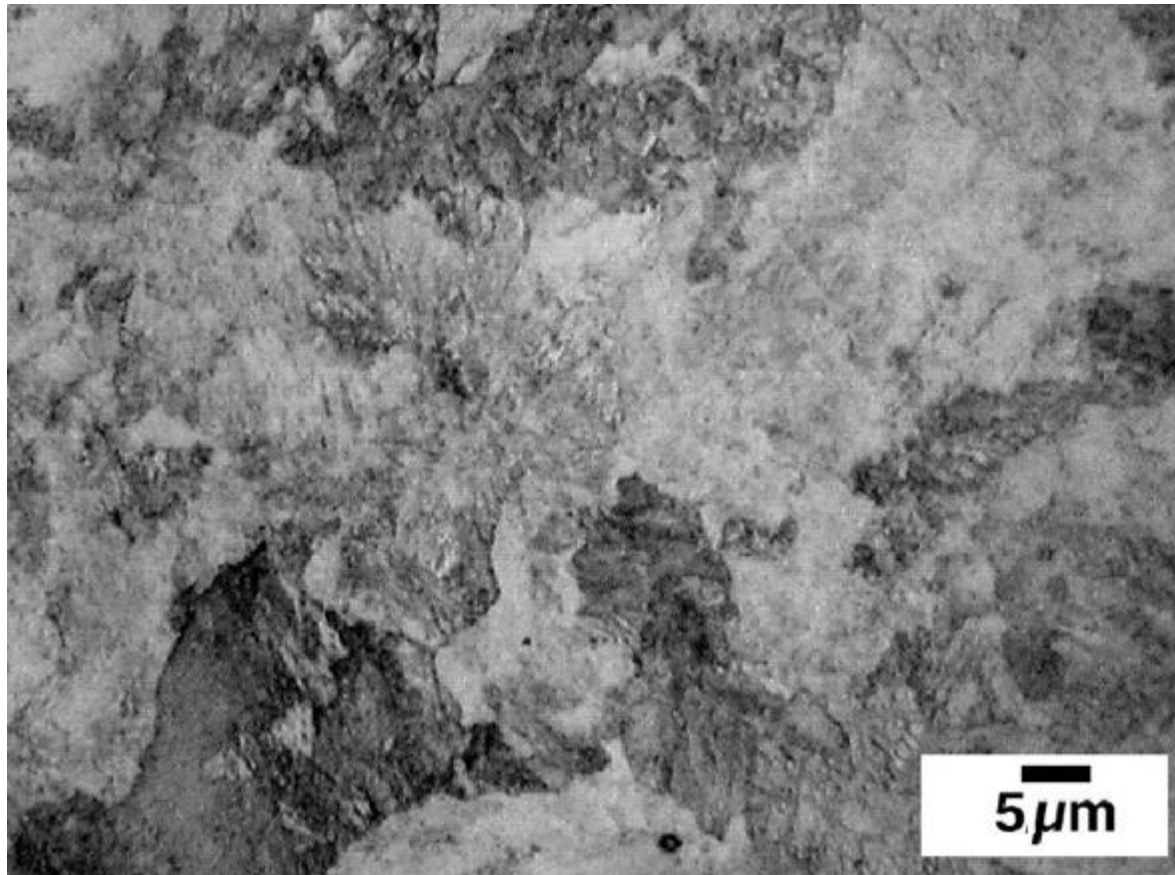
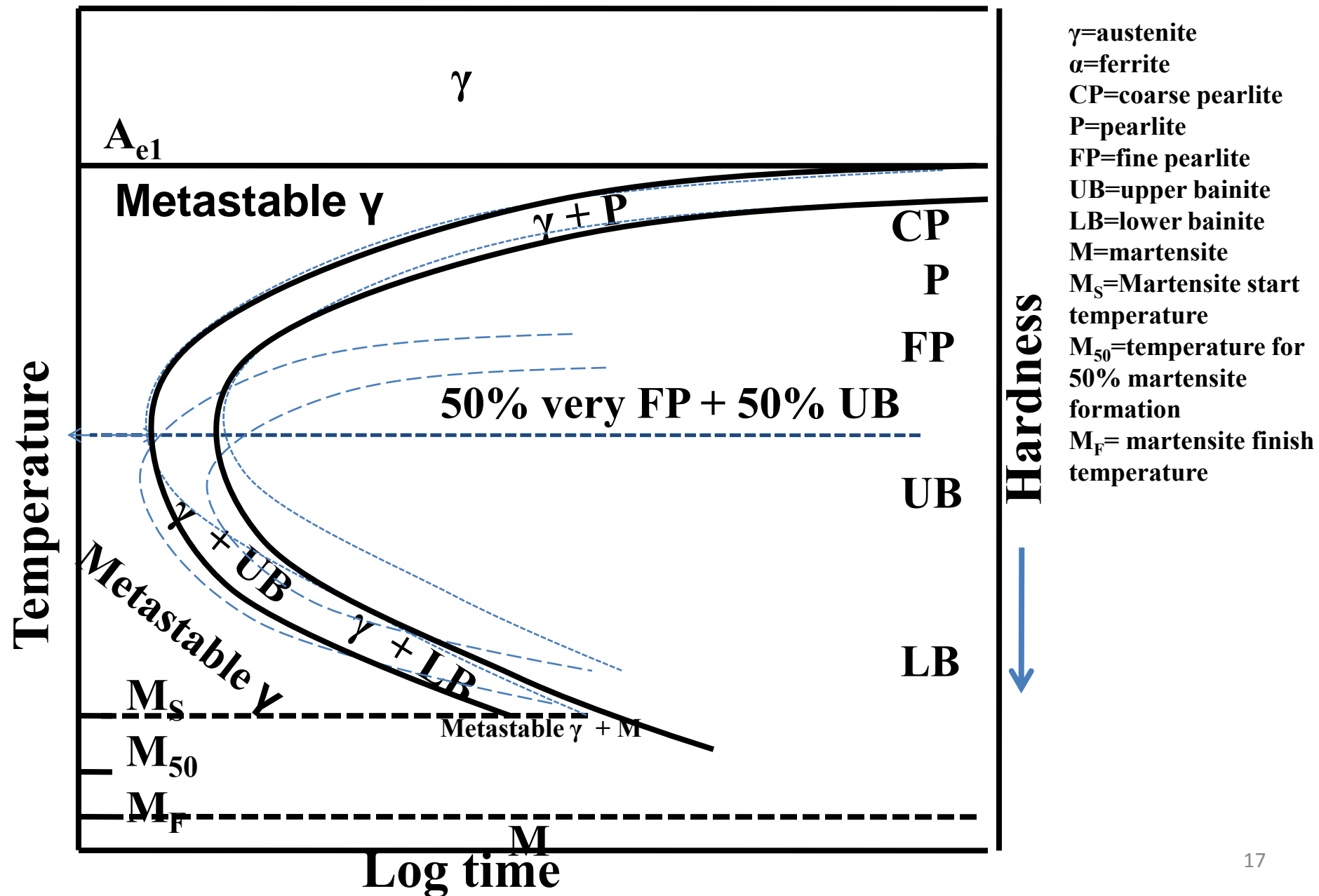


Fig. 5(e): Optical micrograph of extremely fine pearlite from the same sample as used to create Fig. 5(d). The individual lamellae cannot now be resolved.

**Fig. 6: Time Temperature Transformation (schematic) diagram for plain carbon eutectoid steel**



On cooling of metastable austenite 1% martensite forms at about 230°C. The transformation is athermal in nature. i.e. amount of transformation is time independent (characteristic amount of transformation completes in a very short time) but function of temperature alone. This temperature is called the martensite start temperature or  $M_s$ .

Below  $M_s$  while metastable austenite is quenched at different temperature amount of martensite increases with decreasing temperature and does not change with time.

The temperature at which 99% martensite forms is called martensite finish temperature or  $M_f$ . Hardness values are plotted on right Y-axis. Therefore a rough idea about mechanical properties can be guessed about the phase mix.

# TTT diagram gives

Nature of transformation-isothermal or athermal (time independent) or mixed

Type of transformation-reconstructive, or displacive

Rate of transformation

Stability of phases under isothermal transformation conditions

Temperature or time required to start or finish transformation

Qualitative information about size scale of product

Hardness of transformed products

# Factors affecting TTT diagram

Composition of steel-

- (a) carbon wt%,
- (b) alloying element wt%

Grain size of austenite

Heterogeneity of austenite

## **Carbon wt%-**

As the carbon percentage increases  $A_3$  decreases, similar is the case for  $A_{r3}$ , i.e. austenite stabilises. So the incubation period for the austenite to pearlite increases i.e. the C curve moves to right. However after 0.77 wt%C any increase in C,  $A_{cm}$  line goes up, i.e. austenite become less stable with respect to cementite precipitation. So transformation to pearlite becomes faster. Therefore C curve moves towards left after 0.77%C. The critical cooling rate required to prevent diffusional transformation increases with increasing or decreasing carbon percentage from 0.77%C and e for eutectoid steel is minimum. Similar is the behaviour for transformation finish time.

Pearlite formation is preceded by ferrite in case of hypoeutectoid steel and by cementite in hypereutectoid steel. Schematic TTT diagrams for eutectoid, hypoeutectoid and hyper eutectoid steel are shown in **Fig.4**, **Figs. 7(a)-(b)** and all of them together along with schematic Fe-Fe<sub>3</sub>C metastable equilibrium are shown in **Fig. 8**.

**Fig. 7(a) :Schematic TTT diagram for plain carbon hypoeutectoid steel**

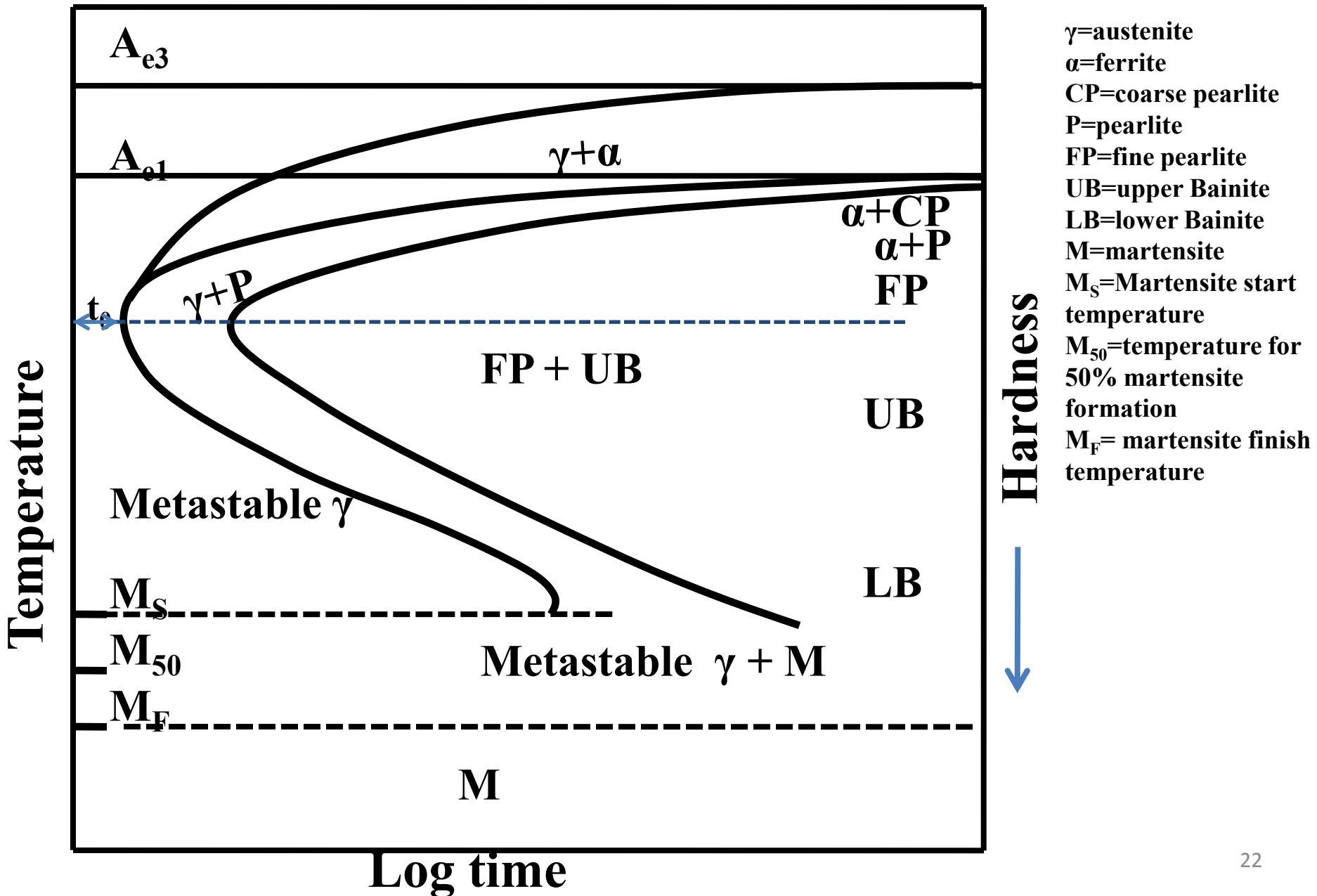


**Fig. 7(b): Schematic TTT diagram for plain carbon hypereutectoid steel**

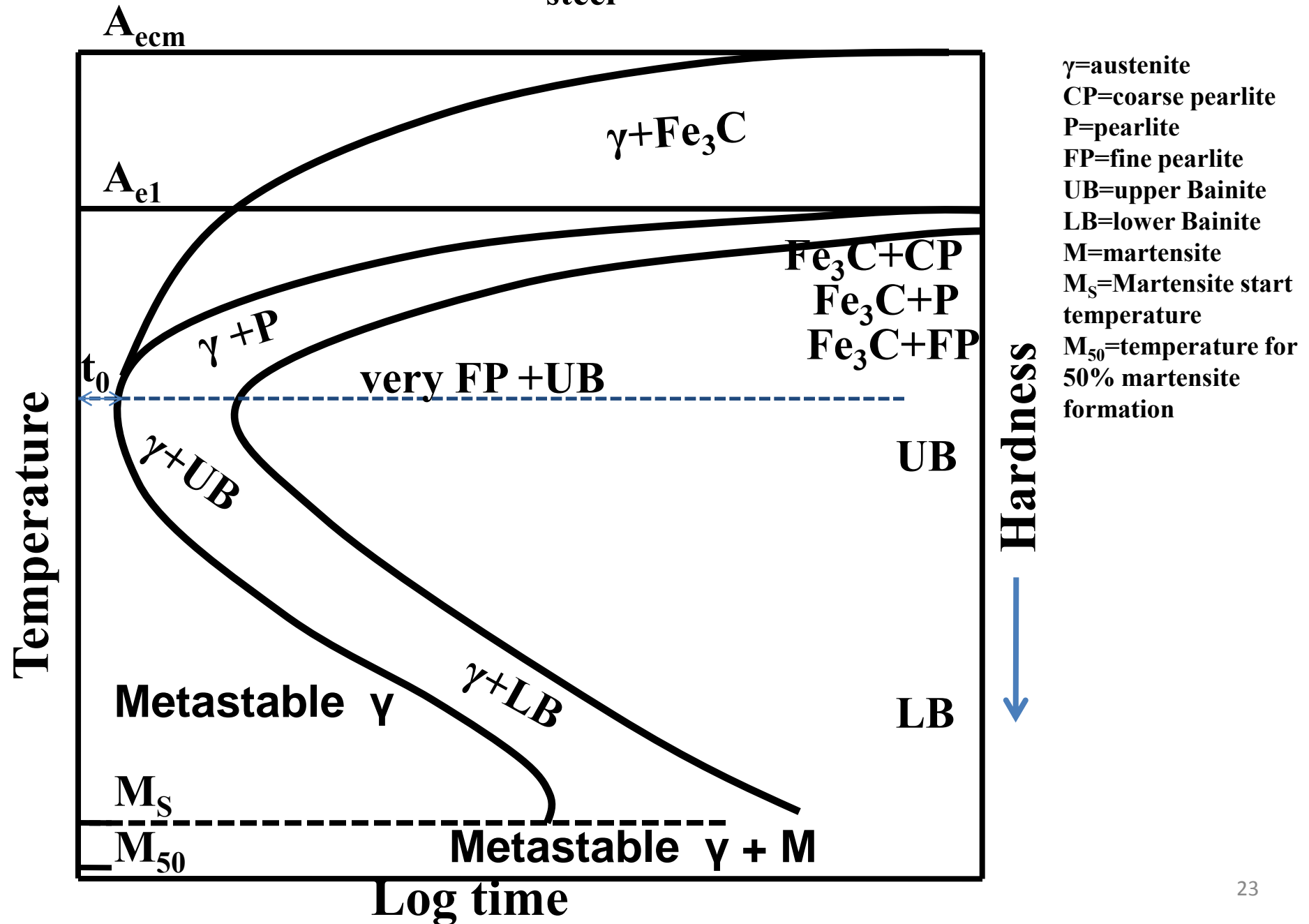


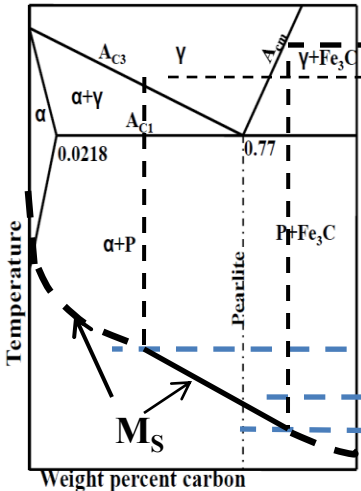
# Fig. 8: Schematic Fe-Fe<sub>3</sub>C metastable equilibrium diagram and TTT diagrams for plain carbon hypoeutectoid, eutectoid and hypereutectoid steels

$\gamma$ =austenite  
 $\alpha$ =ferrite  
 CP=coarse pearlite  
 pearlite

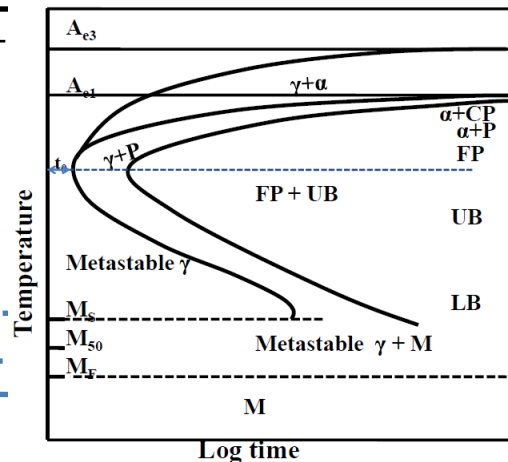
P=pearlite  
 FP=fine pearlite  
 UB=upper bainite  
 LB=lower bainite

M=martensite  
 M<sub>S</sub>=Martensite start temperature  
 M<sub>50</sub>=temperature for 50% martensite formation  
 M<sub>F</sub>= martensite finish temperature

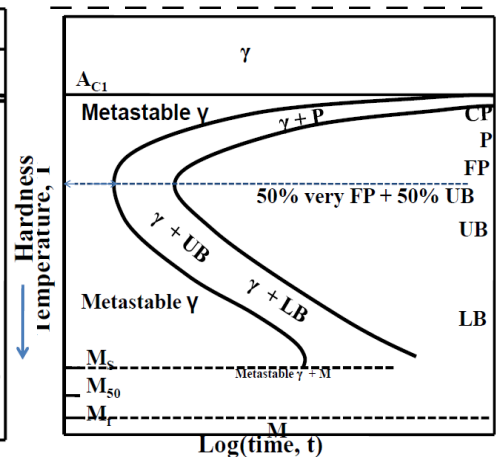
(a) Fe-Fe<sub>3</sub>C metastable phase diagram



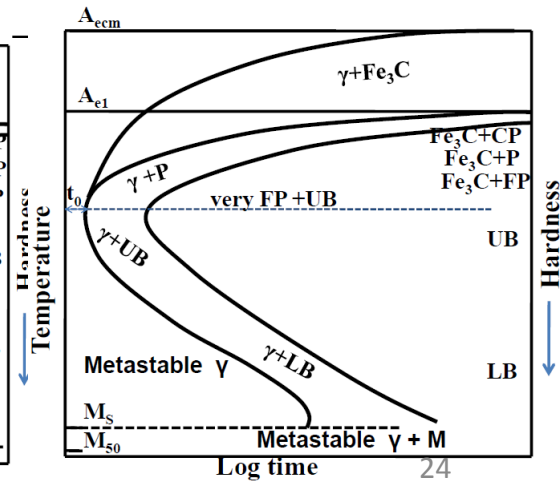
(b) TTT diagram for hypoeutectoid steel



(c) TTT diagram for eutectoid steel



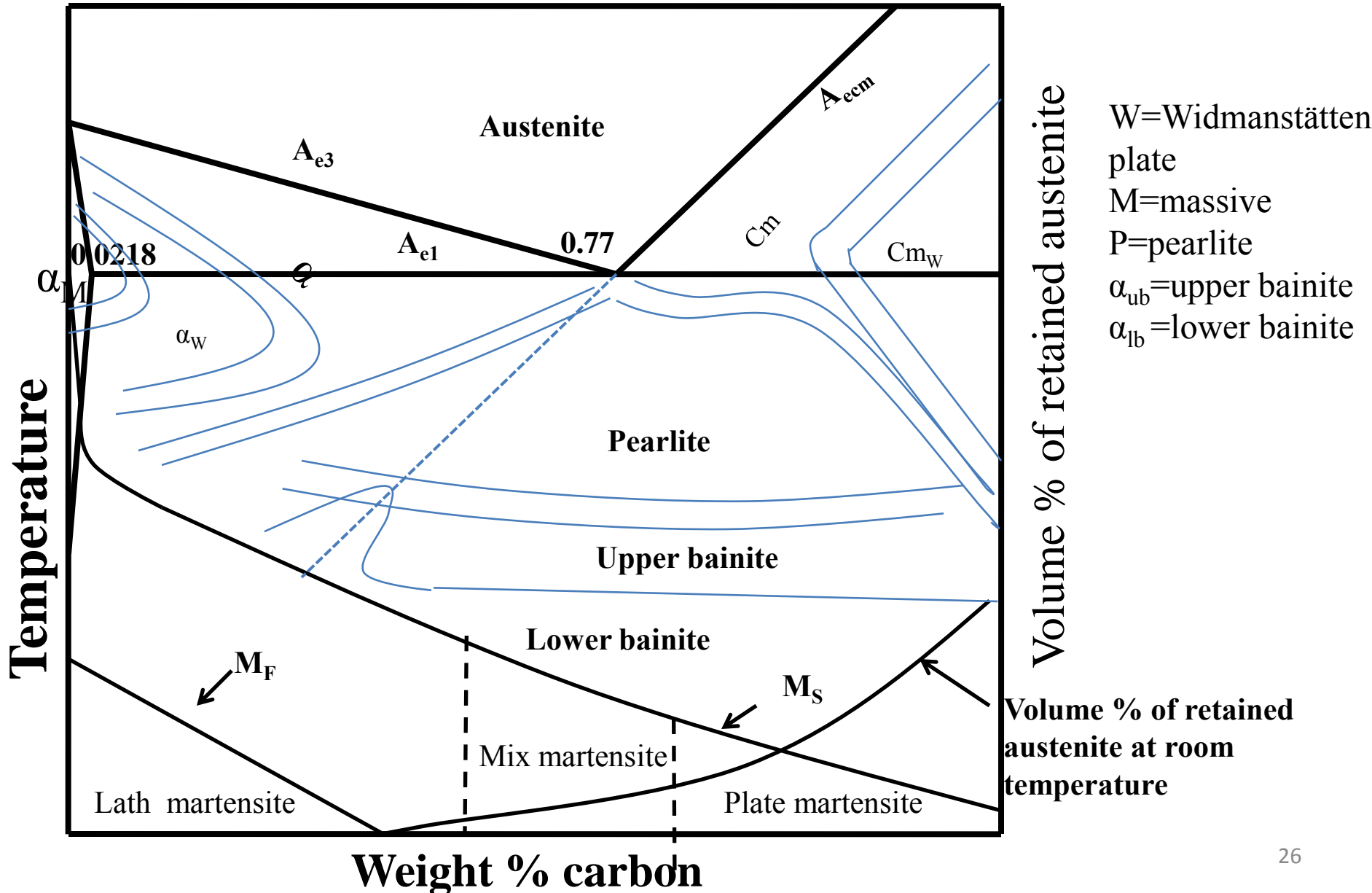
(d) TTT diagram for hypereutectoid steel



Under isothermal conditions for various compositions proeutectoid transformation has been summarised below (**Fig. 9**). In hypoeutectoid steel the observable ferrite morphologies are grain boundary allotriomorph ( $\alpha$ )(**Fig.11(a)-(d)**), Widmanstätten plate ( $\alpha_W$ )(**Figs. 12-16**), and massive ( $\alpha_M$ ) ferrite (**Fig.11(f)**).

Grain boundary allotriomorphs form at close to  $A_{e3}$  temperature or extension of  $A_{ecm}$  line at low undercooling. Widmanstätten plates form at higher undercooling but mainly below  $A_{e1}$ . There are overlap regions where both allotriomorphs and Widmanstätten plates are observed. Equiaxed ferrite forms at lower carbon composition less than 0.29 wt%C.

Fig 9: Temperature versus composition in which various morphologies are dominant at late reaction time under isothermal condition



There are overlapping regions where both equiaxed ferrite and Widmanstätten plates were observed. However at very low carbon percentage massive ferrite forms. The reconstructive and displacive mechanisms of various phase formation is shown in **Fig. 10**.

In hypereutectoid steel both grain boundary allotriomorph and Widmanstätten plates were observed. Massive morphology was not observed in hypereutectoid steel. Grain boundary allotriomorphs were observed mainly close to  $A_{ecm}$  or close to extension of  $A_{e3}$  line but Widmanstätten plates were observed at wider temperature range than that of hypoeutectoid steel. In hypereutectoid steel there are overlapping regions of grain boundary allotriomorph and Widmanstätten cementite.

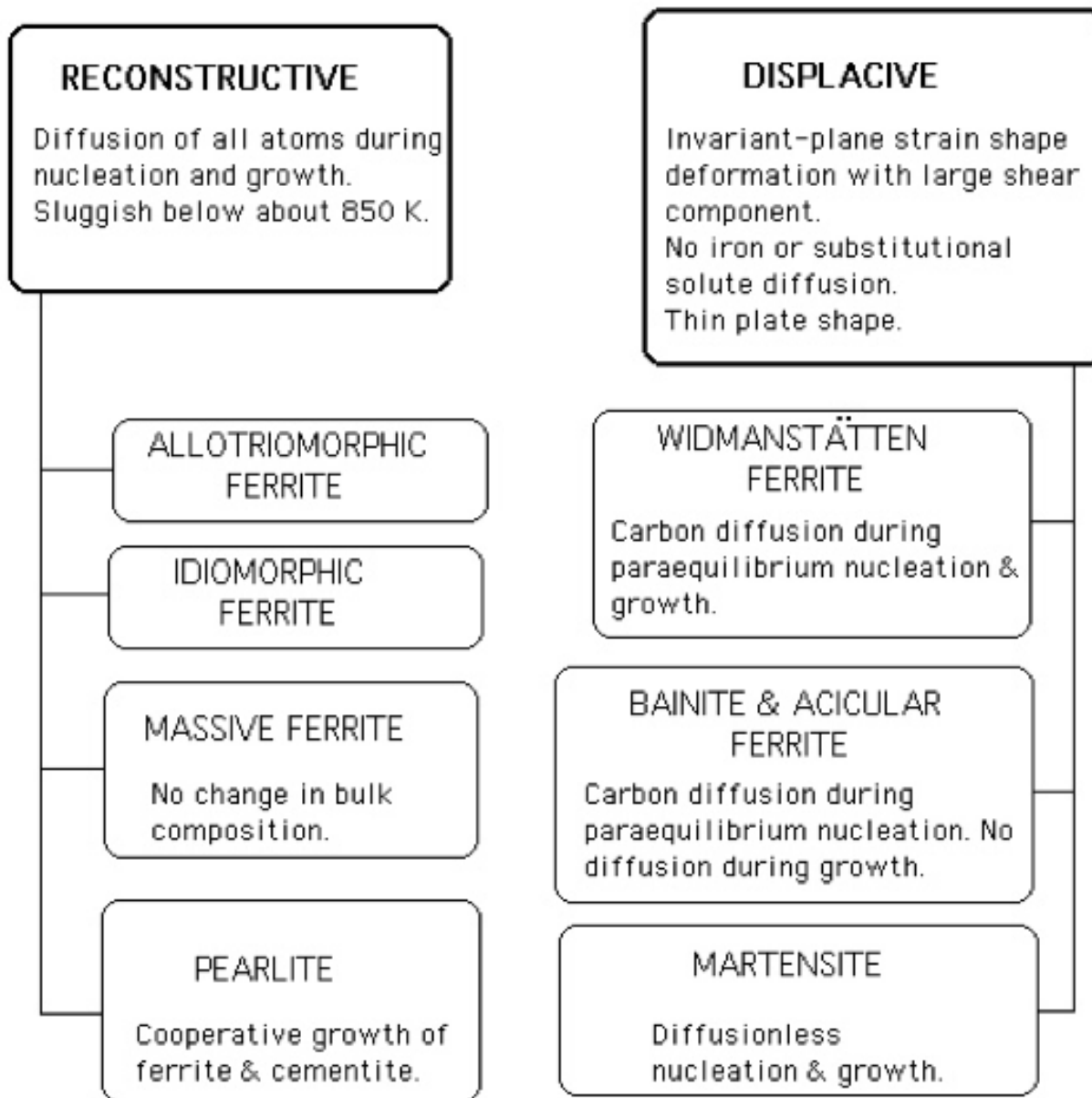


Fig. 10: The reconstructive and displacive mechanisms.

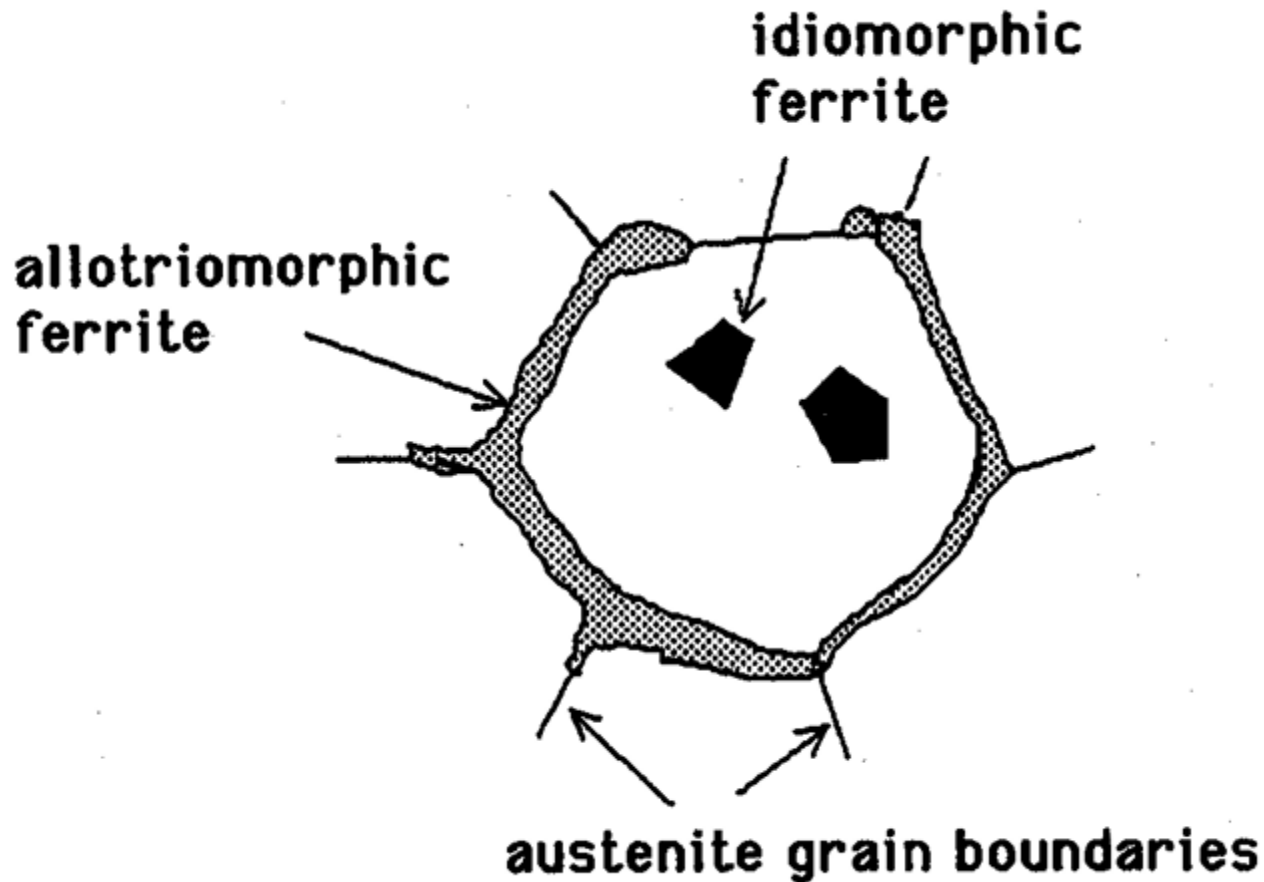


Fig. 11(a): schematic diagram of grain boundary allotriomorphic ferrite, and intragranular idiomorphic ferrite.

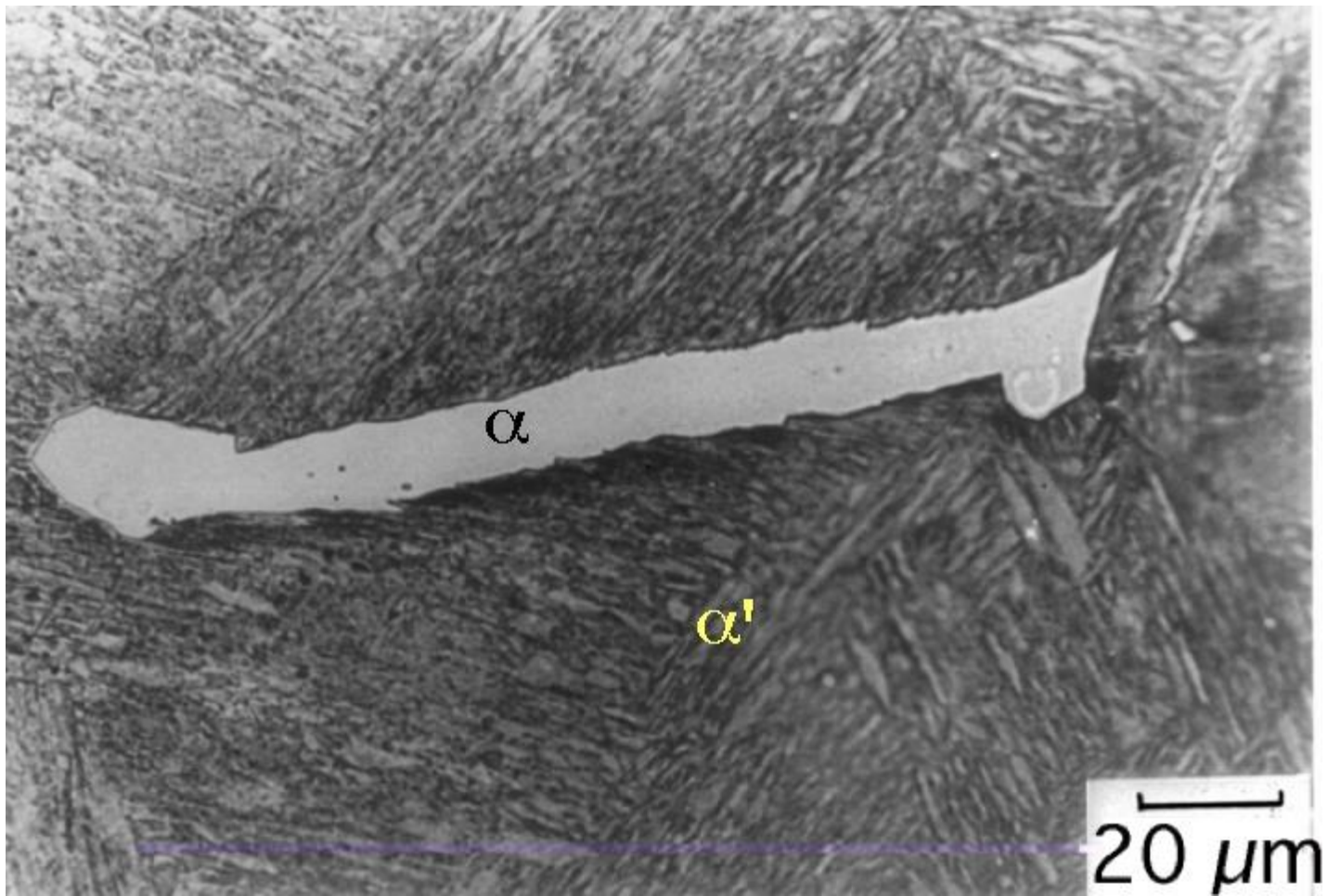


Fig.11(b): An allotriomorph of ferrite in a sample which is partially transformed into  $\alpha$  and then quenched so that the remaining  $\gamma$  undergoes martensitic transformation. The allotriomorph grows rapidly along the austenite grain boundary (which is an easy diffusion path) but thickens more slowly.

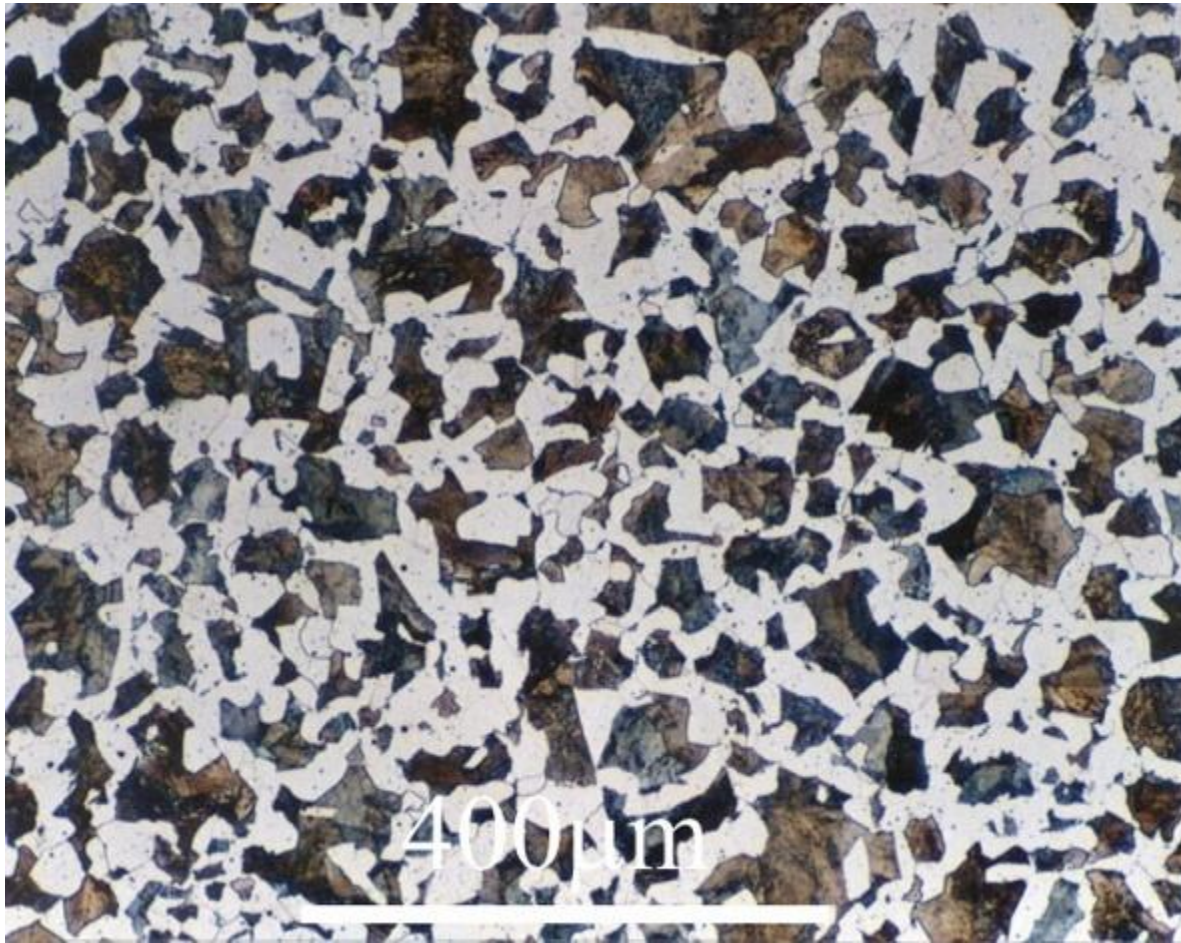


Fig. 11(c): Allotriomorphic ferrite in a Fe-0.4C steel which is slowly cooled; the remaining dark-etching microstructure is fine pearlite. Note that although some  $\alpha$ -particles might be identified as idiomorphs, they could represent sections of allotriomorphs. Micrograph courtesy of the *DoITPOMS* project.

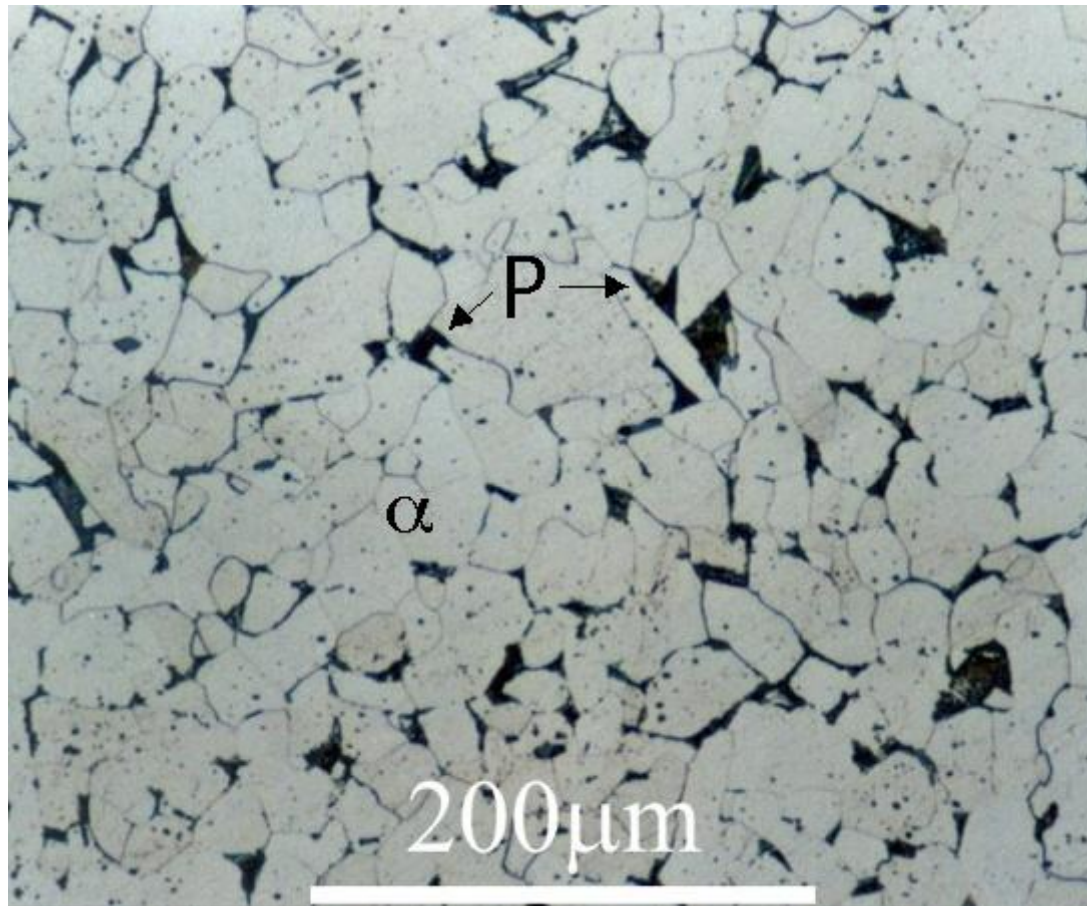


Fig. 11(d): The allotriomorphs have in this slowly cooled low-carbon steel have consumed most of the austenite before the remainder transforms into a small amount of pearlite. Micrograph courtesy of the DoItPoms project. The shape of the ferrite is now determined by the impingement of particles which grow from different nucleation sites.

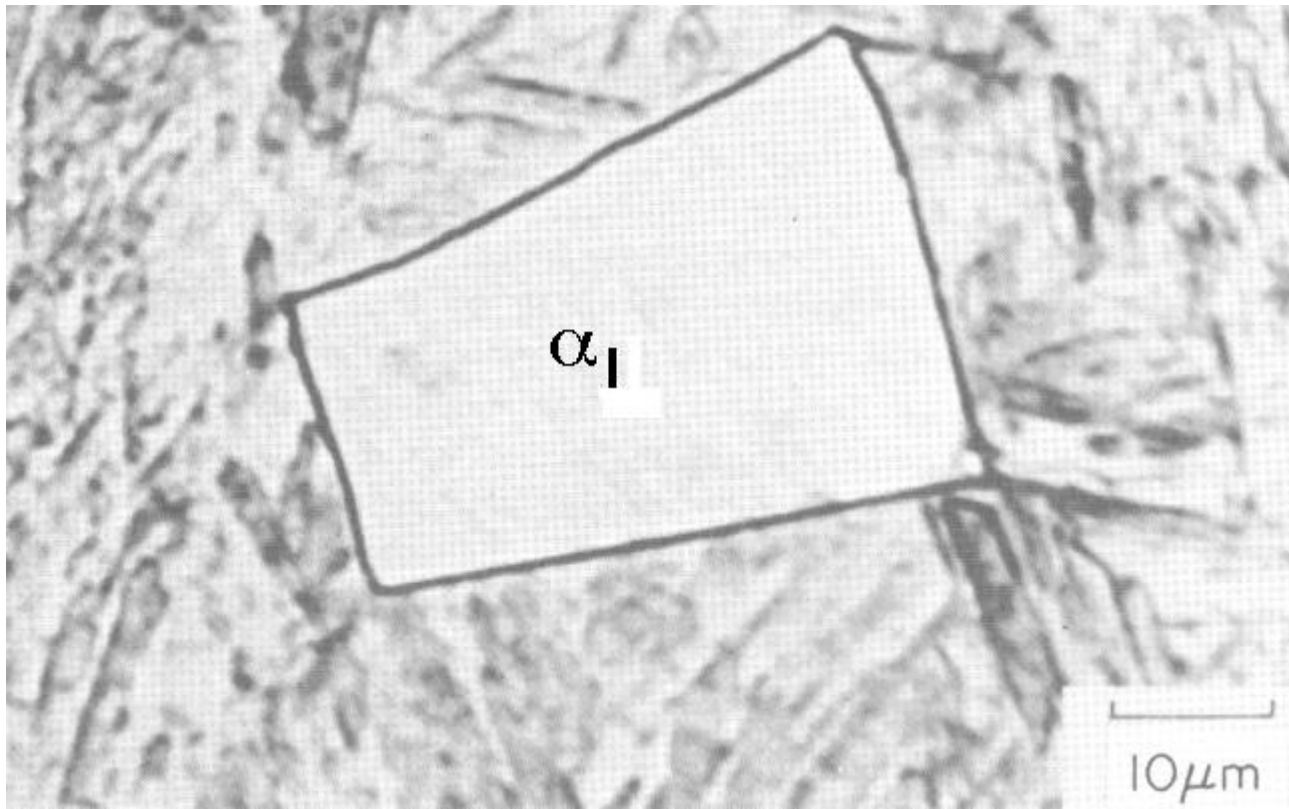


Fig. 11(e): An idiomorph of ferrite in a sample which is partially transformed into  $\alpha$  and then quenched so that the remaining  $\gamma$  undergoes martensitic transformation. The idiomorph is crystallographically faceted.

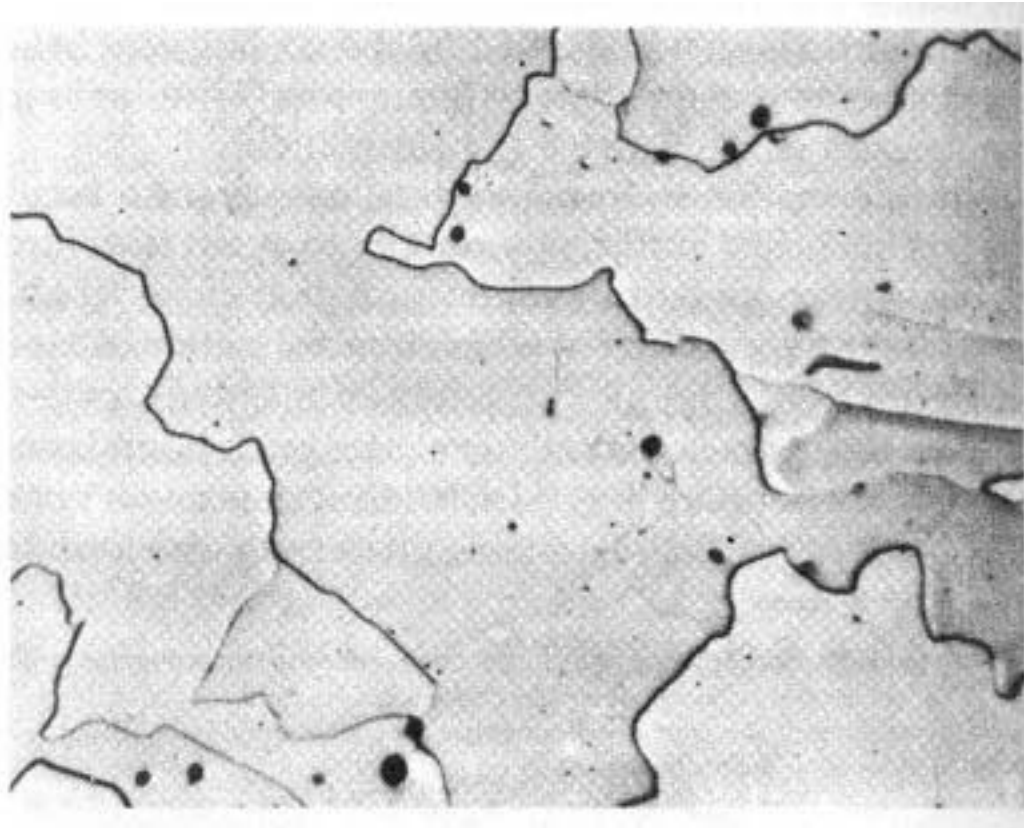


Fig. 11(f): Massive ferrite ( $\alpha_m$ ) in Fe-0.002 wt%C alloy quenched into ice brine from 1000°C. Courtesy of *T. B. Massalski*

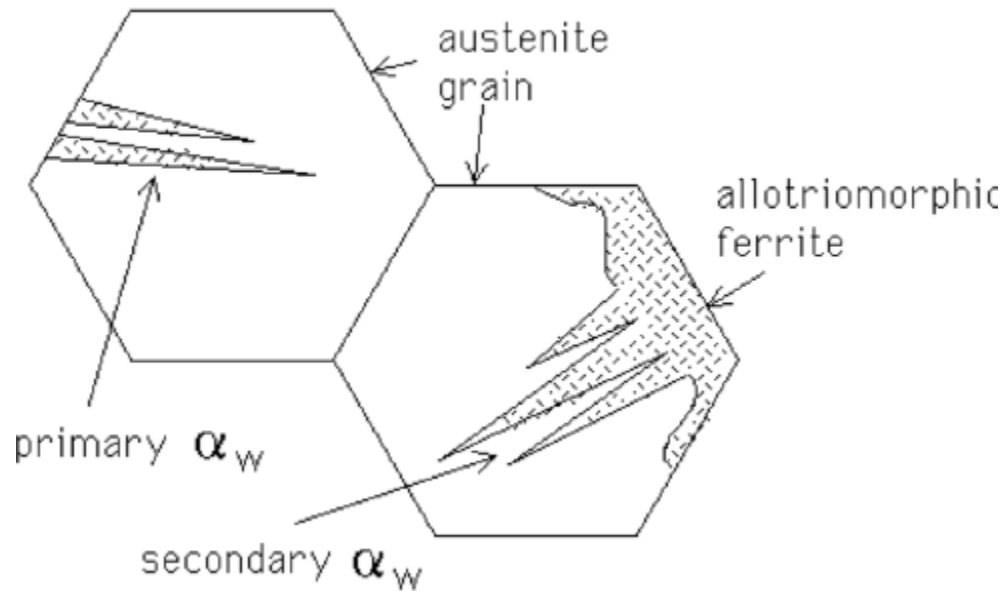


Fig. 12(a): Schematic illustration of primary Widmanstätten ferrite which originates directly from the austenite grain surfaces, and secondary  $\alpha_w$  which grows from allotriomorphs.

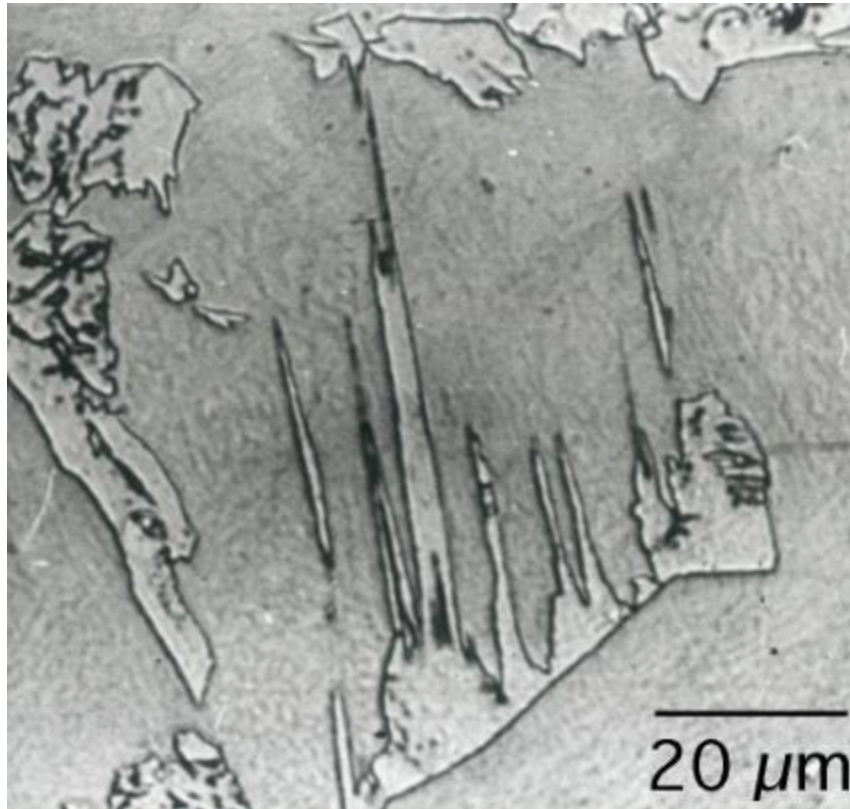


Fig. 12(b): Optical micrographs showing white-etching (nital) wedge-shaped Widmanstätten ferrite plates in a matrix quenched to martensite. The plates are coarse (notice the scale) and etch cleanly because they contain very little substructure.

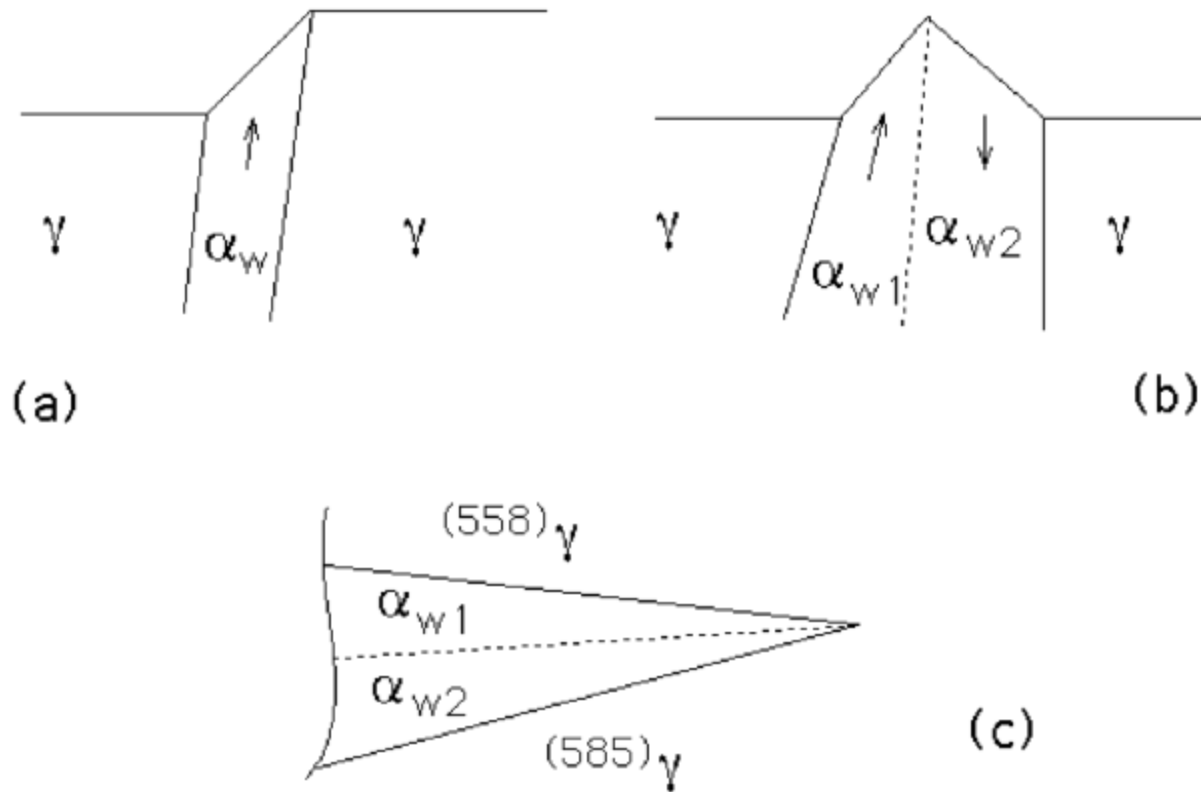


Fig. 13: The simultaneous growth of two self-accommodating plates and the consequential tent-like surface relief.

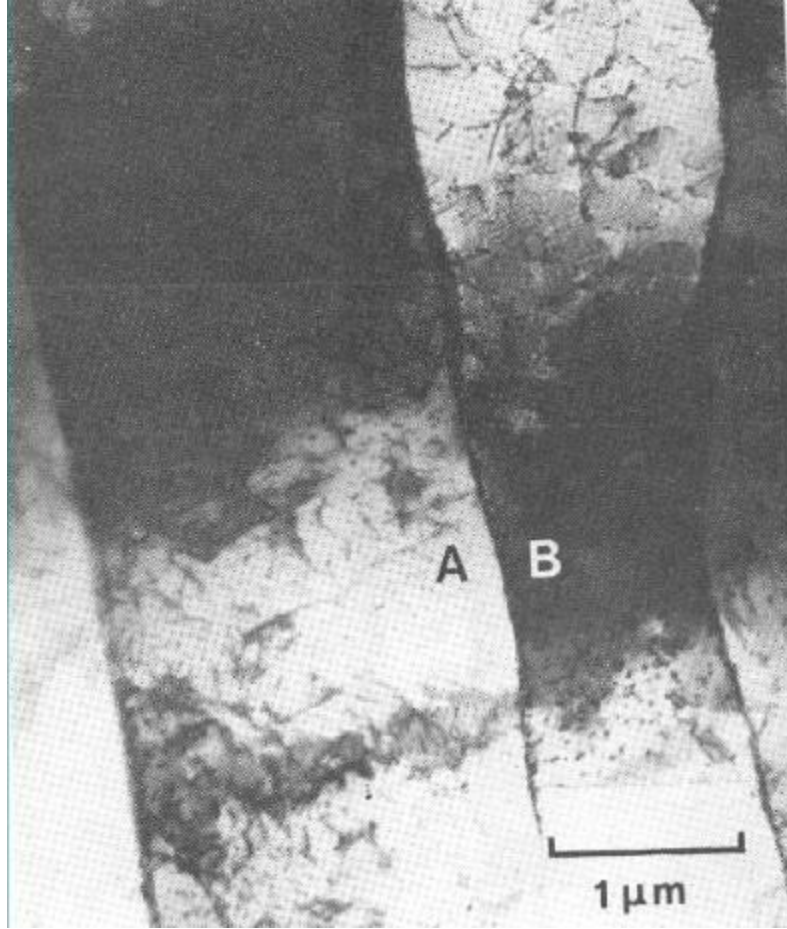


Fig.14: Transmission electron micrograph of what optically appears to be single plate, but is in fact two mutually accommodating plates with a low-angle grain boundary separating them. Fe-0.41C alloy, austenitised at 1200 C for 6 hrs, isothermally transformed at 700 C for 2 min and water quenched.

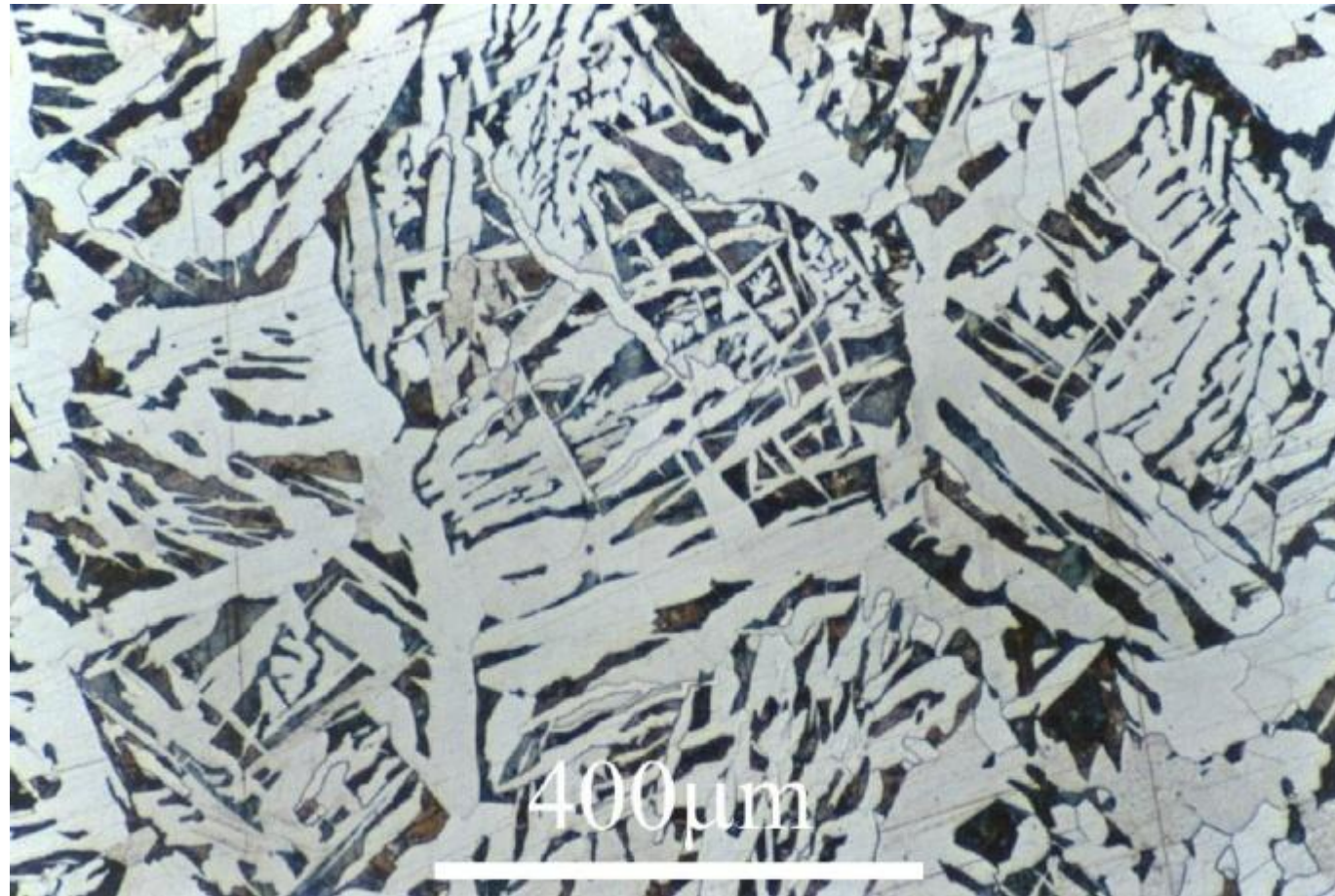


Fig. 15: Mixture of allotriomorphic ferrite, Widmanstätten ferrite and pearlite. Micrograph courtesy of *DOITPOMS project*.

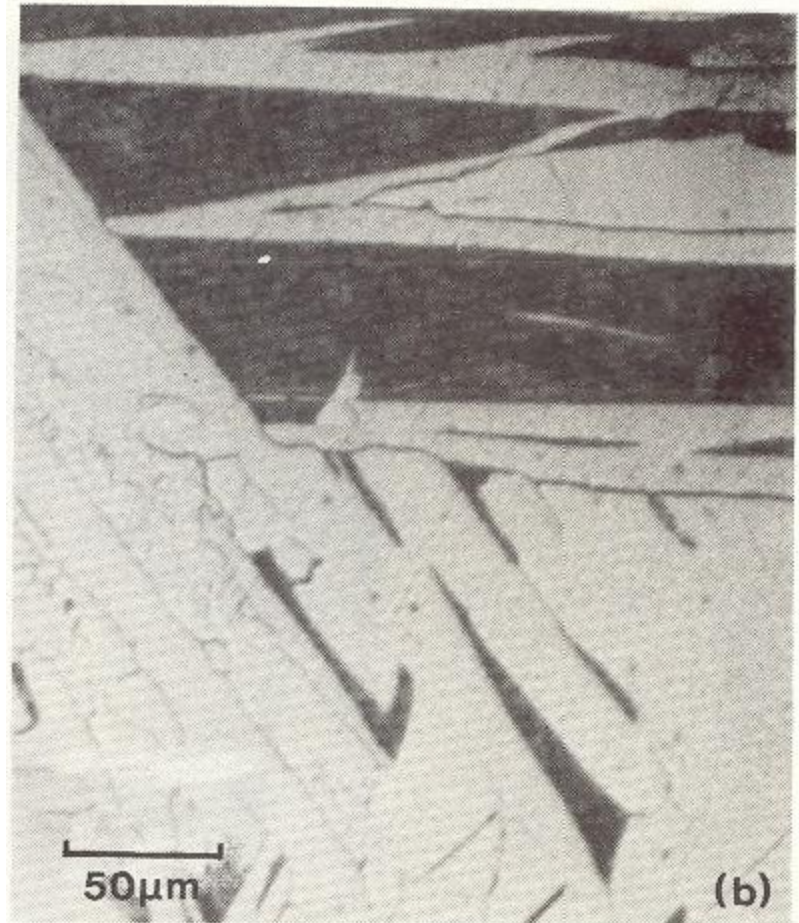
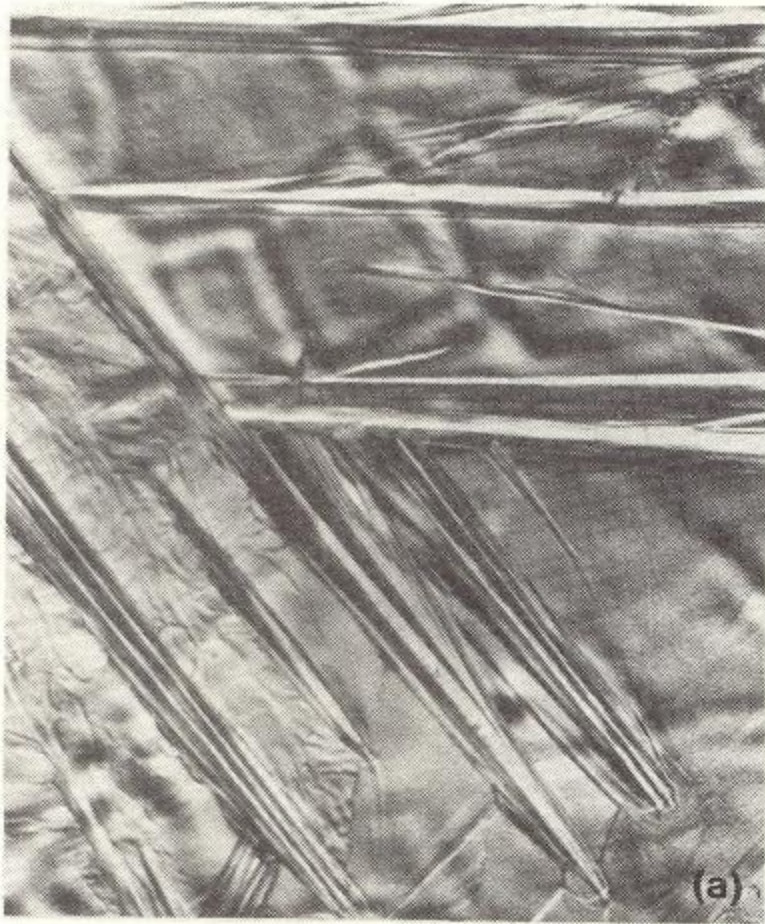


Fig. 16 (a) Surface relief of Widmanstätten ferrite Fe-0.41C alloy, austenitised at 1200 C for 6 hrs, isothermally transformed at 700 C for 30 min and water quenched, (b) same field after light polishing and etching with nital.

For eutectoid steel bainitic transformation occurs at 550 to 250°C. At higher temperature it is upper bainite and at lower temperature it is lower bainite. As C increases the austenite to ferrite decomposition becomes increasingly difficult. As bainitic transformation proceeds by the nucleation of ferrite, therefore bainitic transformation range moves to higher timing and lower temperature. With increasing percentage of carbon the amount of carbide in interlath region in upper bainite increases and carbides become continuous phase. However at lower percentage of carbon they are discrete particles and amount of carbide will be less in both type of bainites. For start and finish temperatures for both types of bainites go down significantly with increasing amount of carbon (**Figs. 8-9**). However increasing carbon makes it easier to form lower bainite.

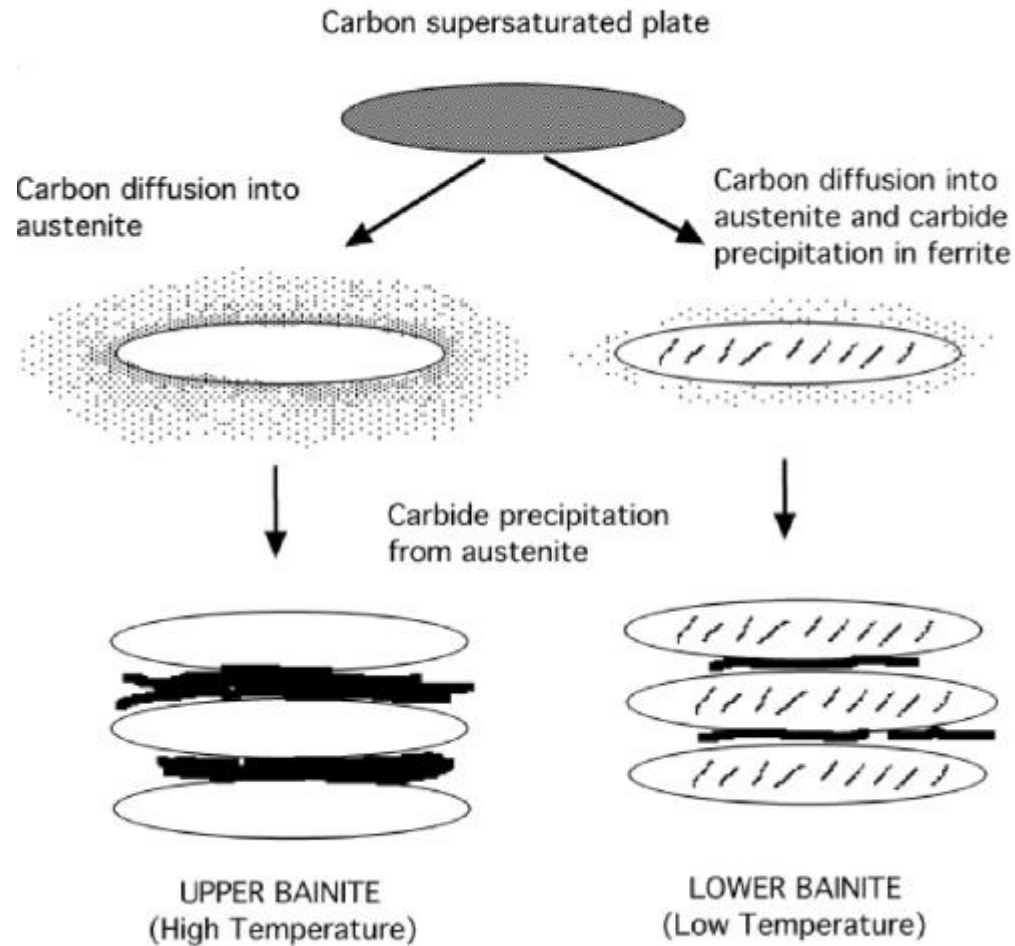


Fig 17: Summary of the mechanism of the bainite reaction.

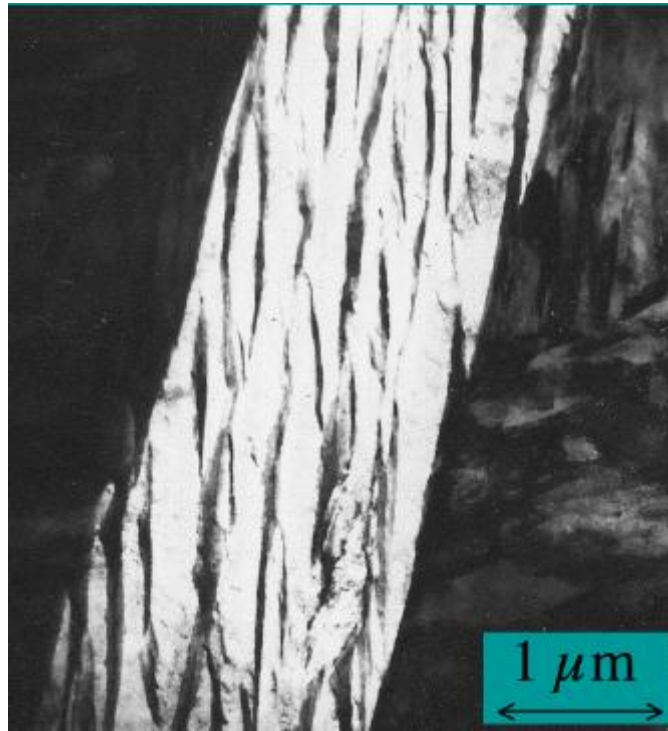


Fig. 18: Upper bainite; the phase between the platelets of bainitic ferrite is usually cementite.

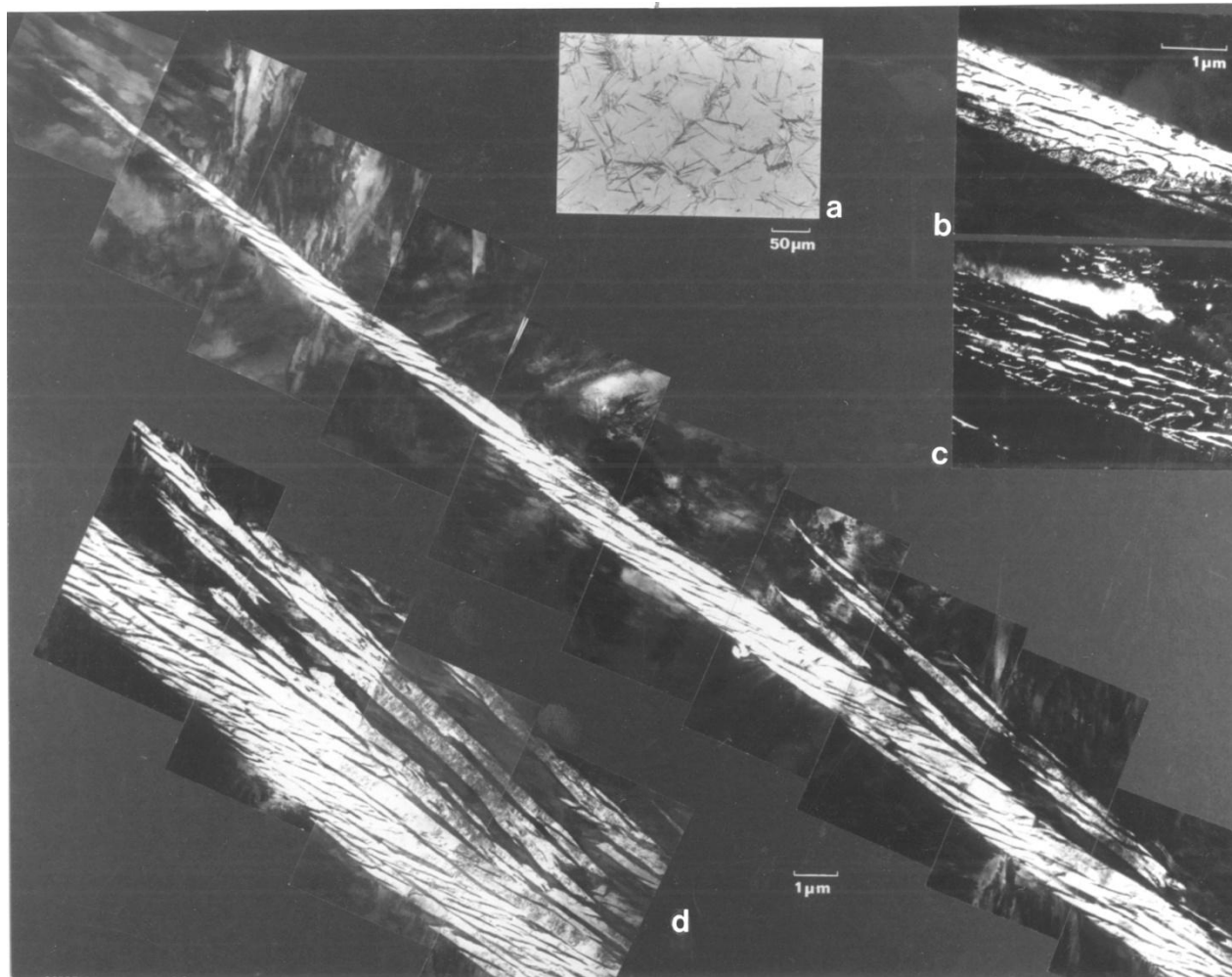


Fig. 19: Transmission electron micrograph of a sheaf of upper bainite in a partially transformed Fe-0.43C-2Si-3Mn wt% alloy (a) optical micrograph, (b, c) bright field and corresponding dark field image of retained austenite between the sub units, (d) montage showing the structure of the sheaf.

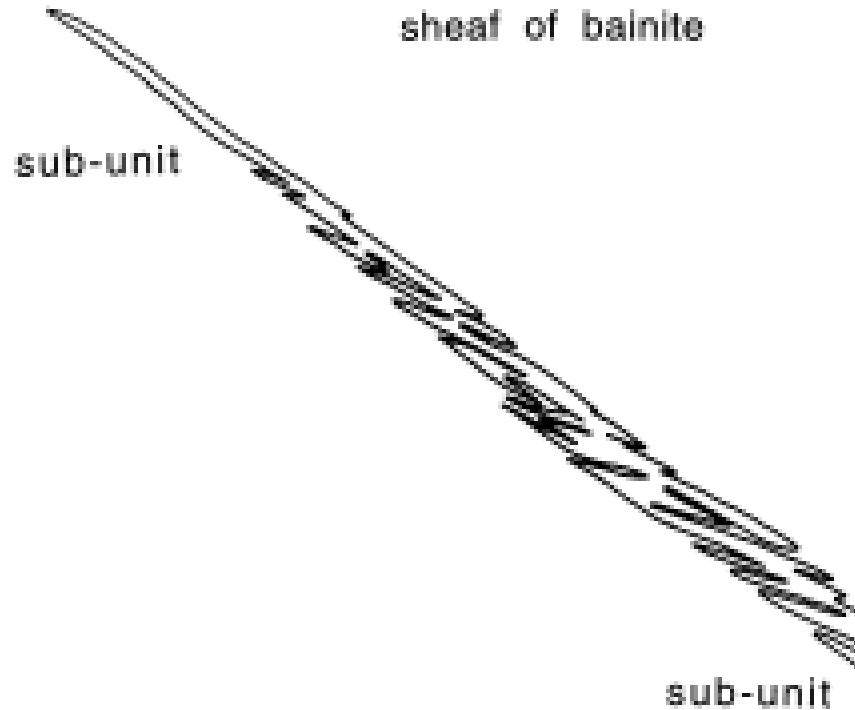


Fig. 20 : Corresponding outline of the sub-units near the sheaf tip region of Fig. 19

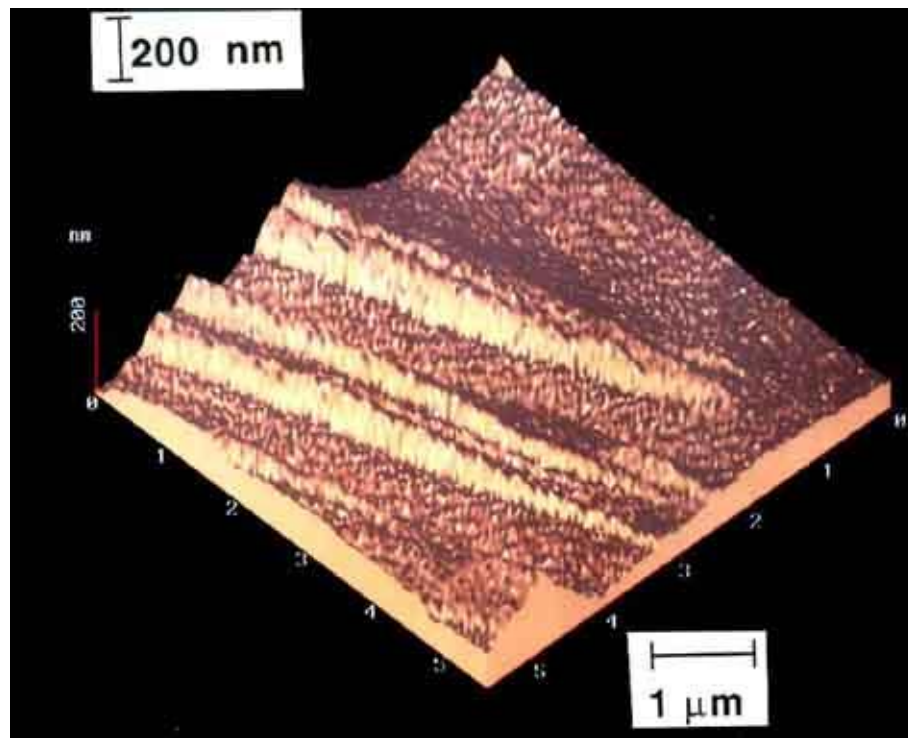


Fig. 21 : AFM image showing surface relief due to individual bainite subunit which all belong to tip of sheaf. The surface relief is associated with upper bainite (without any carbide ) formed at 350°C for 2000 s in an Fe-0.24C-2.18Si-2.32Mn-1.05Ni (wt% ) alloy austenitised at 1200°C for 120 s alloy. Both austenitisation and isothermal transformation were performed in vacuum. The microstructure contains only bainitic ferrite and retained austenite. The measured shear strain is  $0.26 \pm 0.02$ .

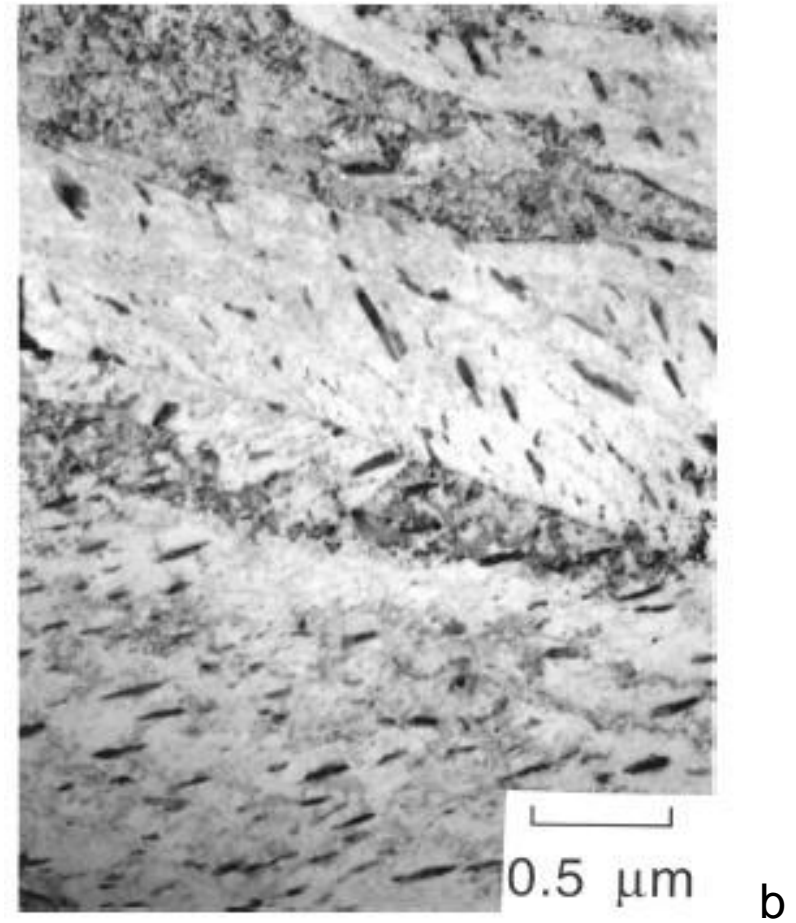
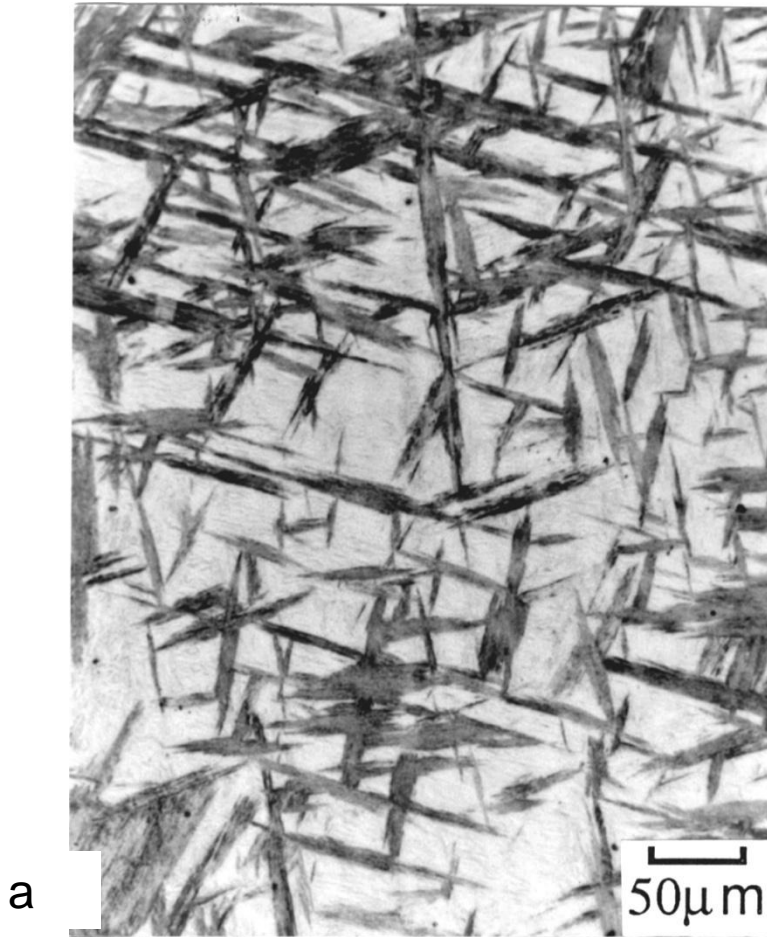


Fig. 22: Optical micrograph illustrating the sheaves of lower bainite in a partially transformed (395C), Fe-0.3C-4Cr wt% ally. The light etching matrix phase is martensite. (b) Corresponding transmission electron micrograph illustrating subunits of lower bainite.

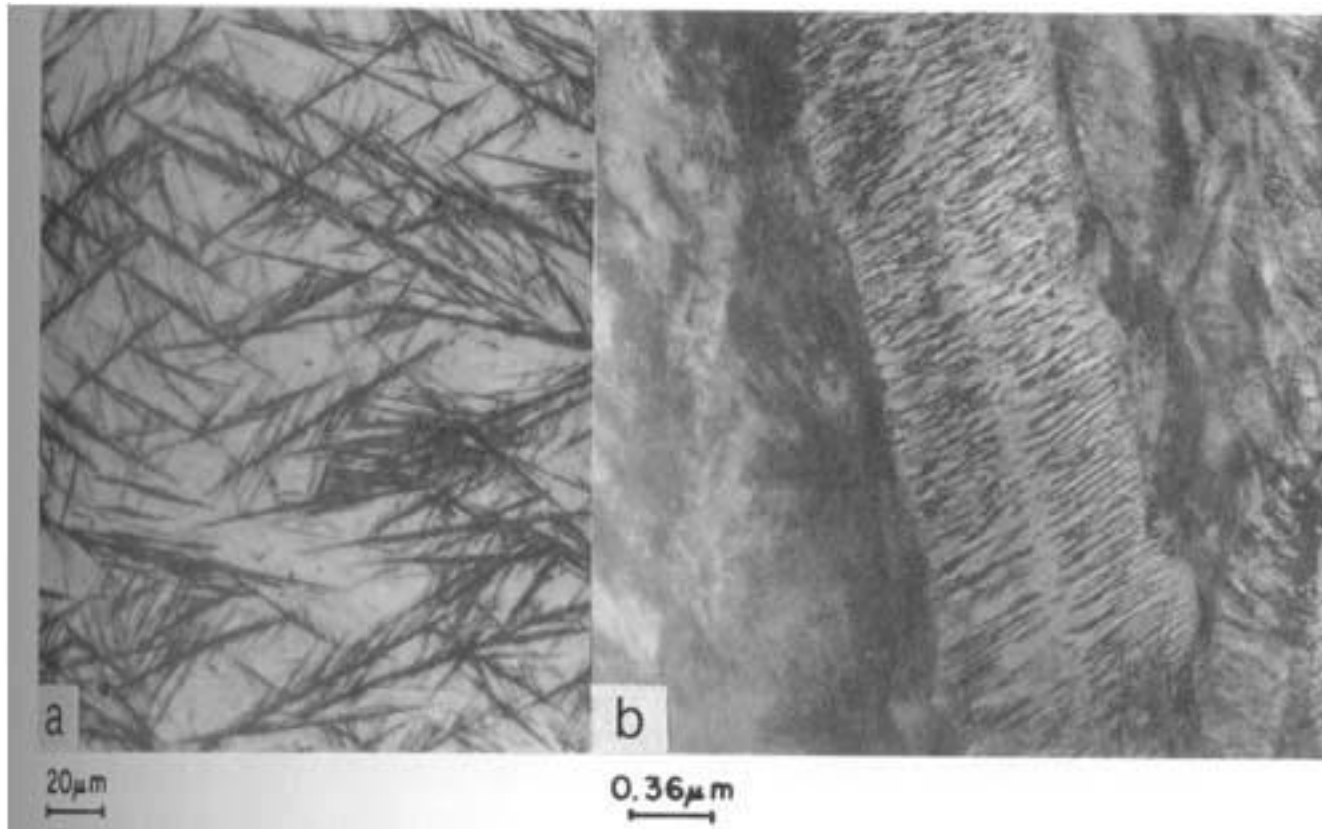
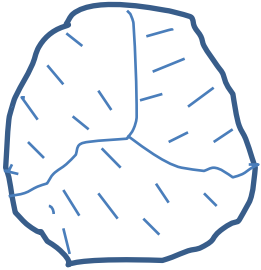
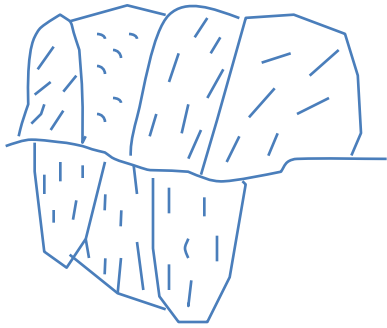


Fig. 23 : (a) Optical micrograph showing thin and spiny lower bainite formed at 190°C for 5 hours in an Fe-1.1 wt% C steel. (b) Transmission electron micrograph showing lower bainite midrib in same steel. Courtesy of *M. Oka*

Fig. 24 : Schematic illustration of various other morphologies: (a) Nodular bainite, (b) columnar bainite along a prior austenite boundary, (c) grain boundary allotriomorphic bainite, (d) inverse bainite



a



b



c



d

Within the bainitic transformation temperature range, austenite of large grain size with high inclusion density promotes acicular ferrite formation under isothermal transformation condition. The morphology is shown schematically (**Figs. 25-27** )

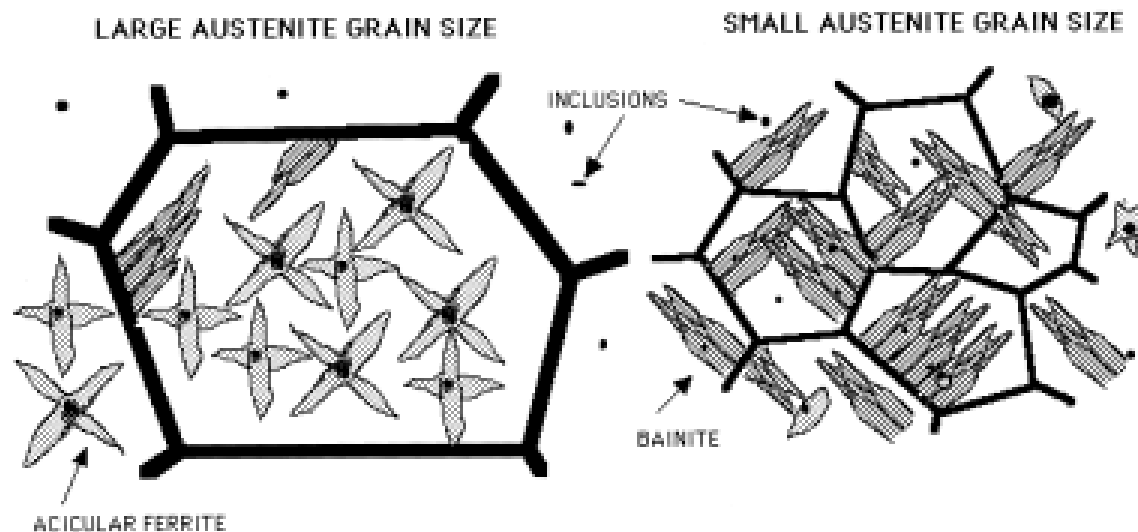


Fig. 25 : shows the morphology and nucleation site of acicular ferrite.

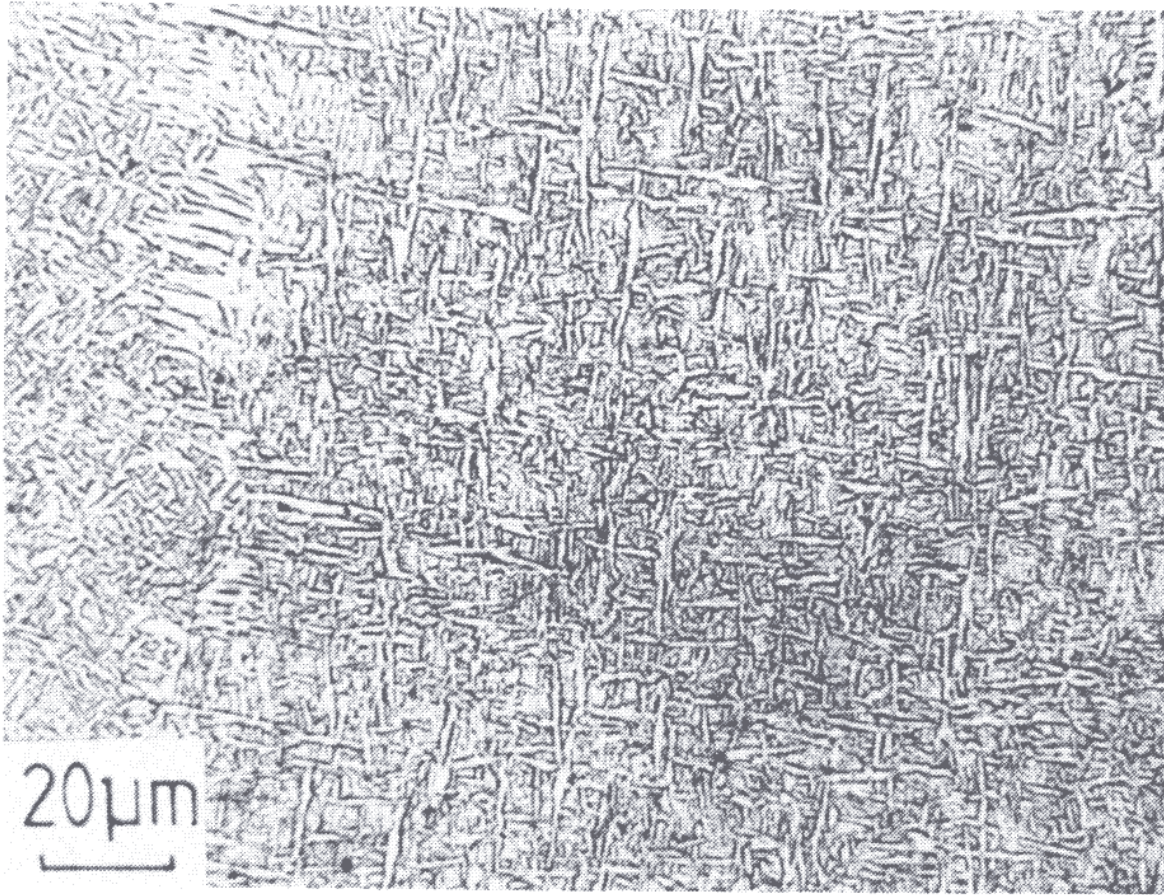


Fig . 26: Acicular ferrite

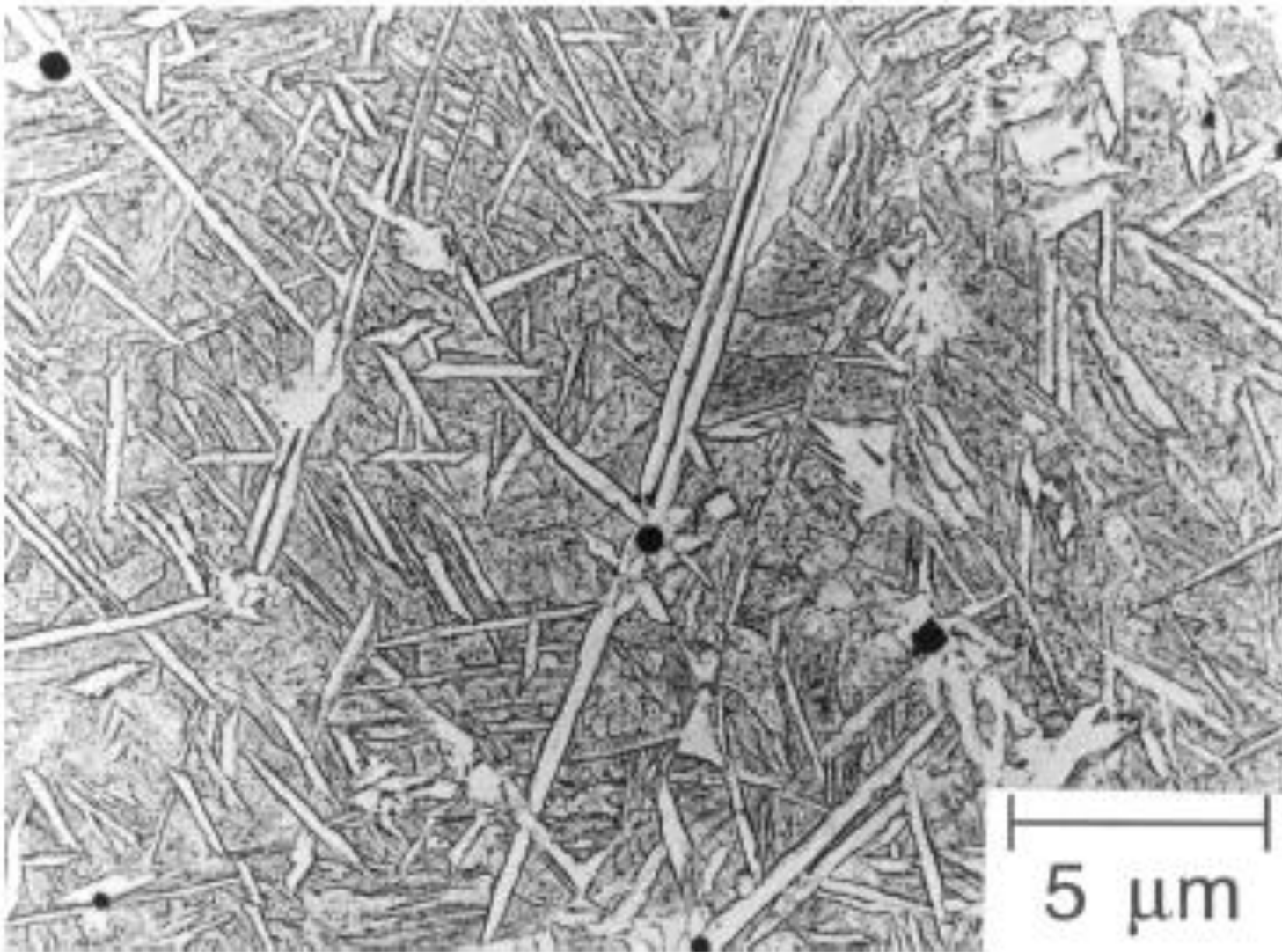


Fig. 27: Replica transmission electron micrograph of acicular ferrite plates in steel weld. Courtesy of *Barritte*.

For eutectoid steel martensite forms at around 230°C. From 230°C to room temperature martensite and retained austenite are seen. At room temperature about 6% retained austenite can be there along with martensite in eutectoid steel. At lower carbon percentage  $M_S$  temperature goes up and at higher percentage  $M_S$  temperature goes down (**Fig. 4, Figs. 7-8, Fig. 28**). Below 0.4 %C there is no retained austenite at room but retained austenite can go up to more than 30% if carbon percentage is more than 1.2%. Morphology of martensite also changes from lath at low percentage of carbon to plate at higher percentage of carbon. Plate formation start at around 0.6 % C. Therefore below 0.6 % carbon only lath martensite can be seen, mixed morphologies are observed between 0.6%C to 1%C and above 1% it is 100% plate martensite (**Figs. 29-39**).

Fig. 28: Effect of carbon on  $M_S$ ,  $M_F$  temperatures and retained austenite in plain carbon steel

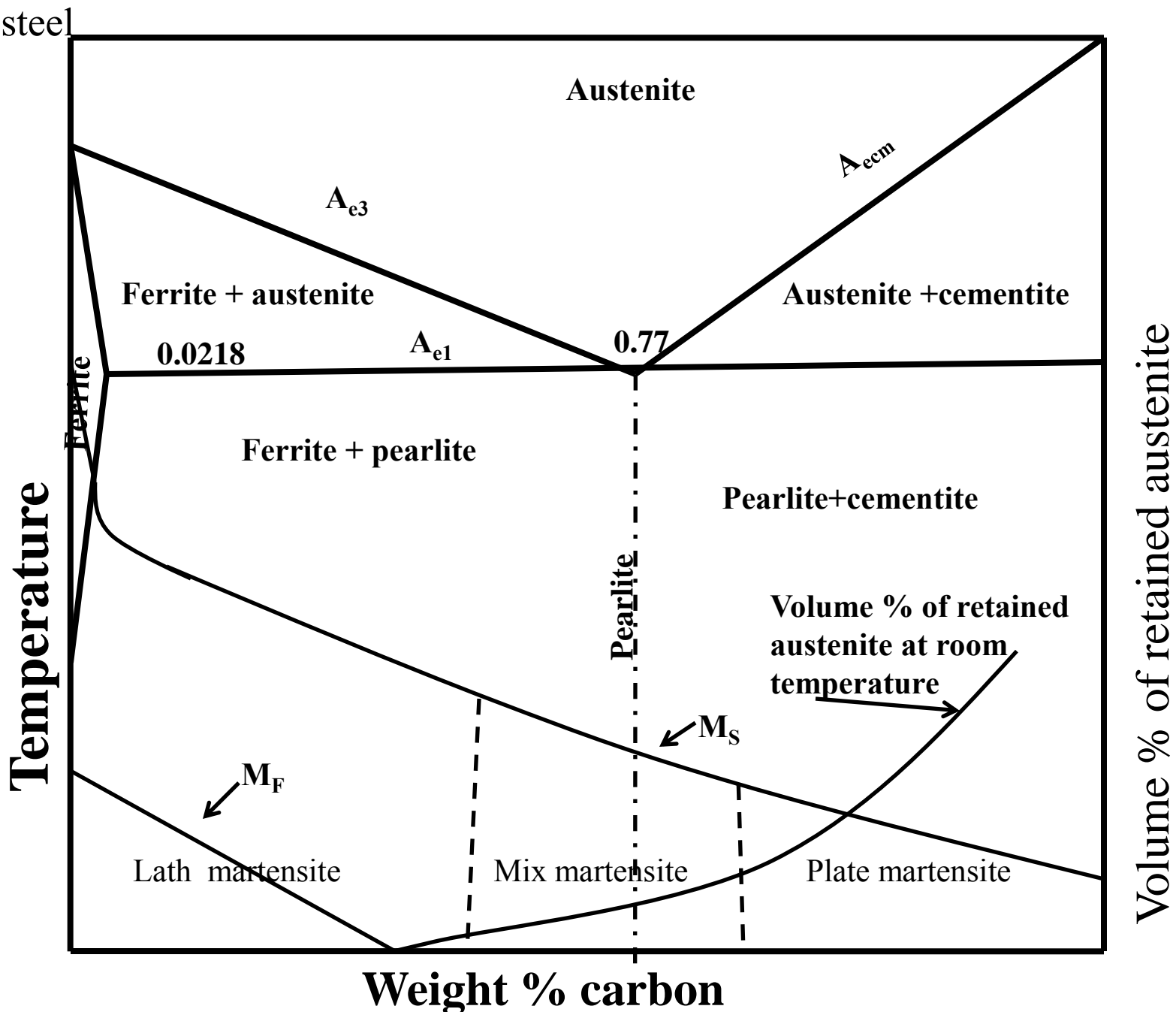


Fig. 29: Morphology and crystallography of (bcc or bct) martensite in ferrous alloys

Courtesy of  
*T. Maki*

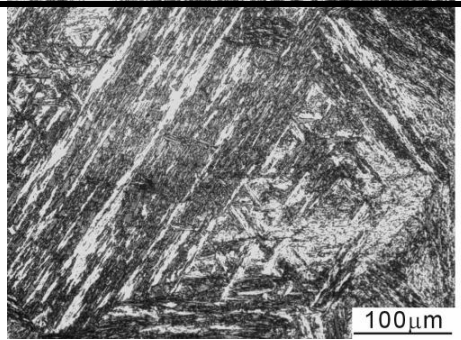
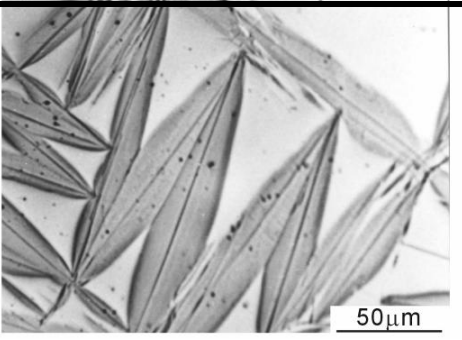
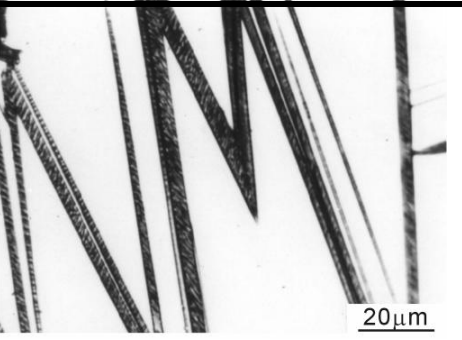
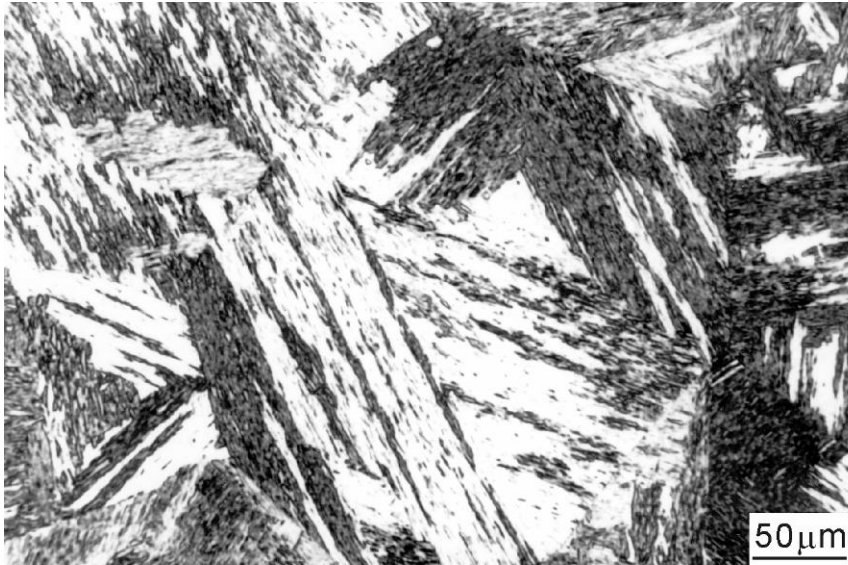
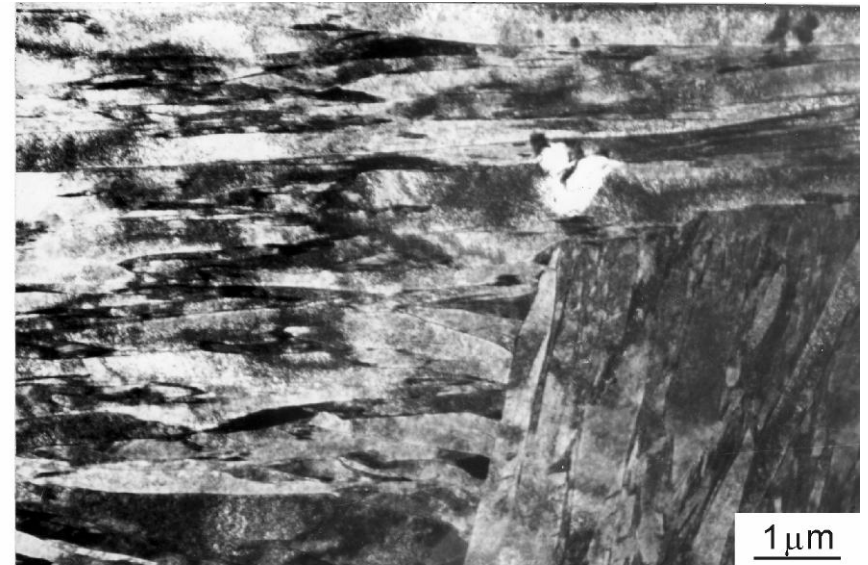
	Lath (Fe-9%Ni-0.15%C)	Lenticular (Fe-29%Ni-0.26%C)	Thin plate (Fe-31%Ni-0.23%C)
			
Substructure	Dislocation	Dislocation Twin (midrib)	Twin
Habit plane	$\{111\}_A$ $\{557\}_A$	$\{259\}_A$ $\{3\ 10\ 15\}_A$	$\{3\ 10\ 15\}_A$
O.R.	K-S	N-W G-T	G-T
Ms	high ←		→ low

Fig. 30: Lath martensite



Optical micrograph



TEM micrograph

(Fe-0.2C)

Courtesy of  
*T. Maki*

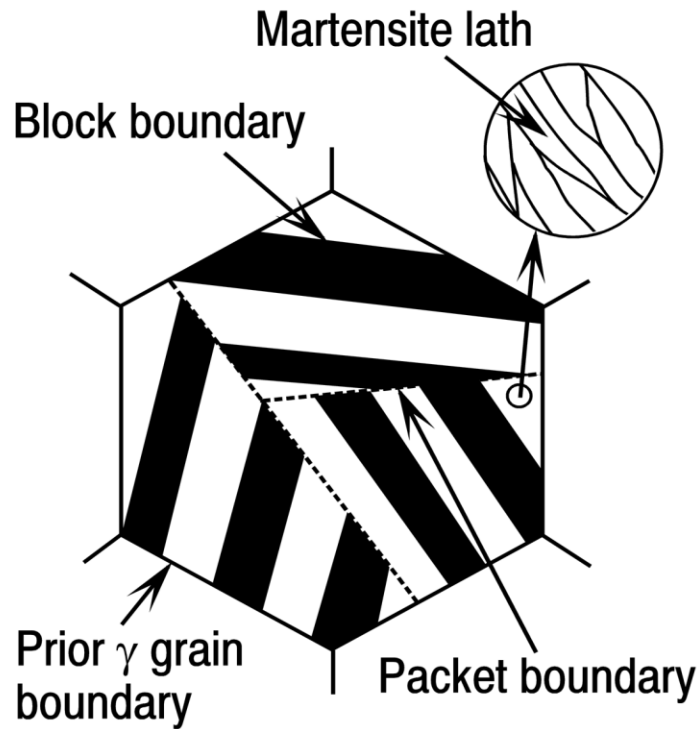


Fig. 31: effect of carbon on martensite lath size

Packet: a group of laths with the same habit plane ( $\sim\{111\}_\gamma$ )

Block : a group of laths with the same orientation (the same K-S variant)

Carbon Content ( wt% )				
0.1 ~ 0.2%	0.3%	0.4%	0.6%	0.8%

(T. Maki , K. Tsuzaki, I. Tamura: Trans. ISIJ, 20(1980), 207.)

# Lenticular martensite (Optical micrograph)

Courtesy of  
*T. Maki*

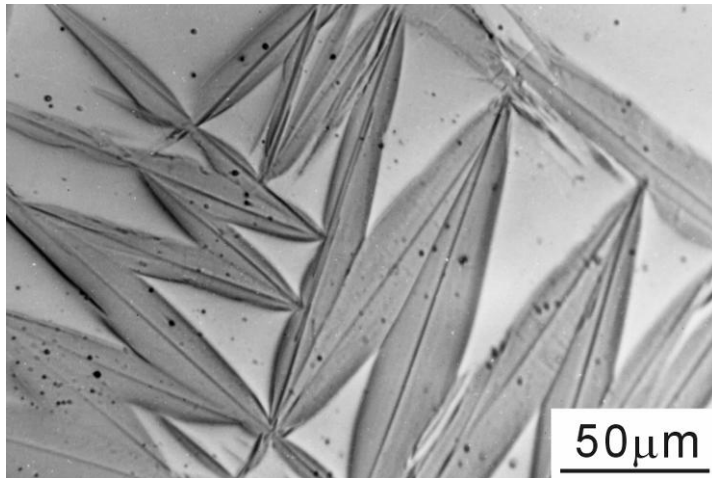


Fig.32: Fe-29%Ni-0.26%C  
( $M_s=203\text{K}$ )

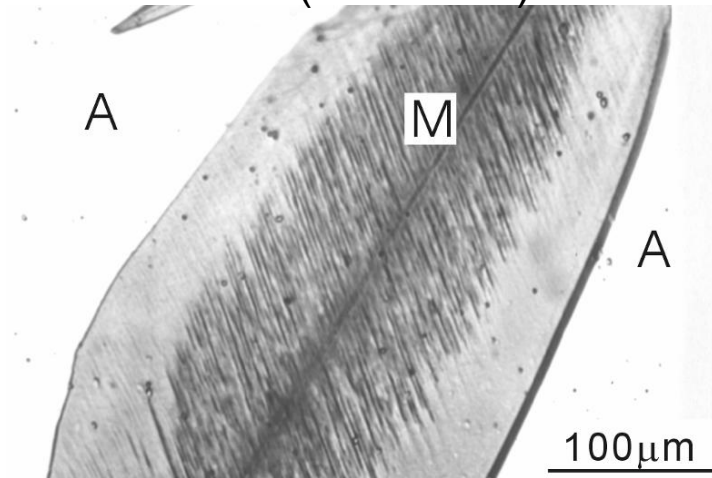


Fig. 33: Fe-31%Ni-0.28%C  
( $M_s=192\text{K}$ )

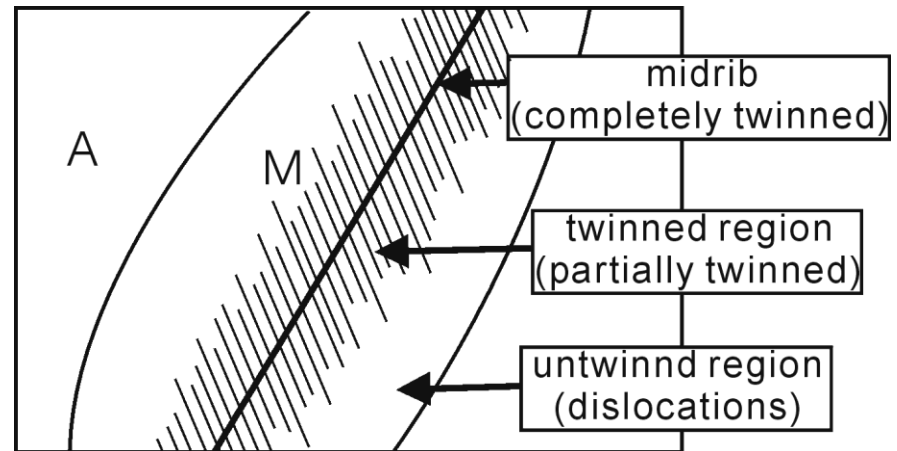
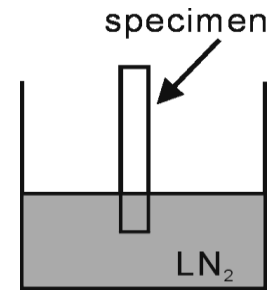
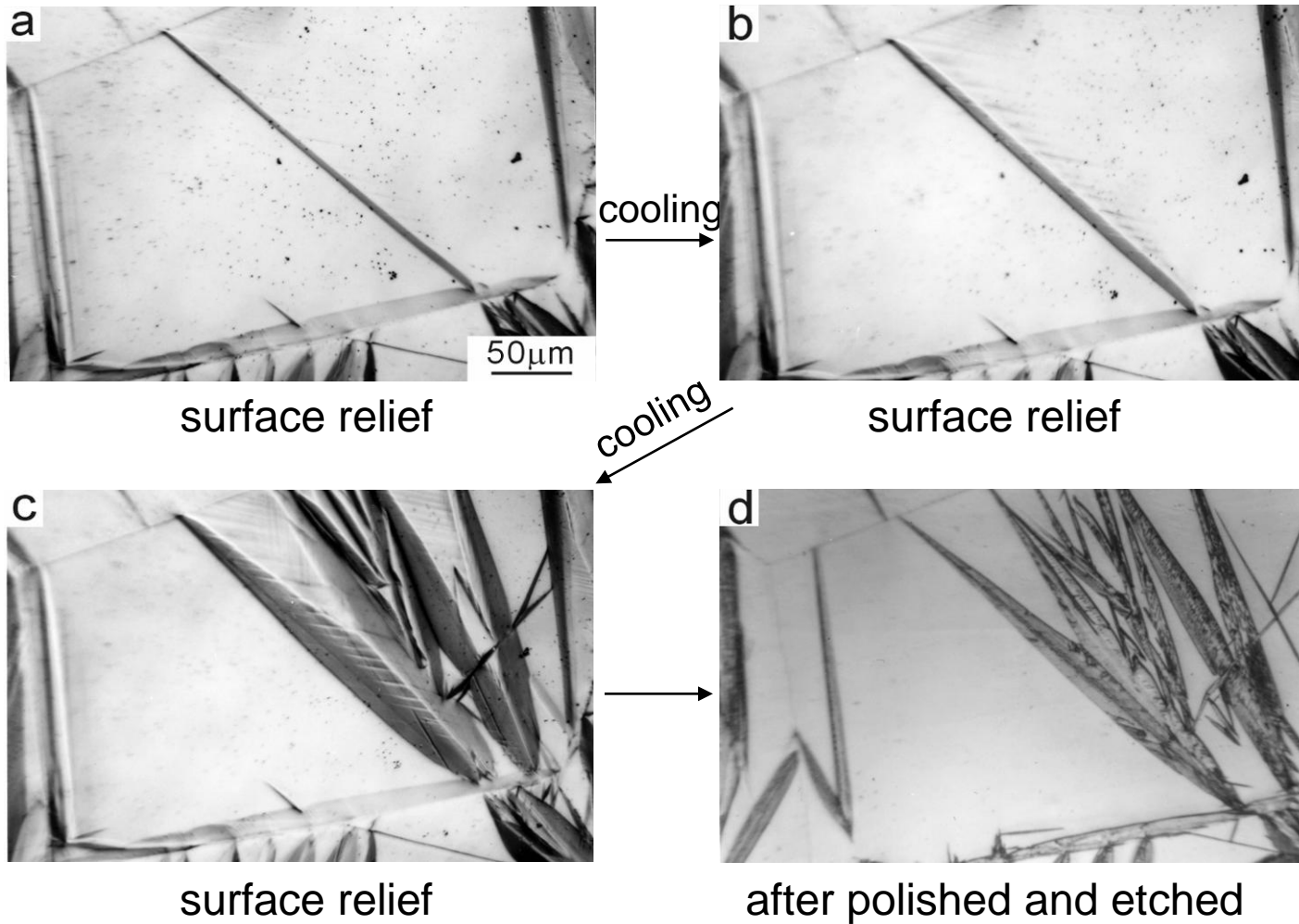


Fig.34: schematic diagram for  
lenticular martensite

Fig. 35: Growth behavior of lenticular martensite in Fe-30.4%Ni-0.4%C alloy



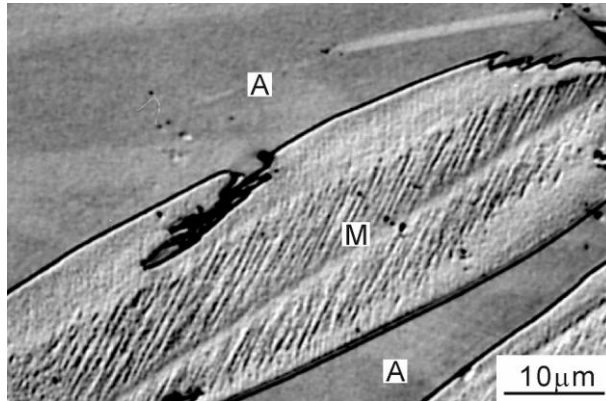
Courtesy of  
*T. Maki*

(T. Kakeshita, K. Shimizu, T. Maki, I. Tamura, Scripta Metall., 14(1980)1067.)

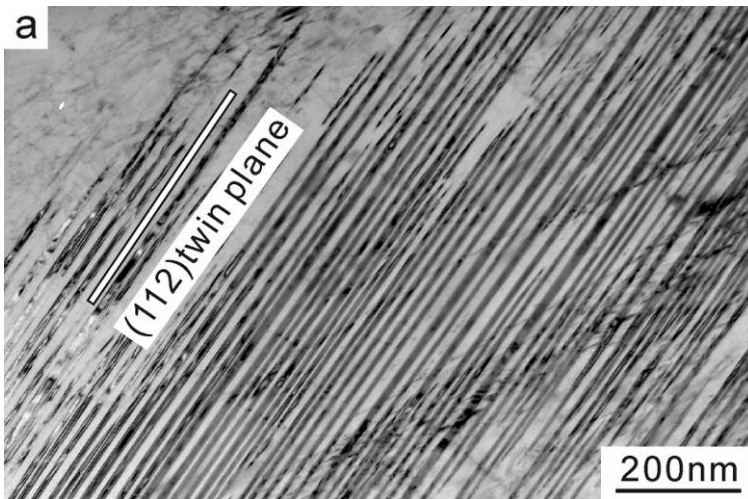
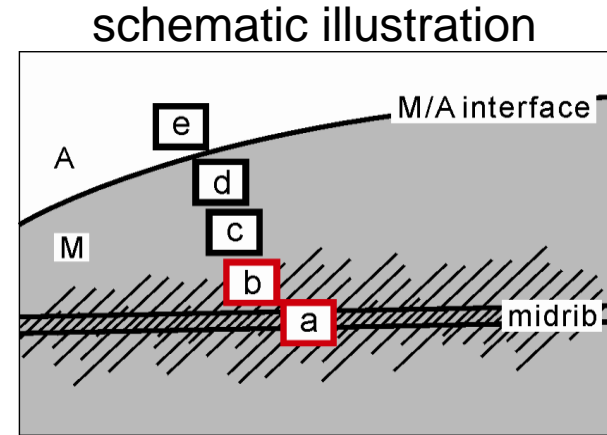
# Fig. 36: Lenticular martensite in Fe-33%Ni alloy

( $M_s=171K$ )

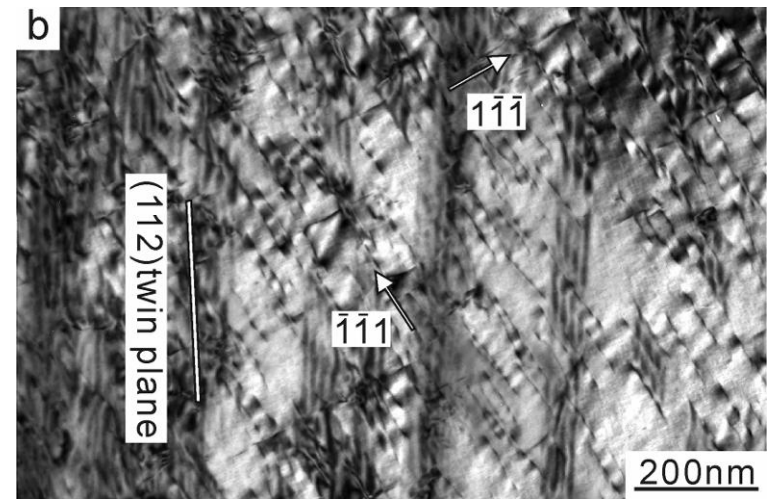
Courtesy of  
*T. Maki*



Optical micrograph

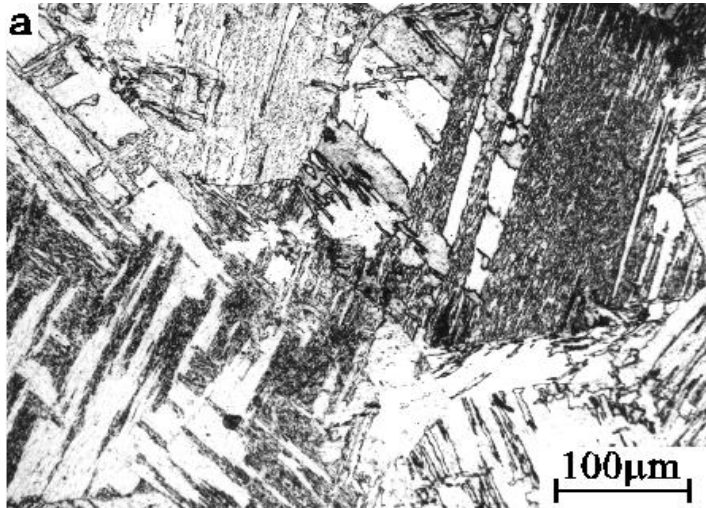


midrib

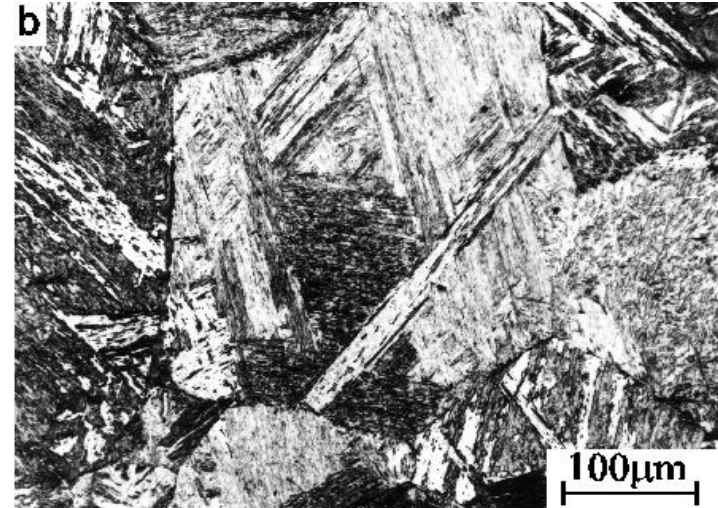


twinned region

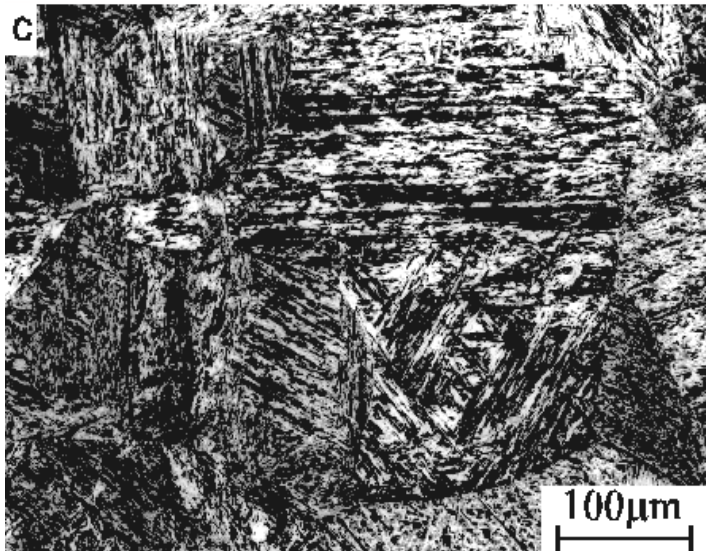
Fig. 37: Optical microstructure of lath martensite (Fe-C alloys) Courtesy of  
*T. Maki*



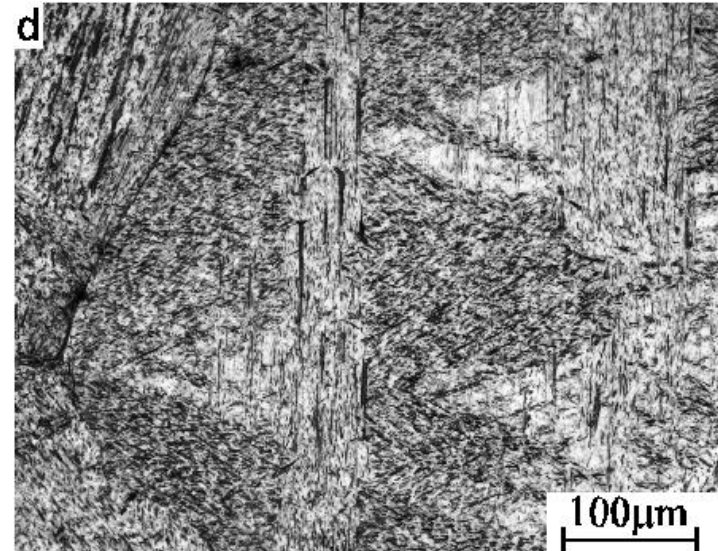
0.0026%C



0.18%C

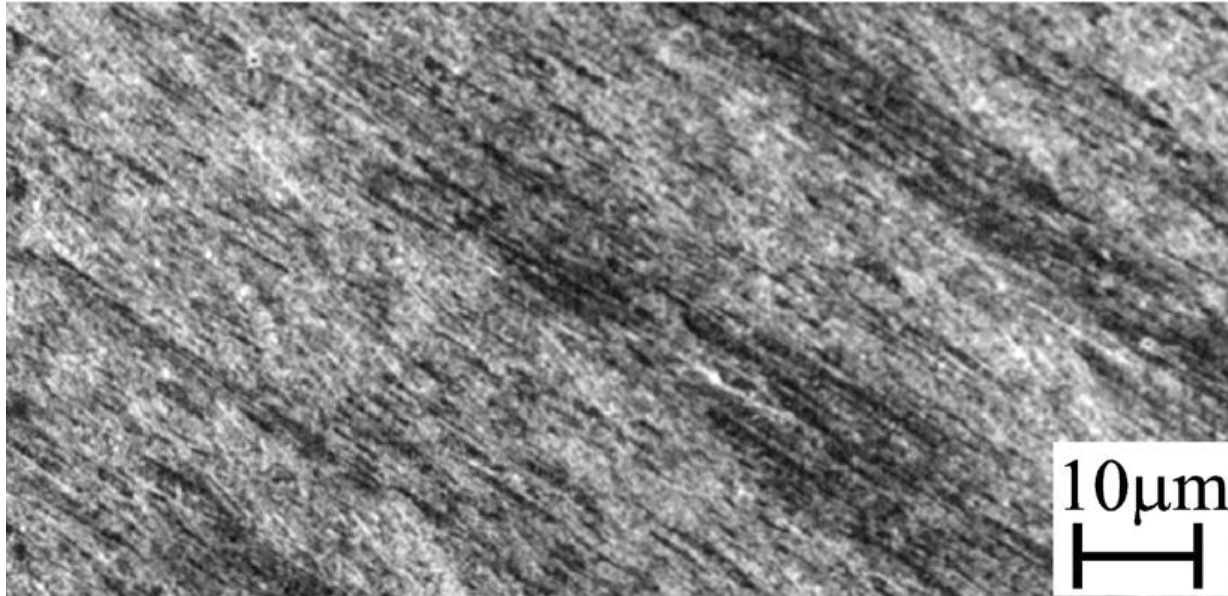


0.38%C



0.61%C

Block structure in a single packet (Fe-0.18%C)



Courtesy of  
*T. Maki*

Fig. 38: SEM image

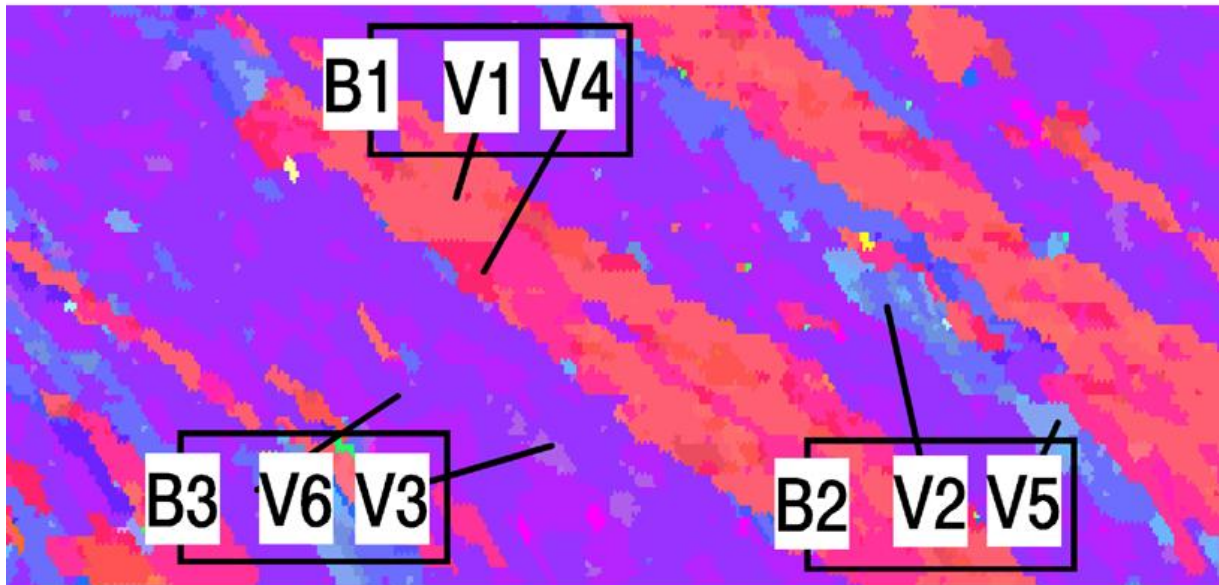


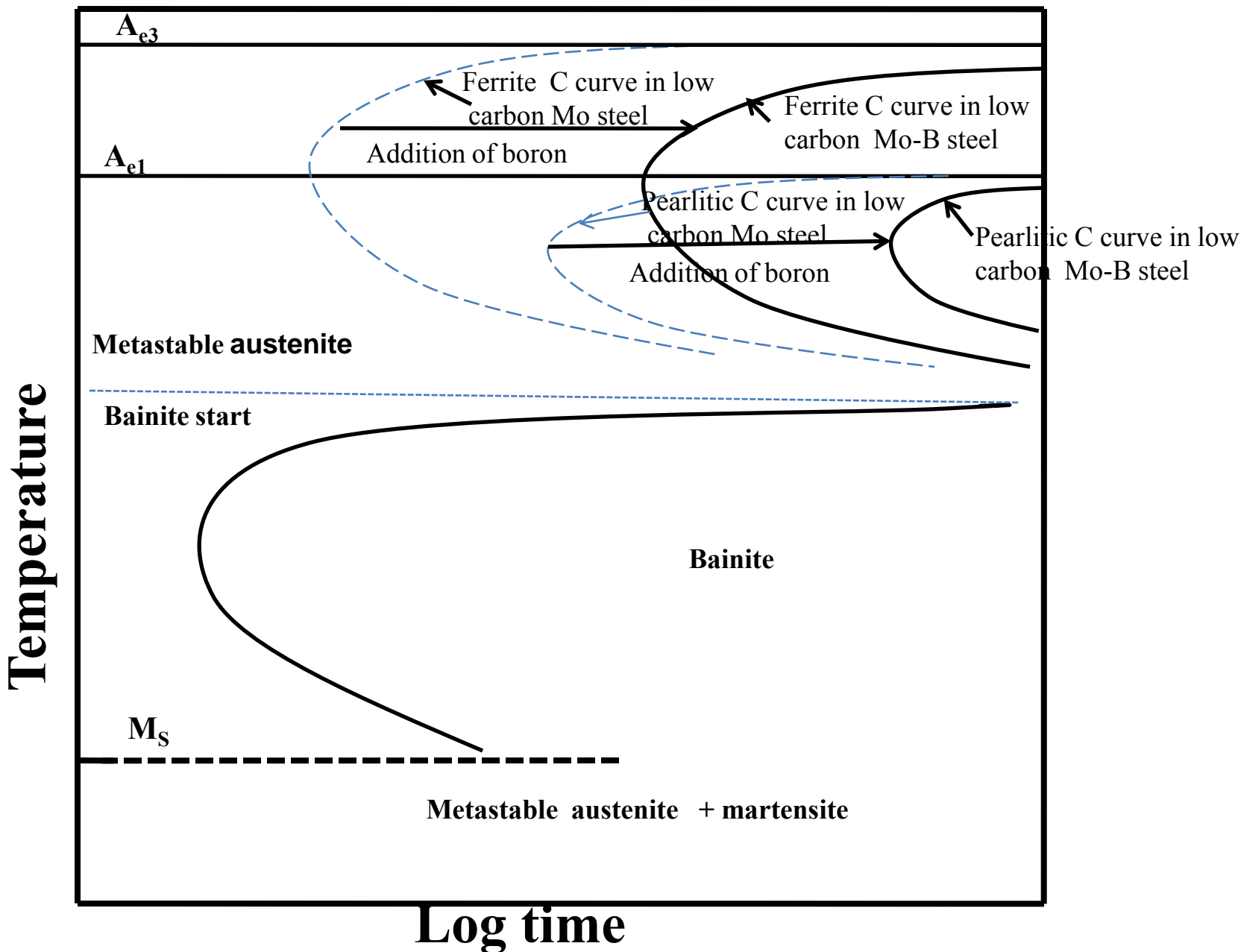
Fig.39 : Orientation  
image map

**Alloying elements:** Almost all alloying elements (except, Al, Co, Si) increases the stability of supercooled austenite and retard both proeutectoid and the pearlitic reaction and then shift TTT curves of start to finish to right or higher timing. This is due to i) low rate of diffusion of alloying elements in austenite as they are substitutional elements, ii) reduced rate of diffusion of carbon as carbide forming elements strongly hold them. iii) Alloyed solute reduce the rate of allotropic change, i.e.  $\gamma \rightarrow \alpha$ , by solute drag effect on  $\gamma \rightarrow \alpha$  interface boundary. Additionally those elements (Ni, Mn, Ru, Rh, Pd, Os, Ir, Pt, Cu, Zn, Au) that expand or stabilise austenite, depress the position of TTT curves to lower temperature. In contrast elements (Be, P, Ti, V, Mo, Cr, B, Ta, Nb, Zr) that favour the ferrite phase can raise the eutectoid temperature and TTT curves move upward to higher temperature.

However Al, Co, and Si increase rate of nucleation and growth of both ferrite or pearlite and therefore shift TTT diagram to left. In addition under the complex diffusional effect of various alloying element the simple C shape behaviour of TTT diagram get modified and various regions of transformation get clearly separated. There are separate pearlitic C curves, ferritic and bainitic C curves and shape of each of them are distinct and different.

The effect of alloying elements is less pronounced in bainitic region as the diffusion of only carbon takes place (either to neighbouring austenite or within ferrite) in a very short time (within a few second) after supersaturated ferrite formation by shear during bainitic transformation and there is no need for redistribution of mostly substitutional alloying elements. Therefore bainitic region moves less to higher timing in comparison to proeutectoid/pearlitic region. Addition of alloying elements lead to a greater separation of the reactions and result separate C-curves for pearlitic and bainitic regions (**Fig. 40**). Mo encourage bainitic reaction but addition of boron retard the ferrite reaction. By addition of B in low carbon Mo steel the bainitic region (almost unaffected by addition of B) can be separated from the ferritic region.

**Fig. 40: Effect of boron on TTT diagram of low carbon Mo steel**



However bainitic reaction is suppressed by the addition of some alloying elements.  $B_S$  temperature (empirical) has been given by Steven & Haynes

$$B_S(^\circ\text{C}) = 830 - 270(\%C) - 90(\%Mn) - 37(\%Ni) - 70(\%Cr) - 83(\%Mo)$$

(elements by wt%)

According to Leslie,  $B_{50}(^\circ\text{C}) = B_S - 60$

$$B_F(^\circ\text{C}) = B_S - 120$$

Most alloying elements which are soluble in austenite lower  $M_S$ ,  $M_F$  temperature except Al, Co.

Andrews gave best fit equation for  $M_S$ :

$$M_S(^\circ\text{C}) = 539 - 423(\%C) - 30.4Mn - 17.7Ni - 12.1Cr - 7.5Mo + 10Co - 7.5Si$$

(concentration of elements are in wt%).

Effect of alloying elements on  $M_F$  is similar to that of  $M_S$ . Therefore, subzero treatment is must for highly alloyed steels to transform retained austenite to martensite.

Addition of significant amount of Ni and Mn can change the nature of martensitic transformation from athermal to isothermal (**Fig. 41**).

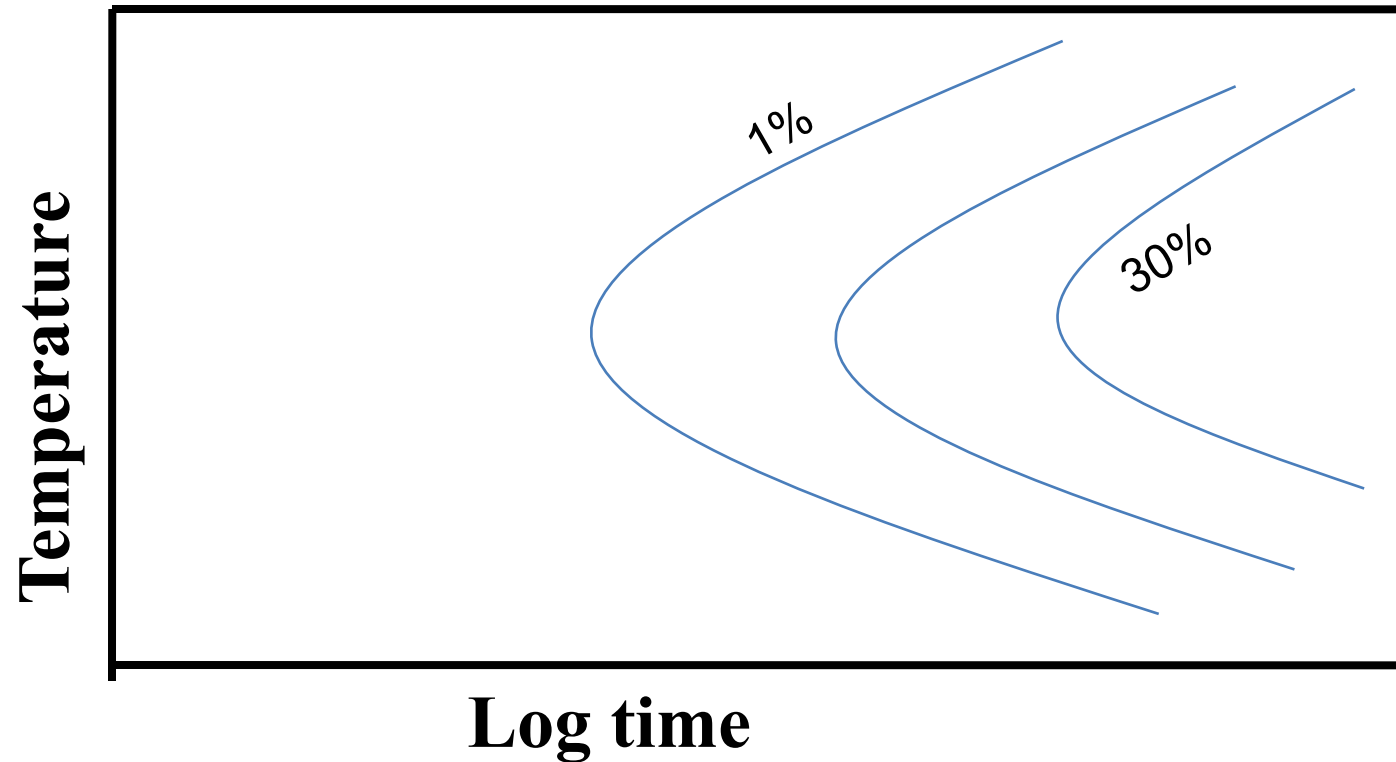


Fig. 41: kinetics of isothermal martensite in an Fe-Ni-Mn alloy

**Effect of grain size of austenite:** Fine grain size shifts S curve towards left side because it helps for nucleation of ferrite, cementite and bainite (**Fig. 43**). However Yang and Bhadeshia et al. have shown that martensite start temperature ( $M_S$ ) is lowered by reduction in austenite grain size (**Fig. 42**).

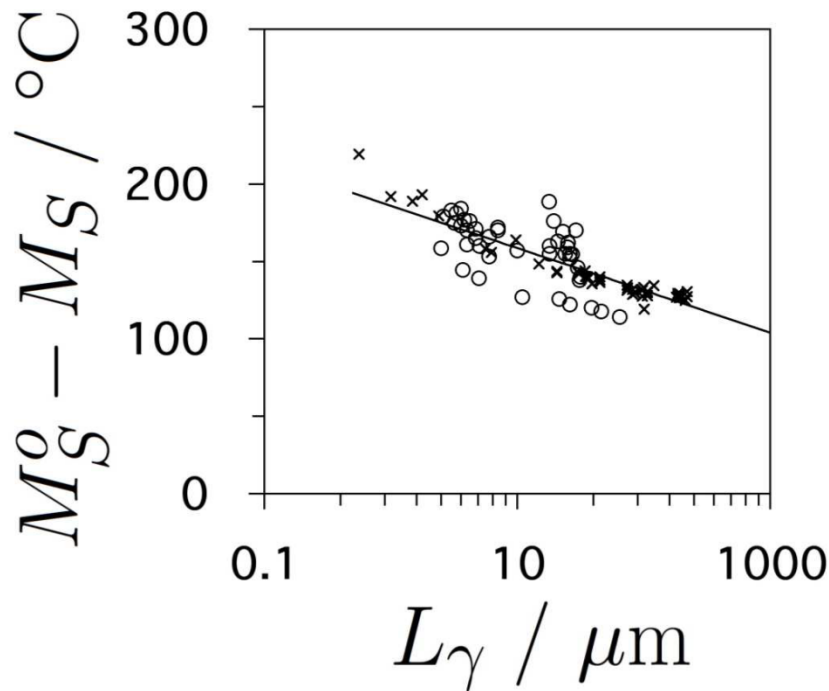


Fig. 42: Suppression of Martensite start temperature as a function austenite grain size  $L_\gamma$ .  $M_S^0$  is the highest temperature at which martensite can form in large austenite grain.  $M_S$  is the observed martensite start temperature (at 0.01 detectable fraction of martensite). Circles represent from low alloy data and crosses from high alloy data.

$$M_S^o - T = \frac{1}{b} \ln \left[ \frac{1}{aV_\gamma} \left\{ \exp \left( -\frac{\ln(1-f)}{m} \right) - 1 \right\} + 1 \right]$$

$T = M_S$ .  $a, b$  are fitting empirical constants,

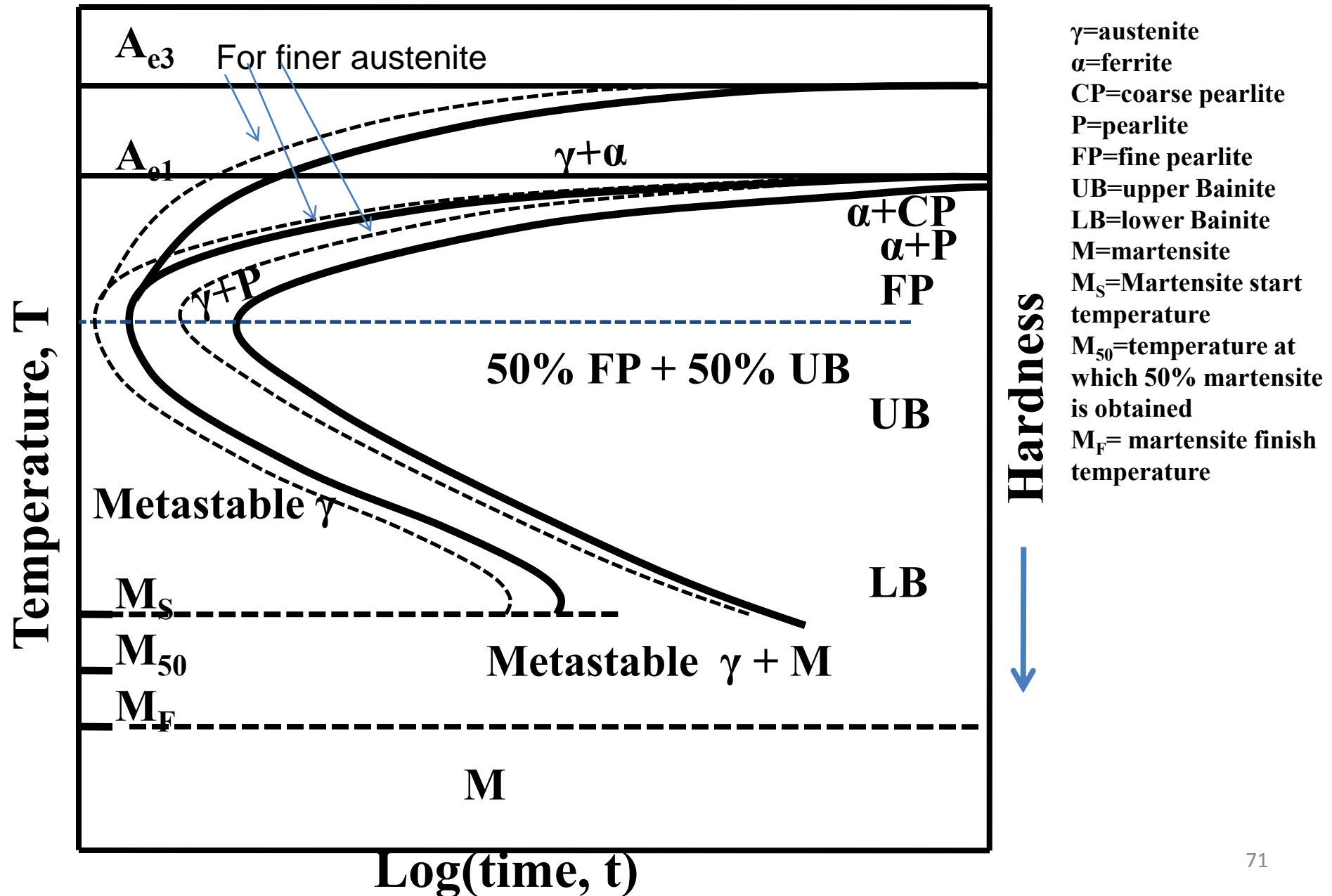
$$(a = 1.57 \times 10^{-21} \mu\text{m}^3 \text{ and } b = 0.253)$$

$m$  = average aspect ratio of martensite = 0.05 assumed,  $V_\gamma$  = average volume of austenite.  $f$  = detectable fraction of martensite = 0.01 (taken).

It is expected similar effect of grain size on  $M_F$  as on  $M_S$ .

Grain size of austenite affects the maximum plate or lath size.  
i.e. larger the austenite size the greater the maximum plate size or lath size

**Fig. 43 : Effect of austenite grain size on TTT diagram of plain carbon hypoeutectoid steel**



**Heterogeneity of austenite:** Heterogeneous austenite increases transformation time range, start to finish of ferritic, pearlitic and bainitic range as well as increases the transformation temperature range in case of martensitic transformation and bainitic transformation. Undissolved cementite, carbides act as powerful inoculant for pearlite transformation. Therefore heterogeneity in austenite increases the transformation time range in diffusional transformation and temperature range of shear transformation products in TTT diagram.

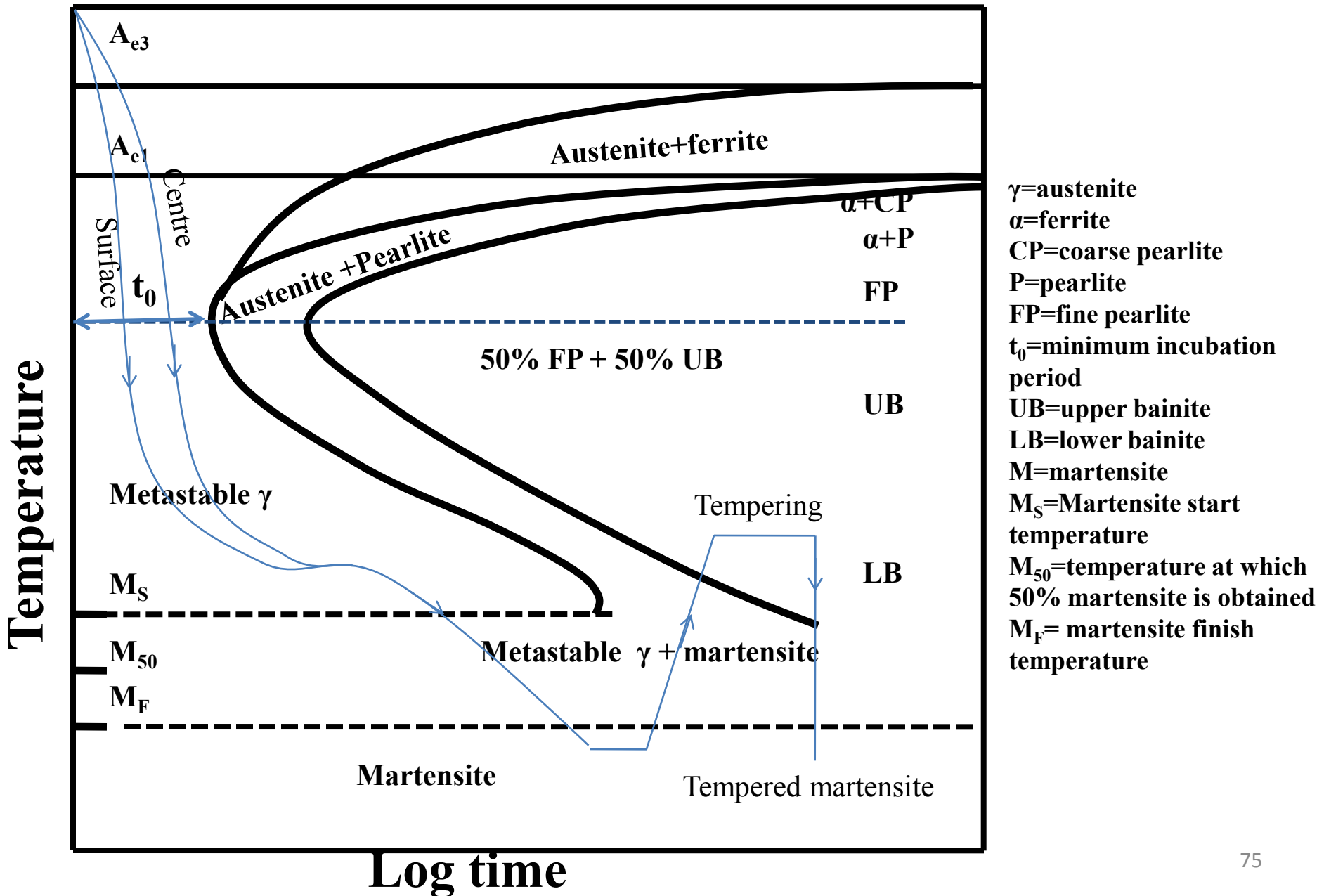
# Applications of TTT diagrams

- **Martempering**
- **Austempering**
- **Isothermal Annealing**
- **Patenting**

**Martempering** : This heat treatment is given to oil hardenable and air hardenable steels and thin section of water hardenable steel sample to produce martensite with minimal differential thermal and transformation stress to avoid distortion and cracking. The steel should have reasonable incubation period at the nose of its TTT diagram and long bainitic bay. The sample is quenched above  $M_S$  temperature in a salt bath to reduce thermal stress (instead of cooling below  $M_F$  directly) **(Fig. 44)**

Surface cooling rate is greater than at the centre. The cooling schedule is such that the cooling curves pass behind without touching the nose of the TTT diagram. The sample is isothermally hold at bainitic bay such that differential cooling rate at centre and surface become equalise after some time. The sample is allowed to cool by air through  $M_S$ - $M_F$  such that martensite forms both at the surface and centre at the same time due to not much temperature difference and thereby avoid transformation stress because of volume expansion. The sample is given tempering treatment at suitable temperature.

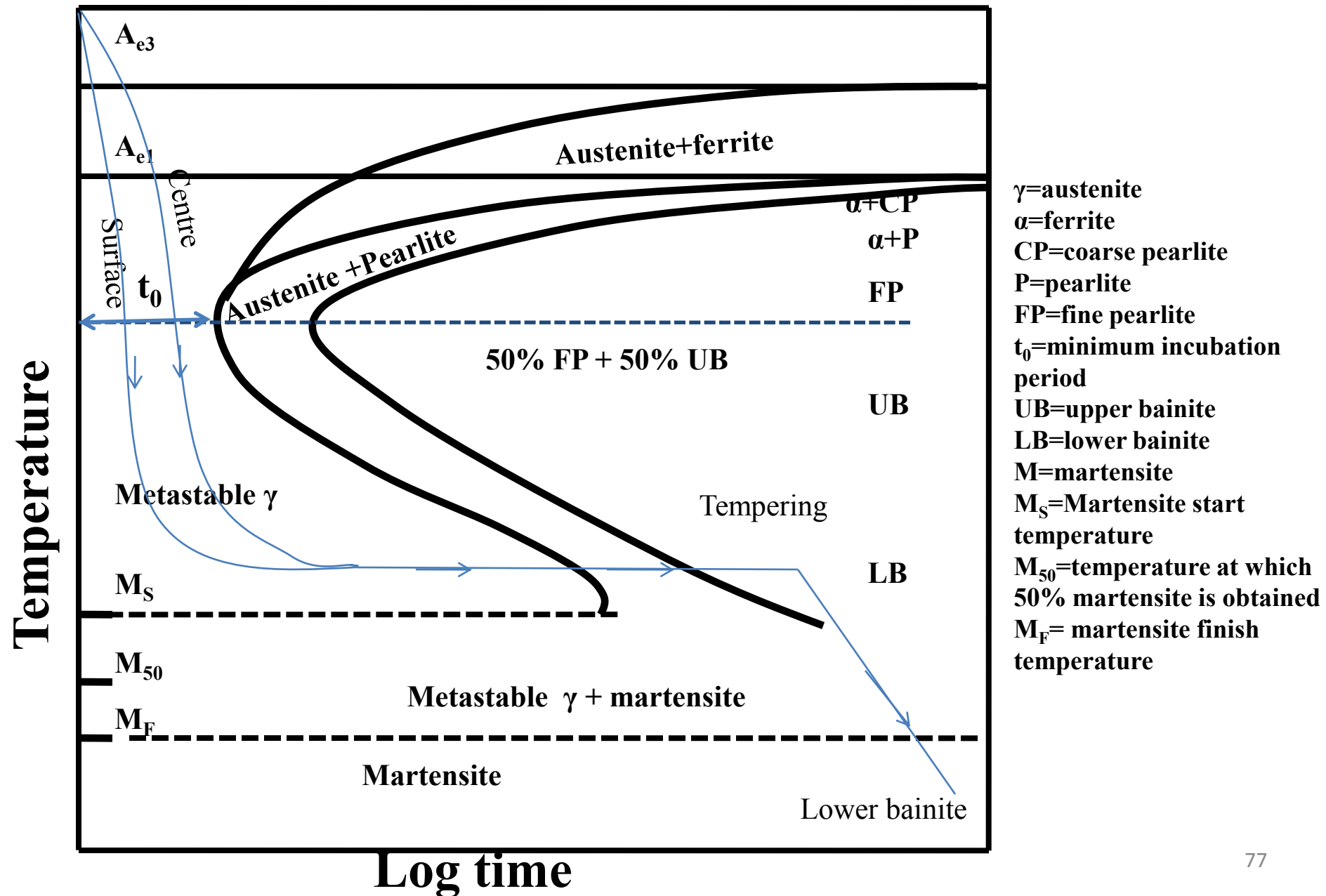
**Fig. 44: Martempering heattreatment superimposed on TTT diagram for plain carbon hypoeutectoid steel**



# Austempering

Austempering heat treatment is given to steel to produce lower bainite in high carbon steel without any distortion or cracking to the sample. The heat treatment is cooling of austenite rapidly in a bath maintained at lower bainitic temperature (above  $M_s$ ) temperature (avoiding the nose of the TTT diagram) and holding it here to equalise surface and centre temperature (**Fig. 45**) and . till bainitic finish time. At the end of bainitic reaction sample is air cooled. The microstructure contains fully lower bainite. This heat treatment is given to 0.5-1.2 wt%C steel and low alloy steel. The product hardness and strength are comparable to hardened and tempered martensite with improved ductility and toughness and uniform mechanical properties. Products donot required to be tempered.

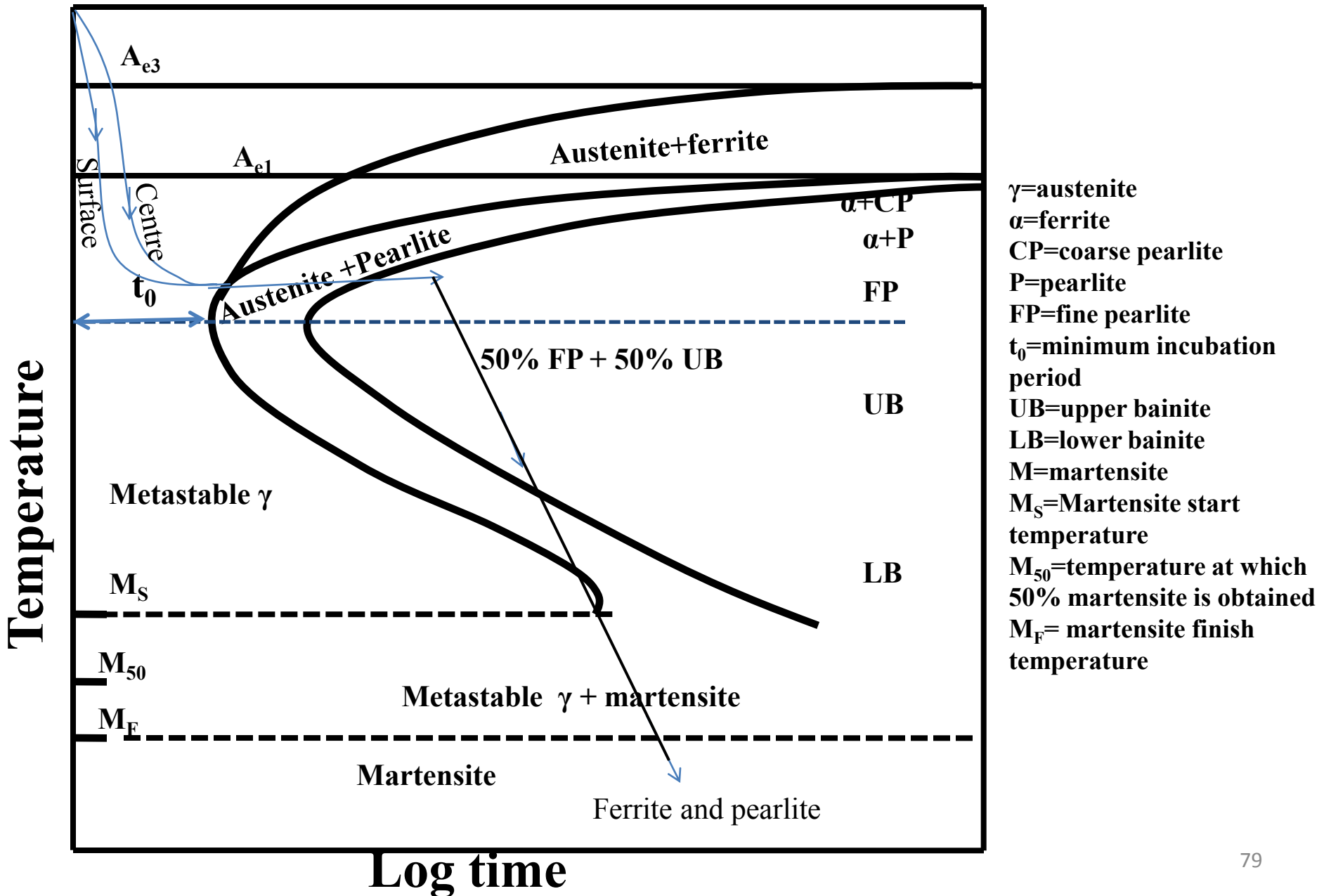
**Fig. 45: Austempering heattreatment superimposed on TTT diagram for plain carbon hypoeutectoid steel**



# Isothermal annealing

- Isothermal annealing is given to plain carbon and alloy steels to produce uniform ferritic and pearlitic structures. The product after austenising taken directly to the annealing furnace maintained below lower critical temperature and hold isothermally till the pearlitic reaction completes (**Fig. 46**). The initial cooling of the products such that the temperature at the centre and surface of the material reach the annealing temperature before incubation period of ferrite. As the products are hold at constant temperature i.e. constant undercooling) the grain size of ferrite and interlamellar spacing of pearlite are uniform. Control on cooling after the end of pearlite reaction is not essential. The overall cycle time is lower than that required by full annealing.

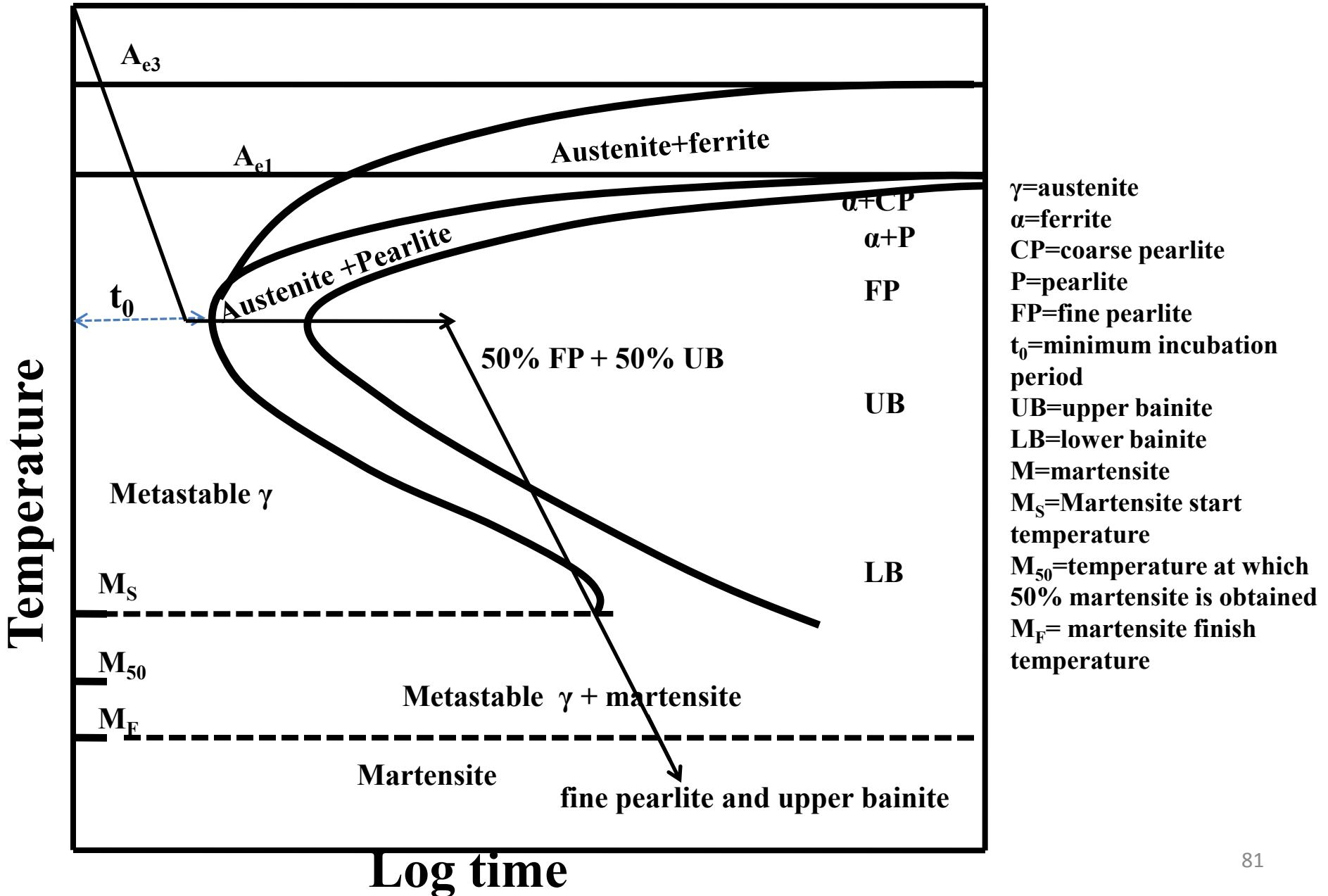
**Fig. 46: Isothermal annealing heat treatment superimposed on TTT diagram of plain carbon hypoeutectoid steel**



# Patenting

Patenting heat treatment is the isothermal annealing at the nose temperature of TTT diagram (**Fig. 47**). Followed by this the products are air cooled. This treatment is to produce fine pearlitic and upper bainitic structure for strong rope, spring products containing carbon percentage 0.45 %C to 1.0%C. The coiled ropes move through an austenitising furnace and enters the salt bath maintained at 550°C(nose temperature) at end of salt bath it get recoiled again. The speed of wire and length of furnace and salt bath such that the austenitisation get over when the wire reaches to the end of the furnace and the residency period in the bath is the time span at the nose of the TTT diagram. At the end of salt bath wire is cleaned by water jet and coiled.

**Fig. 47: Patenting heat treatment superimposed on TTT diagram of plain carbon hypoeutectoid steel**



# Prediction methods

TTT diagrams can be predicted based on thermodynamic calculations.

MAP\_STEEL\_MUCG83 program [transformation start curves for reconstructive and displacive transformations for low alloy steels, Bhadeshia et al.], was used for the following TTT curve of Fe-0.4 wt%C-2 wt% Mn alloy (**Fig. 48**)

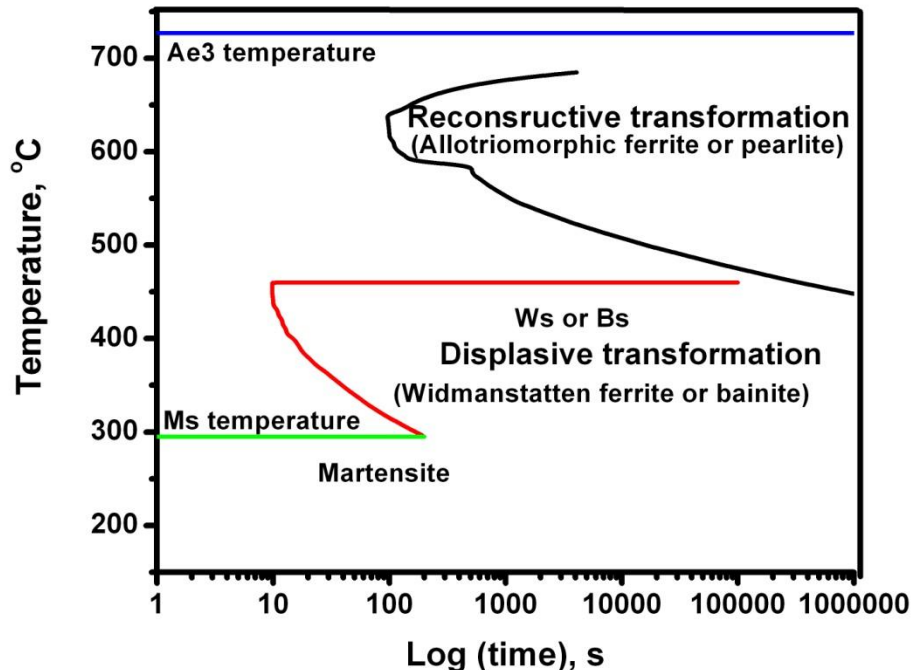


Fig. 48: Calculated transformation start curve under isothermal transformation condition

# The basis of calculating TTT diagram for ferrous system

1. Calculation of  $A_{e3}$  Temperature below which ferrite formation become thermodynamically possible.
2. Bainite start temperature  $B_S$  below which bainite transformation occurs.
3. Martensite start temperature  $M_S$  below which martensite transformation occurs
4. A set of C-curves for reconstructive transformation (allotriomorphic ferrite and pearlite).  
A set of C-curves for displacive transformations (Widmanstätten ferrite, bainite)  
A set of C-curves for fractional transformation
5. Fraction of martensite as a function of temperature

# 1. Calculation of $A_{e3}$ temperature for multicomponent system. [Method adopted by Bhadeshia et al.]

(This analysis is based on Kirkaldy and Barganis and is applicable for total alloying elements of less than 6wt% and Si is less than 1 wt%)

General procedure of determination of phase boundary

Assume T is the phase boundary temperature at which high temperature phase L is in equilibrium with low temperature phase  $\gamma$ .

In case of pure iron then T is given by

$$X_0^{\gamma\gamma} = X_0^{L\gamma} \exp\left(\frac{\Delta^{\circ}G_0^{\gamma \rightarrow L}}{RT}\right)$$

for  $A_{e3}$  temperature, low temperature phase  $\gamma$  to be substituted by  $\alpha$  and high temperature phase L to be substituted by  $\gamma$ )

Where  $X_0$  is the mole fraction of iron then

$$X_0 = 1 - \sum_{i=1}^n X_i$$

Where  $X_i$ =mole fraction of component i,  $\gamma_i$ =activity coefficient of component i, R=universal gas constant, assuming 0 for Fe, 1 for C, i=2 to n for Si, Mn, Ni, Cr, Mo, Cu, V, Nb, Co, W respectively.

$$\Delta^{\circ}G^{\gamma \rightarrow L} = {}^{\circ}G_L - {}^{\circ}G_{\gamma}$$

and  ${}^{\circ}G_L$  = standard Gibbs free energy of pure high temperature phase and  ${}^{\circ}G_{\gamma}$  = Standard Gibbs free energy of pure low temperature phase

Similarly for carbon ( n=1) or component i

$$X_i^{\gamma} \gamma_i^{\gamma} = X_i^L \gamma_i^L \exp \left( \frac{\Delta^{\circ}G_i^{\gamma \rightarrow L}}{RT} \right)$$

The Wagner Taylor expansion for the activity coefficients are substituted in the above equations.

The Wagner-Taylor expansions for activity coefficients are

$$\ln \gamma_0 = -1/2 \sum_{i, k=1}^7 \epsilon_{ik} X_i X_k$$

**$k=1$  to  $11$  in this case**

and

$$\ln \gamma_i = \sum_{k=1}^7 \epsilon_{ik} X_k$$

Where  $\epsilon_{ii} = 0$  (assumed)

$$\epsilon_{ik} (i \neq k, i \text{ and } k > 1)$$

are the Wagner interaction parameters i.e. interaction between solutes are negligible. The substitution of Wagner-Taylor expansions for activity coefficients gives temperature deviation  $\Delta T$  for the phase boundary temperature (due to the addition of substitutional alloying elements

In multicomponent system, the temperature deviations due to individual alloying additions are additive as long as solute-solute interactions are negligible. Kirkaldy and co-workers found that these interactions are negligible as long as total alloying additions are less than 6wt% and Si is less than 1wt%].

Eventually  $\Delta T$  takes the following form

$$\Delta T = RT_0^2 \sum_{i=2}^n A_i X_i^L$$

Where  $T_0$  is the phase boundary temperature for pure Fe-C system and  $T_0$  is given by .

$$T_0 \text{ (K)} = 1115 - 150.3 \text{ (pct C)} + 216 \text{ (0.765 - pct C)}^{4.26}$$

And where

$$A_1 = \frac{A_1^0 - [1 + X_1^L(1 - X_1^L)(\varepsilon_{11}^L - \varepsilon_{11}^V A_1^0 A_1^0)] \exp B}{[X_1^L \Delta^\circ H_1 A_1^0 + (1 - X_1^L) \Delta^\circ H_0] \exp B}$$

for which

$$B = \left\{ \frac{\Delta^\circ G_0}{RT_0^2} - \frac{(X_1^L)^2}{2} [\varepsilon_{11}^L - \varepsilon_{11}^V (A_1^0)^2] \right\}$$

and

$$A_n^0 = \frac{\exp [(\Delta^\circ G_n / RT_0) + \varepsilon_{1n}^L X_1^L]}{1 + \varepsilon_{1n}^V X_1^L \exp (\Delta^\circ G_1 / RT_0)}$$

where  $n=1$  or  $i$  and  $\Delta^\circ H_0$  and  $\Delta^\circ H_1$  are standard molar enthalpy changes corresponding to  $\Delta^\circ G_0$  and  $\Delta^\circ G_1$ .

If the relevant free energy changes  $\Delta^{\circ}G$  and the interaction parameters  $\varepsilon$  are known then  $\Delta T$  can be calculated for any alloy.

Since all the thermodynamic functions used are dependent on temperature,  $\Delta T$  cannot be obtained from single application of all values (used from various sources) but must be deduced iteratively. Initially  $T$  can be set as  $T_0$ ,  $\Delta T$  is calculated. Then  $T=T+\Delta T$  is used for  $T$  and  $\Delta T$  is found. Iteration can be repeated for a few times (typically five times) about till  $T$  changes by less than 0.1K.

This method obtains  $A_{e3}$  temperature with accuracy of  $\pm 10K$ .

## 2. Bainite start temperature $B_S$ from Steven and Haynes formula

$$B_S(^\circ\text{C}) = 830 - 270(\%C) - 90(\%Mn) - 37(\%Ni) - 70(\%Cr) - 83(\%Mo)$$

(% element by wt)

Both bainite and Widmanstätten ferrite nucleate by same mechanism. The nucleus develops into Widmanstätten ferrite if at the transformation temperature the driving force available cannot sustain diffusionless transformation. By contrast bainite form from the same nucleus if the transformation can occur without diffusion. Therefore in principle  $B_S = W_S$ .

Bainite transformation does not reach completion if austenite enriches with carbon. But in many steels carbide precipitation from austenite eliminates the enrichment and allow the austenite to transform completely. In those cases bainite finish temperature is given (according to Leslie) by

$$B_F(^\circ\text{C}) = B_S - 120$$

### 3. $M_S$ Temperature:

At the  $M_S$  temperature

$$\begin{aligned}
 \Delta F_{M_s}^{\gamma \rightarrow \alpha'} &= 2xRT \ln x + x[\Delta \bar{H}_\alpha - \Delta \bar{H}_\gamma - (\Delta S_\alpha - \Delta S_\gamma)T \\
 &\quad + 4\omega_\alpha - 6\bar{\omega}_\gamma] \\
 &\quad - 4RT(1-x) \ln(1-x) + 5RT(1-2x) \ln(1-2x) \\
 &\quad - 6RTx \ln \left| \frac{\delta_\gamma - 1 + 3x}{\delta_\gamma + 1 - 3x} \right| \\
 &\quad - 6RT(1-x) \ln \left| \frac{1 - 2J_\gamma + (4J_\gamma - 1)x - \delta_\gamma}{2J_\gamma(2x - 1)} \right| \\
 &\quad + 3RTx \ln(3 - 4x) + 4RTx \ln \left| \frac{\delta_\alpha - 3 + 5x}{\delta_\alpha + 3 - 5x} \right| \\
 &\quad + (1-x) \left| 141 \sum Y_i (\Delta T_{\text{mag}_i} - \Delta T_{\text{NM}_i}) \right. \\
 &\quad \left. + \Delta F_{F_c}^{\gamma \rightarrow \alpha'} \{ T - 100 \sum_i Y_i \Delta T_{\text{mag}_i} \} \right| + \Delta f^* \tag{1}
 \end{aligned}$$

where

$$\delta_x = |9 - 6x(2J_x + 3) + (9 + 16J_x)x^2|^{1/2}$$

$$\delta_y = |1 - 2(1 + 2J_y)x + (1 + 8J_y)x^2|^{1/2}$$

$$J_x = 1 - \exp(-\omega_x/RT)$$

$$J_y = 1 - \exp(-\bar{\omega}_y/RT).$$

In the above equation, T refers to  $M_S$  temperature in absolute scale, R is universal gas constant, x=mole fraction of carbon,  $Y_i$  is the atom fraction of the  $i$ th substitutional alloying element,  $\Delta T_{\text{magi}}$  and  $\Delta T_{\text{NMi}}$  are the displacement in temperature at which the free energy change accompanying the  $\gamma \rightarrow \alpha$  transformation in pure iron (i.e.  $\Delta F_{\text{Fe}}^{\gamma \rightarrow \alpha}$ ) is evaluated in order to allow for the changes (per at%) due to alloying effects on the magnetic and non-magnetic components of  $\Delta F_{\text{Fe}}^{\gamma \rightarrow \alpha}$ , respectively. These values were taken from Aaronson, Zenner.  $\Delta F_{\text{Fe}}^{\gamma \rightarrow \alpha}$  value was from Kaufmann.

The other parameters are as follows

(i) the partial molar heat of solution of carbon in ferrite,  
 $\Delta^{\bar{}}H_{\alpha}=111918 \text{ J mol}^{-1}$  (from Lobo) and

$\Delta^{\bar{}}H_{\alpha}=35129+169105x \text{ J mol}^{-1}$  (from Lobo)

ii) the excess partial molar non-configurational entropy of solution of carbon in ferrite  $\Delta S_{\alpha}=51.44 \text{ J mol}^{-1}\text{K}^{-1}$  (from Lobo)

$\Delta S_{\gamma}=7.639+120.4x \text{ J mol}^{-1}\text{K}^{-1}$  (from Lobo)

$\omega_{\alpha}$ =the C-C interaction energy in ferrite= $48570 \text{ J mol}^{-1}$ (average value) (from Bhadeshia)

$\omega_{\gamma}$ =the corresponding C-C interaction energy in austenite values were derived , as a function of the concentrations of various alloying elements, using the procedure of Shiflet and Kingman and optimised activity data of Uhrenius. These results were plotted as a function of mole fraction of alloying elements and average interaction parameter  $\omega^{\bar{}}_{\gamma}$  was calculated following Kinsman and Aaronson.

$\Delta f^*$ =Zener ordering term was evaluated by Fisher.

The remaining term,  $\Delta F_{Fe}^{\gamma \rightarrow \alpha}$ =free energy change from austenite to martensite as only function of carbon content. and is identical for Fe-C and Fe-C-Y steels as structure for both cases are identical (Calculated by Bhadeshia )=-900 to -1400 J mol<sup>-1</sup> (for C 0.01 to 0.06 mole fraction, changes are not monotonic). However Lacher-Fowler-Guggenheim extrapolation gives better result of -1100 to -1400 J mol<sup>-1</sup> (Carbon mole fraction 0.01-0.06).

The equation was solved iteratively until the both sides of the equation balanced with a residual error of <0.01%. The results underestimate the temperature of 10-20K. The error may be due to critical driving force for transformation calculation consider only a function of carbon content.

## 4. Transformation start and finish C curves

The incubation period ( $\tau$ ) can be calculated from the following equation [Bhadeshia et al.]

$$\ln \left\{ \frac{\tau G_{\max}^p}{T^z} \right\} = \frac{Q}{RT} + C$$

Where T is the isothermal transformation temperature in absolute scale, R is universal gas constant,  $G_{\max}$  is the maximum free energy change available for nucleation, Q is activation enthalpy for diffusion, C, p, z=20 are empirical constant obtained by fitting experimental data of T,  $G_{\max}$ ,  $\tau$  for each type of transformation (ferrite start, ferrite finish, bainite start and bainite finish). By systematically varying p and plotting  $\ln(\tau G_{\max}^p / T^{z=20})$  against  $1/RT$  for each type of transformation (reconstructive and displacive) till the linear regression coefficient  $R_1$  attains an optimum value. Once p has been determined Q and C follow from respectively the slope and intercept of the of plot. The same equation can be used to predict transformation time.

Table-I: Chemical compositions, in wt% of the steel chosen to test the model

Alloy	C	Si	Mn	Ni	Mo	Cr
En13	0.19	0.14	1.37	0.56	0.31	0.20
En14	0.29	0.26	1.67	0.21	0.04	0.12
En15	0.33	0.23	1.54	0.18	0.05	0.15
En16	0.33	0.18	1.48	0.26	0.27	0.16
En17	0.38	0.25	1.49	0.24	0.41	0.14
En18	0.48	0.25	0.86	0.18	0.04	0.98
En19	0.41	0.23	0.67	0.20	0.23	1.01
En20L	0.27	0.13	0.60	0.19	0.55	0.74
En20H	0.41	0.28	0.58	0.15	0.74	1.39
En24	0.38	0.20	0.69	1.58	0.26	0.95
En110	0.39	0.23	0.62	1.44	0.18	1.11
US1050	0.50	0.13	0.91	—	—	—
US4140	0.37	0.15	0.77	—	0.21	0.98
US4150	0.55	—	0.60	0.36	0.19	1.03
US4340	0.42	—	0.78	1.79	0.33	0.80
US5140	0.42	0.16	0.68	—	—	0.93

The optimum values of  $p$  and corresponding values of  $C$ ,  $Q$  for different types of steels (**Table-I**) where concentrations are in wt% are summarised below [Bhadeshia et.al.] (**Table-II**).

Table-II: The optimum values of fitting constants

FS=ferrite start, FF=ferrite finish, BS=bainite start and BF=bainite finish

FS	$p = 4, C = -155 - 9\text{Ni} - 30\text{Mo},$ $Q = 331340 + 83000\text{Ni} + 255000\text{Mo} + 129000\text{Cr}$
FF	$p = 8, C = -155 - 9\text{Ni} - 30\text{Mo},$ $Q = 596750 + 78000\text{Ni} + 265000\text{Mo} + 115000\text{Cr}$ $- 110000\text{C}$
BS	$p = 5, C = -133,$ $Q = 219880 + 10000\text{C} + 6000\text{Ni} - 3000\text{Mo}$ $+ 5000\text{Cr}$
BF	$p = 5, C = -133,$ $Q = 234860 + 27000\text{C} + 4000\text{Ni} + 11000\text{Cr}$

The bainite finish C-curve of the experimental TTT diagram not only shifts to longer time but also but is also shifts to lower temperature by about 120°C. Therefore this is taken care by plotting  $\ln[\tau G_{\max}^p / (T + 120)^{20}]$  against  $1/R(T + 120)$  in order to determine p, Q and C for the bainitic finish curve.

Based on Q, C and Gmax value it can be predicted that Mo strongly retard the formation of ferrite through its large influence on Q. however it can promote bainite via the small negative coefficient that it has for the Q of the bainitic C-curve. Cr retard both both bainite and ferrite but net effect is to promote the formation of bainite since the influence on the bainitic C-curve is relatively small. Ni has a slight retarding effect on transformation rate. Mn has also retarding effect on ferrite as as well as bainitic transformation

# Fractional transformation curves

Fractional transformation time can be estimated from the following Johnson-Mehl-Avrami equation.

$$x = 1 - \exp\left(\frac{K_1 t^n}{d^m}\right)$$

X=transformation volume fraction,  $K_1$  is rate constant which is a function of temperature and austenite grain size  $d$ ,  $n$  and  $m$  are empirical constants. By selecting steels of similar grain size, the austenite grain size can be neglected then the above equation simplifies to

$$x = 1 - \exp\{K_1 t^n\}$$

Assuming  $x=0.01$  for transformation start and  $x=0.99$  for transformation finish. For a given temperature transformation start time and finish time can be calculated then  $K_1$  and  $n$  can be solved for each transformation product as a function of temperature.

Then fractional transformation curves for arbitrary values of  $x$  can therefore be determined using

Representation of intermediate state of transformation between 0% and 100% can be derived by fitting to the experimental TTT diagram as follows:

$$B_x(^{\circ}\text{C}) = B_S - 300x \quad x \leq 0.1$$

$$B_x(^{\circ}\text{C}) = B_S - 30 - 75(x - 0.1) \quad 0.1 < x \leq 0.9$$

$$B_x(^{\circ}\text{C}) = B_S - 90 - 300(x - 0.9) \quad 0.9 < x \leq 1$$

Where  $x$  refers to the fraction of transformation.

In most of TTT diagrams of Russell has a plateau at its highest temperature. Therefore a horizontal line can be drawn at  $B_S$  and joining it to a C-curve calculated for temperatures below  $B_S$ .

Relation between observed and predicted values for ferrite start (FS), ferrite finish (FF), bainite start (BS) and bainite finish (BF) are shown in **Fig. 49**. Predicted value closely matches the observed values for selected low alloy steels. Predicted TTT diagrams are projected on experimental diagrams (**Figs. 50-52**). The model correctly predicts bainite bay region in low alloy as well as in selected high alloy steels. The model reasonably predicts the fractional C curves (**Fig. 52**). Mo strongly retard the formation of ferrite through its large influence on Q. however it can promote bainite via the small negative coefficient that it has for the Q of the bainitic C-curve. Cr retard both both bainite and ferrite but net effect is to promote the formation of bainite since the influence on the bainitic C-curve is relatively small. Ni has a slight retarding effect on transformation rate. Mn has also retarding effect on ferrite as well as bainitic transformation. The model is empirical in nature but it can nevertheless be useful in procedure for the calculation of microstructure in steel.

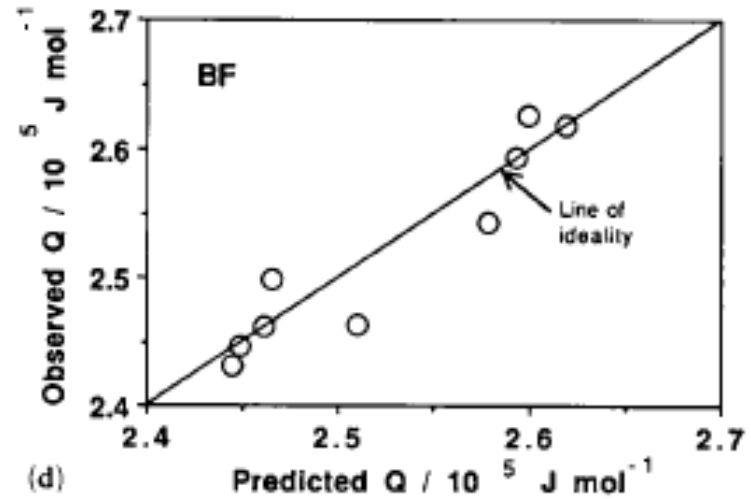
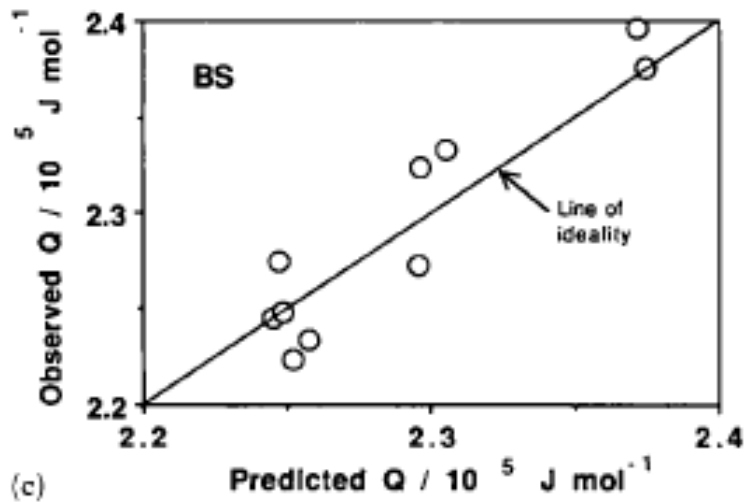
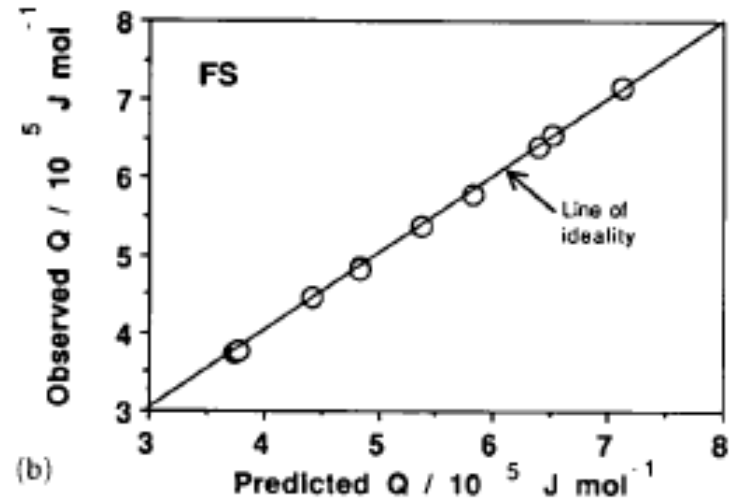
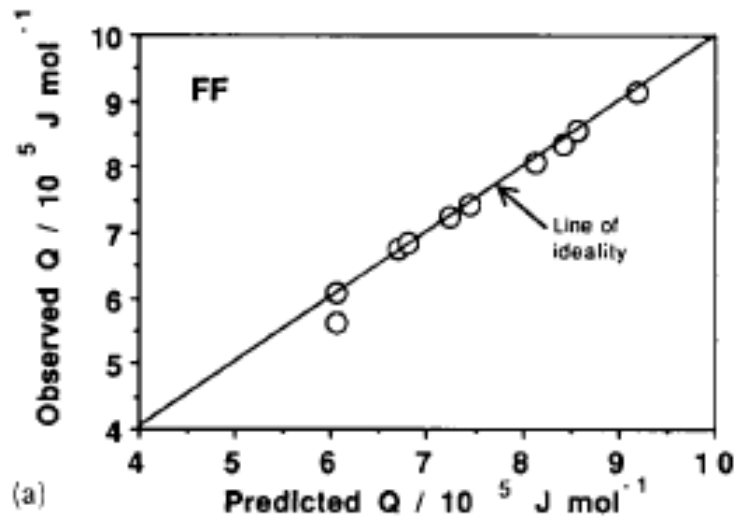


Fig. 49: Relation between observed and predicted  $Q(\text{Jmol}^{-1})$  value for: (a) FS-ferrite start, (b) FF-ferrite finish, (c) BS-bainite start and (d) BF-bainite finish curves.

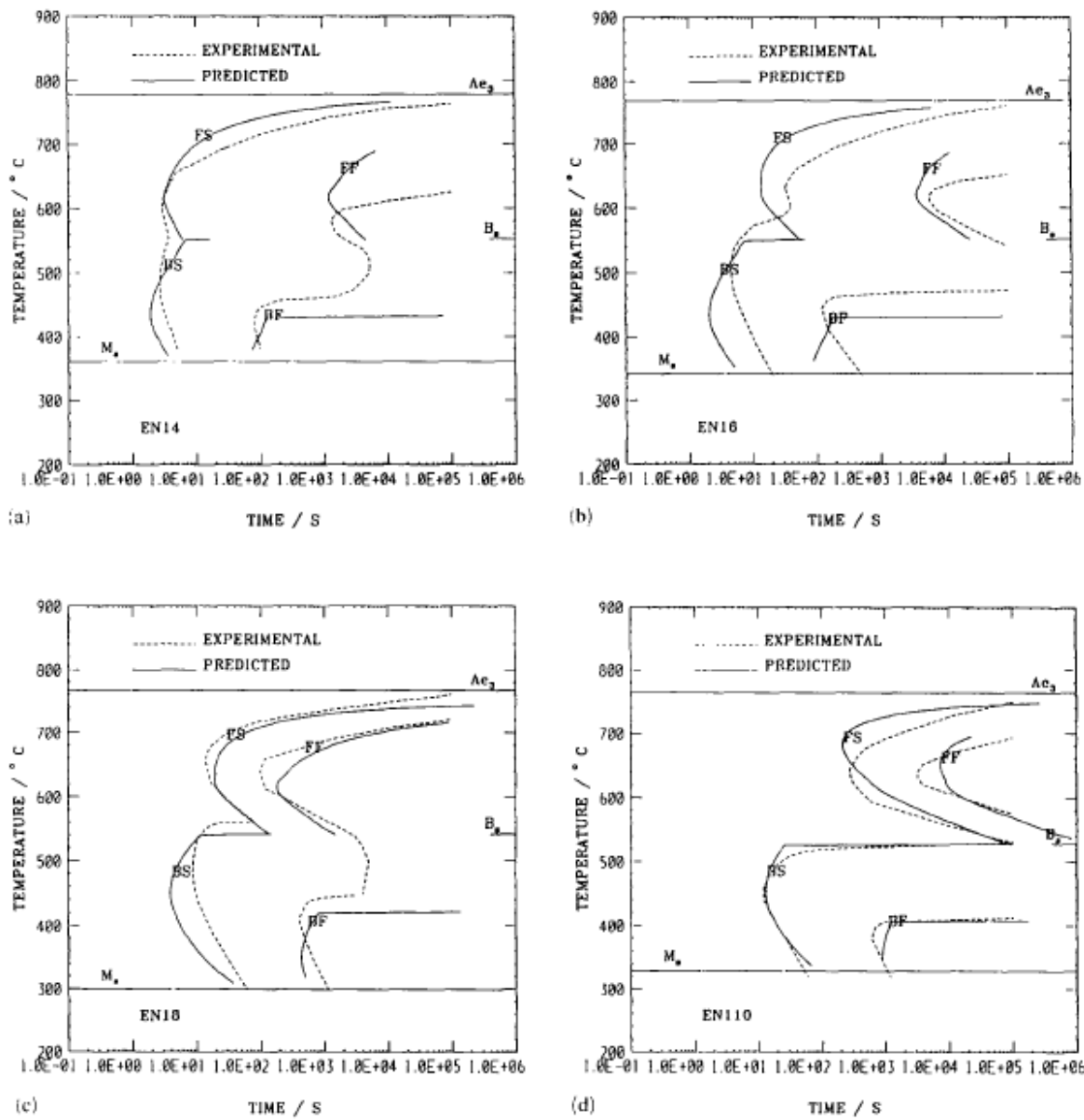
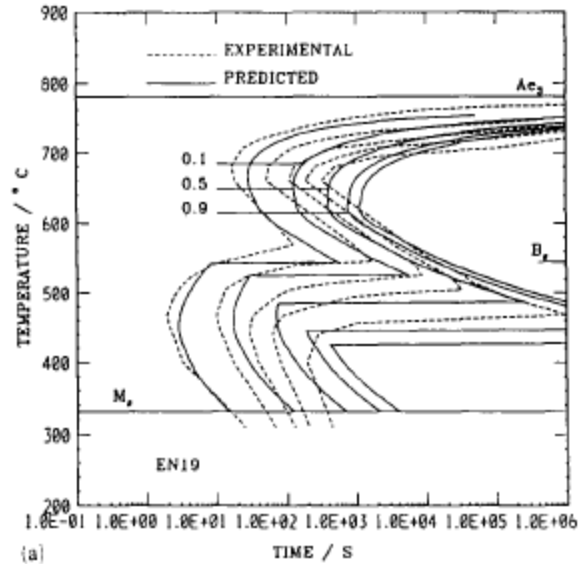
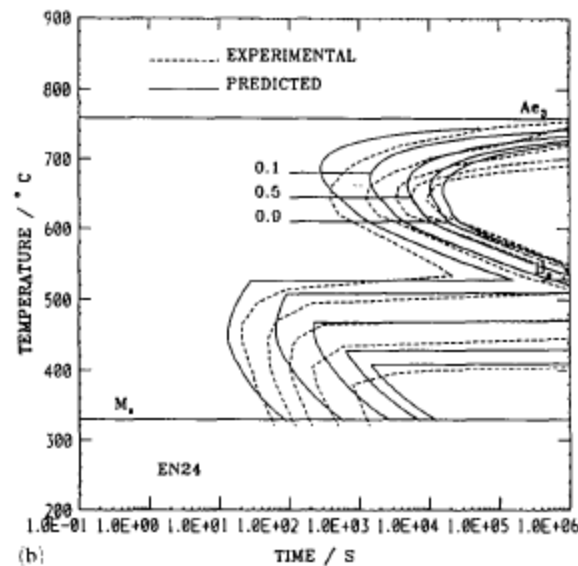


Fig. 50: Comparison of experimental and predicted TTT diagram for BS steel:(a) En14, (b) En 16, (c) En 18 and (d) En 110.





(a)



(b)

Fig. 52: Comparison of the experimental and predicted TTT diagrams including fractional transformation curves at 0.1, 0.5 and 0.9 transform fractions: (a) En 19 and (b) En24.

## Limitations of model

The model tends to overestimate the transformation time at temperature just below  $A_{e3}$ . This is because the driving force term  $\Delta G_{\max}$  is calculated on the basis of paraequilibrium and becomes zero at some temperature less than  $A_{e3}$  temperature.

The coefficients utilized in the calculations were derived by fitting to experimental data, so that the model may not be suitable for extrapolation outside of that data set. Thus the calculation should be limited to the following concentration ranges (in wt%): C 0.15-0.6, Si 0.15-0.35, Mn 0.5-2.0, Ni 0-2.0, Mo 0-0.8 Cr 0-1.7.

## 5. Fraction of martensite as a function of temperature

Volume fraction of martensite formed at temperature  $T = f$  and

$$f = 1 - \exp[-BV_p d\Delta G_v / dT (M_s - T)]$$

Where,  $B = \text{constant}$ ,  $V_p = \text{volume of nucleus}$ ,  $\Delta G_v = \text{driving force for nucleation}$ ,  $M_s = \text{martensite start temperature}$ . Putting the measured values

the above equation becomes

$$f = 1 - \exp[-0.011(M_s - T)] \quad [\text{Koistinen and Marburger equation}].$$

The above equation can be used to calculate the fraction of martensite at various temperature.